CHALMERS
UNIVERSITY OF TECHNOLOGY

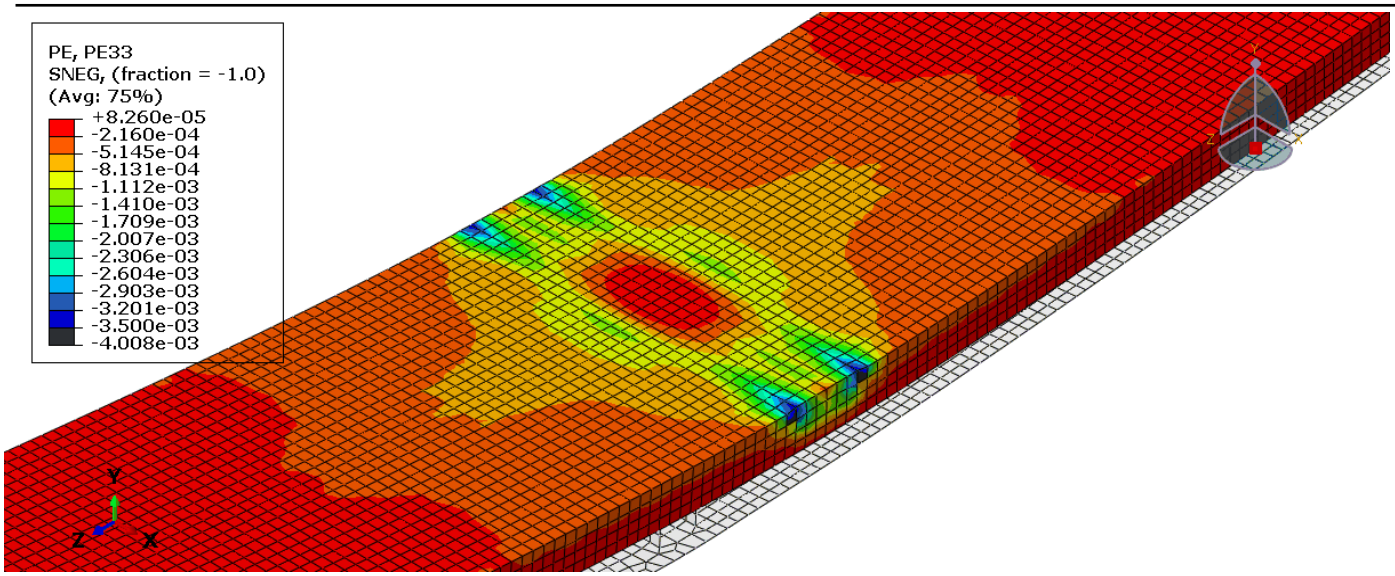

Finite Element Analysis and Design Models for Composite Action in Stainless Steel Corrugated Web I Girders Bridges

Master's thesis in Structural Engineering and Building Technology

AMER ALI
HASSAN ABUDAHER

Department of Architecture and Civil Engineering
Division of Structural Engineering
Light Weight Structures
CHALMERS UNIVERSITY OF TECHNOLOGY
Master's Thesis ACEX30
Gothenburg, Sweden 2022

MASTER'S THESIS ACEX30-22-06

Finite Element Analysis and Design Models for Stainless Steel Corrugated Web I-Girder Bridges

Master's Thesis in Structural Engineering and Building Technology

AMER ALI

HASSAN ABUDAHER

CHALMERS

Department of Architecture and Civil Engineering

Division of Structural Engineering

Lightweight Structures

CHALMERS UNIVERSITY OF TECHNOLOGY

Göteborg, Sweden 2022

Finite Element Analysis and Design Models for Composite Action in Stainless Steel Concrete Corrugated I-Girder Bridges

Master's Thesis in Structural Engineering and Building Technology

AMER ALI

HASSAN ABUDAHER

Examensarbete ACEX30-22-06

Institutionen för arkitektur och samhällsbyggnadsteknik

Chalmers Tekniska Högskola, 2022

Department of Architecture and Civil Engineering
Division of Structural Engineering
Light Weight Structures
Chalmers University of Technology

SE-412 96 Göteborg
Sweden
Telephone: + 46 (0)31-772 1000

Cover:
Strain distribution in the longitudinal direction of a concrete slab illustrating concrete crushing.

Department of Architecture and Civil Engineering

Göteborg, Sweden, 2022-06

Finite Element Analysis and Design Models for Composite Action in Stainless Steel Concrete Corrugated I-girder Bridges

Master's thesis in Structural Engineering and Building Technology

AMER ALI

HASSAN ABUDAHER

Department of Architecture and Civil Engineering
Division of Structural Engineering
Light Weight Structures
Chalmers University of Technology

ABSTRACT

Using stainless steel corrugated web I-girders in steel-concrete composite bridges has made it possible to achieve greater sustainability than the conventional designs since stainless steel has a lower life cycle cost and the corrugation reduces the amount of needed material. The composite action in the innovative design concept needs performance assessment, therefore a literature study has been carried out to review the existing design models for steel-concrete composite bridges and to examine their application in the case using corrugation and stainless steel. In addition, the composite action using stainless steel has been modeled, analyzed, and compared with carbon steel by using ABAQUS software in order to study the nonlinearities effects due to the used materials, geometries, and boundary conditions. Although the results showed that corrugation will contribute to a reduced flexural capacity and increase the ductility of composite cross-section, meanwhile stainless steel could sustain a higher flexural capacity due to its remarkable strain hardening.

Keywords:

Composite bridges, I-Girders, Carbon Steel, Stainless Steel, Corrugated Web, Strain Hardening.

Preface

This master's thesis is a part of a research project at Chalmers University of Technology that has been carried out at the master's program Structural Engineering and Building Technology at the Department of Architecture and Civil Engineering in Gothenburg between January 2022 to June 2022.

First and foremost, we would like to thank our supervisor and examiner Mozhdeh Amani for the great support during the whole thesis. We really appreciate your hard work and motivation.

We would like to extend our thanks to Mohammad Al-Emrani and Robert Hällmark for participating in our meetings, sharing their opinions, suggestions and many valuable ideas to guide this work forward.

Gothenburg June 2022

Amer Ali and Hassan Abudaher

Contents

LIST OF FIGURES

List of tables

List of symbols

Roman upper-case letters

A_a	The steel cross-section area.
A_b	area of bottom transverse reinforcement.
A_{bh}	The area of bottom transverse haunch reinforcement
A_c	The sectional area of the concrete slab.
$A_{c,L}$	The transformed area of the concrete cross-section depends on the loading term.
$A_{s,tot}$	The total area of reinforcement steel.
$A_{s,i}$	The total amount of reinforcement in the slab
$\frac{A_{sf}}{s_f}$	The area of transverse reinforcement divided by the spacing.
A_t	The area of top transverse reinforcement.
$A_{t,i}$	An increased area for the effective beam.
$A_{1,L}$	The composite cross-section area.
$A_{2,sa}$	The area of the cracked composite section
E_S	Secant modulus of elasticity of stainless steel
E_{S1}	The secant modulus corresponds to stress in the tension flange.
E_{S2}	The secant modulus corresponds to stress in the compression flange.
E_{cm}	Young's modulus of elasticity of concrete
E_y	the tangent modulus of the stress-strain curve at the yielding point
G_a	Shear modulus of elasticity.
G_F	Fracture energy.
I_a	The moment of inertia of structural steel cross-section.
$I_{1,L}$	The moment of inertia for the composite cross-section

$I_{2,sa}$	The area and moment of inertia of the cracked composite section
$I_{c,L}$	The transformed moment of inertia of concrete cross-section
, Ks	A rotational stiffness per unit length of the steel beam
N_{cs}	The transferred force to the beam by shear connectors.
$N_{c,el}$	The compressive force in the concrete flange associated with $M_{el,Rd}$.
N_{sh}	An equal compression force will act on the composite section.
$M_{a,Ed}$	The design bending moment applied to the structural steel before composite behaviour.
$M_{c,Ed}$	The part of the design bending moment acting on the composite section.
$M_{el,Rd}$	The elastic bending resistance of composite cross/section
$M_{pl,Rd}$	The design plastic bending moment
$M_{1,pl,Rd}$	The plastic moment for sagging bending moment region
$M_{2,pl,Rd}$	The plastic moment for hogging bending moment region
$M_{1,pl,V,Rd}$	The reduced plastic moments for sagging due to shear forces.
$M_{2,pl,V,Rd}$	The reduced plastic moments for hogging due to shear forces.
M_{sh}	The moment that will make tensile and compressive forces equal each other.
P_{Rd}	The vertical shear resistance of headed studs.
$S_{1,L}$	The static moment of composite cross-section
S	The first moment of inertia of the concrete slab with respect to the center of gravidity of the composite section for the considered time and load case.
S_{rm}	Mean smeared distance
$V_{C,Rd}$	the crushing resistance of the struts
V_{ED}	The design of vertical shear force or shear buckling resistance.

$V_{Lc,Ed}$	The design shear flow at sagging bending moment sections.
$V_{L,ED}$	The design value horizontal shear flow
$V_{L,Ed,max}$	The longitudinal shear develops at the ends of the bridge.
$V_{L,Rd}$	The longitudinal shear resistance of headed studs
$V_{s,Rd}$	The shear resistance of the ties
$\bar{Z}_{1,L}$	The distance of center gravity of the composite cross-section to the center gravity of the concrete slab section.
$\bar{z}_{1,s}$	The gravity centre of the equivalent section calculated with n_s
$\bar{Z}_{2,sa}$	The center of gravity for the cracked composite section from the center of reinforcement

Roman lower-case letters

b_0	The distance between the centers of the outstand shear connectors
b_{ei}	The value of the effective width of the concrete flange on each side of the web and taken
b_{eff}	The effective width of the concrete flange
d	The diameter of the shank of the stud
d_c	Plasticity damage variable for compressive stress-strain curve
d_t	Plasticity damage variable for tensile stress-strain curve
e_L	The longitudinal spacing of connectors
f_{cd}	The compressive design strength of concrete
f_{ck}	The characteristic value of the compressive stress.
f_{ctm}	The mean tensile strength of concrete
f_{sk}	The characteristic yield strength of reinforcement steel.
f_{sd}	The design yield strength of reinforcement steel.
f_{yd}	The design yield strength of steel-grades

f_u	The ultimate strength of steel-grades
h	The total depth of composite cross/section.
h_{sc}	The overall nominal height of the stud.
$l_{element}$	Length of a finite element
n	The number of shear connectors at one cross-section
n_0	The modular ratio of concrete for short-term loading
n_L	The modular ratio of concrete for long-term loading
n_s	The long-term modular ratio for shrinkage
x_{pl}	The plastic neutral axis

Greek letters

α_{cc}	Reduction factor that considers the long-term effects on the compressive strength.
α_T	Coefficient of Thermal expansion
β	Reduction factor of plastic bending moment.
$\beta_c(t, t_0)$	
$\varphi(t, t_0)$	Creep coefficient
σ_{true}	True value of stress in plastic region of stress/strain curve
ε_{ca}	The autogenous shrinkage strain.
ε_{cd}	The drying shrinkage strain.
ε_{cs}	Total shrinkage strain
ε_{true}	True value of strain in plastic region of stress/strain curve.
ε_{true}^{pl}	The logarethmic plastic strain
ρ	Reduction factor of design strength of structural steel.
$\rho_{s,tot}$	The total reinforcement ratio.
γ_a	Specific weight
γ_c	The resistance factor for permanent and load variable

γ_s	The partial factor for reinforcement steel
γ_V	The partial safety factor for calculating shear stud resistance
γ_{M0}	Resistance of cross-section whatever the class is
γ_{M1}	Resistance of members to instability assessed by member checks
γ_{M2}	Resistance of cross-section in tension to fracture
v_a	Passion ratio

1 Introduction

This chapter gives a background about the topic of this thesis, the method that is used, and the limitations of the study.

1.1 Background

Composite bridges are a good example of sustainable bridges as they take the advantage of steel in tension and concrete in compression. Additionally, having new types of steel such as stainless steel makes it possible to have more sustainable solutions. Although stainless steel has a lower life cycle cost compared with carbon steel; nevertheless, using stainless steel in composite bridges still needs further studies. The reason behind that is stainless steel's high initial cost. Furthermore, using corrugated web plates in the beams will contribute to reducing the amount of needed material and having more sustainable solutions.

1.2 Aim

Corrugated web stainless steel composite bridges need performance assessments in different aspects and the aim of this master thesis is to review the existing design models for composite sections and evaluate their application for the case of design in stainless steel and corrugated web. The composite action of stainless steel and corrugated web will be modeled, analyzed, and compared with carbon steel.

1.3 Limitations

Limitations for the thesis are presented as follows:

- The study will consider simply supported plate girder composite bridges.
- The study will focus on the design models for composite sections in the ultimate limit state. Therefore, construction phase is not included in this study.
- The study will review the design models of flexural capacity of composite cross section whereas shear capacity is not included in the scope area of the study.

2 Theory

2.1 Steel-concrete composite bridges

In steel-concrete composite bridges, two or more parallel steel girders are rigidly connected with a reinforced concrete slab using shear connectors (Vayas & Iliopoulos, 2014).An example of shear connectors is welded studs that allow the composite action between steel and concrete. The composite action is essential to generate a stiff cross-section. Where bending moment is positive, steel will be in tension and concrete in compression taking the advantage of each material's superior properties. Thus, composite bridges can be considered as an efficient and sustainable design solution. However, at internal supports, concrete will be in tension, and it is considered cracked. The focus of this thesis will be on a single span where there is no negative moment.

2.1.1 Structural Systems

The structural system of the bridge depends on different parameters, for instance, the depth of the bridge, the type of the soil, and the potential reconstruction activities in the future (Vayas & Iliopoulos, 2014).

Choosing a simply supported bridge has many advantages. Thermal effects, creep, and shrinkage does not affect the internal forces of the bridge. Moreover, no cracking in the concrete of the slab occurs since the concrete is under compression.

On the other hand, continuous bridges are known for their small deformations, higher redundancy, and the possibility for moment redistribution. Continues bridges are efficient for small and medium spans. The focus of this thesis will be on simply supported plate girder bridges.

2.1.2 Composite Action

Composite action is when steel, which has a high tensile resistance, and concrete, which has a high compression resistance act as one structural member (Hällmark, 2018). Shear connectors are important to provide the composite action and they must have sufficient strength, stiffness, and ductility.

Without the composite action, a slip between steel and concrete will occur when the beam is loaded. Therefore, the plane section will not remain plane after bending. The concrete slab defects separately with its own neutral axis while structural steel girders defect similarly with its neutral axis in the longitudinal direction see Figure 2.1. In fact, the concrete slab elongates at its bottom fiber whereas the top fiber of the top steel flange shortens, the differential displacements come up at the interface section between the concrete slab and the structural steel. Therefore, there is a need to connect both parts by shear connectors that restrain the differential displacements and make concrete slab and structural steel girders behave as one composite section with a common single neutral axis. In that case, full development of moment resistance of the composite section will be achieved and the connection between the composite section's components is denoted as a full connection. (Vayas & Iliopoulos, 2014).

When rigid connectors are used, no-slip between steel and concrete will occur, and the composite action will make the two materials as one structural member as shown in Figure 2.1. Nevertheless, real structures will always have a degree of slip between steel and concrete caused by bending of the shear connectors and concrete crashing (Hällmark, 2018).

If shear connectors have sufficient strength, stiffness, and ductility, Eurocode 4-2 (EN 1994-2, 2005) allows the section to be designed assuming full composite action. In this case, the strength of the cross-section will be governed by the steel girder or the concrete slab. However, if the shear connection is the weakest part or if the number of shear connectors is not sufficient, the design can be based on a partial shear connection, but the requirements in (EN 1994-1-1, 2005) shall be fulfilled.

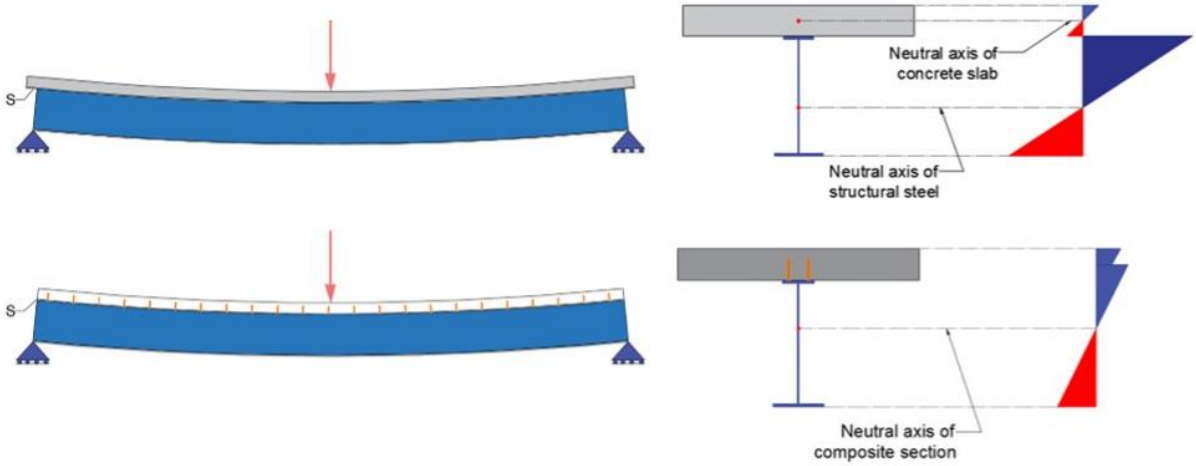

Figure 2.1 Girders in flexure with and without full shear connection, redrawn from (Vayas & Iliopoulos, 2014)

2.2 Corrugated webs

The idea of using corrugation in steel and steel-concrete composite beams has been used in various nations around the world for building structures. Recently, the idea transfers to bridge structures where it is a beneficial solution to reduce needed materials. Beam with corrugated web, top and bottom flanges is the traditional model that has been used instead of conventional flat web beams. There are many advantages of using corrugated webs specially the trapezoidal webs which are the common type of corrugated web beams used for bridges, for instance, hight out of plane stiffness due supporting from both longitudinal and inclined folds to each other according to (Elammary, Saddek, & Alwetaishi, 2017). Furthermore, corrugated web beams have higher global and local shear resistance than flat plate webs. Moreover, the corrugated webs have transverse stiffness greater than conventional flat plate webs. Thus, number of transverse stiffeners and cross girders that are used in case of flat web beams can be reduced in case of using corrugated web instead. Additionally, the thickness of corrugated web is usually thinner due to its sufficient shear capacity and the fact that corrugated web does not contribute to flexural capacity and flanges only resist the applied stresses due to bending moment according to (ELgaaly & Seshadri, 1997).

Therefore, there is no need to increase the thickness of web. Thereby, corrugated web beams are considered as a sufficient economical solution. This fact is considered as a disadvantage of using corrugated web that the outstanding length of compressive flange and web eccentricity forms due to the depth of corrugation. Noteworthy, failure modes of corrugated web beams are web yielding in shear, flange yielding in compression and tension, flange buckling in compression, and lateral torsional buckling.

The typical configuration of trapezoidal corrugated web is illustrated in Figure 2.2, which is used in this study.

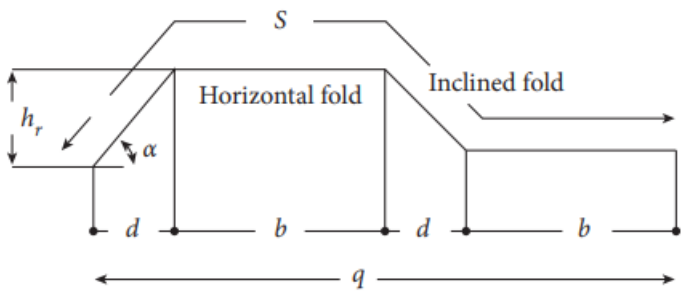

Figure 2.2 : Corrugated web: profile configuration of trapezoidal web from (Elammary, Saddek, & Alwetaishi, 2017)

2.3 Stainless steel

In structures that have demands for corrosion resistance such as bridges, stainless steel is considered as a good alternative for its significant high strength, fire and corrosion resistance. Furthermore, stainless steels give an efficient economical solution for large construction projects even though the cost of stainless steel is higher than carbon steel in the construction stage. The real investment of stainless steel appears in the renovation and maintenance stage. Moreover, stainless steel is considered a recyclable material, which makes stainless steel an investable material for other applications after its cycle life is gone (Design manual for structural stainless steel, 2018).

2.3.1 Different types of stainless steel

The stainless steel contains a family of corrosion-resistant and high-strength steels that have a minimum containing Chromium about 10.5%. There is a wide range of various types of stainless steel with different grades that give the opportunity to use them in structural applications that require a specific level of corrosion resistance and strength. (Design manual for structural stainless steel, 2018)

Austenitic stainless steel contains up to18% of Chromium and 11% of additional Nickel. This type is relevant to cold forming and is easier for welding in comparison with carbon steel. It has high ductility and better toughness during variations of surrounding temperatures. On the other hand, Ferritic stainless steel is without

additional Nickel. ferritic has less than ductility and toughness that results in the ferritic type is not suitable for cold forming and less weldable.

Duplex stainless steel has a mixed ferritic and austenitic atomic structure that results in a duplex type stronger than austenitic type twice. The duplex stainless steel contains up to 26% of Chromium, up to 8 % of Nickel, and 0.3% Nitrogen. Furthermore, the duplex stainless steel has good ductility, the resistance of corrosion cracking, and higher strength than austenitic stainless steel with restricted formability. The most common application is that duplex stainless steel is used in heavier such as bridges in aggressive corrosive environments (Design manual for structural stainless steel, 2018).

Duplex stainless-steel grade 1.4462 is the most appropriate for structural elements that are exposed to corrosive environments. In addition, it becomes more available to use in constructions that require high strength and good resistance corrosion of cracking according to Eurocode 3 (EN 1993-1-4, 2020).

2.3.2 Stainless steel behaviour

Different stainless steels have different stress-strain relations. The most important aspect of stainless-steel behavior is that there is no specific identified point for yielding strength in the stress-strain curve as shown in Figure 2.3. The shape of the stress-strain curve is rounded even before reaching to yielding level. Whereas carbon steels have elastic behavior before they yield at a specific point (Design manual for structural stainless steel, 2018).

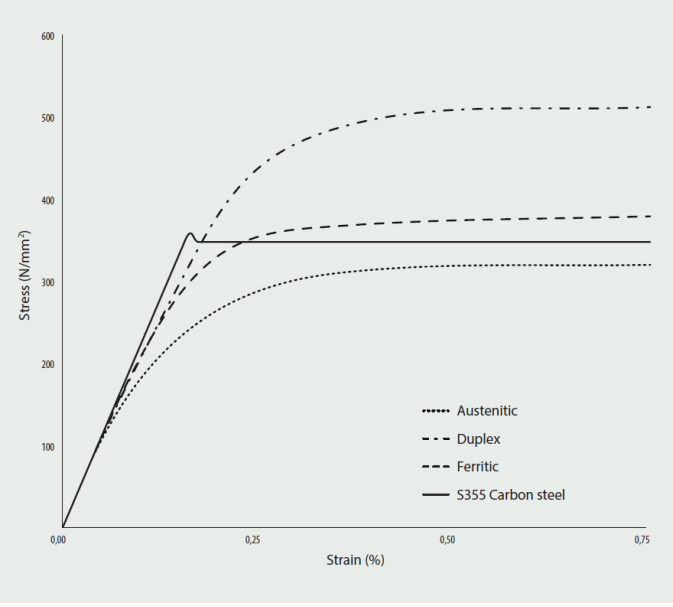

Figure 2.3:stress- strain relation for different types of steels, from (Design manual for structural stainless steel, 2018)

2.3.3 Corrosion control

Corrosion problem in noble metals like stainless steel is more dangerous than in carbon steel, this is because the damaged area in stainless steel is larger and deeper. Thus, the choice of appropriate types and grades of stainless steel are important. It is necessary to assess the environment of project and study potential accidents for instance, presence of chloride higher than expected on the stainless-steel member surface. Also, the manufacturing process has its effect on the corrosion resistance of stainless. Duplex stainless steel provides increased corrosion resistance with high strength that reduces the cross-section area and thus needed materials decrease in large projects such as bridges. It is worth to note that several practical considerations shall be considered to prevent corrosion problems are listed in Table 3.2 (Design manual for structural stainless steel, 2018).

2.3.4 Modulus of elasticity

The modulus of elasticity of stainless steel is recommended to be taken as 200 GPa for Duplex and Austenitic in the ultimate limit state according to Eurocode 3 (EN 1993-1-4, 2020). Whereas the secant modulus of elasticity should be used in serviceability limit state where it is considered more accurate than the modulus of elasticity when estimating the deflections in elastic beams. The secant modulus of elasticity can be calculated based on the current level of stresses in the flanges of members. The reason for using secant modulus of elasticity is the nonlinearity stress-strain relation that appears in terms of the variation of modulus of elasticity with load combinations in different cross-sections along with the stainless-steel member (Design manual for structural stainless steel, 2018).

The secant modulus of elasticity of stainless-steel in-service limit state can be calculated by equation **(2.1)**.

$$E_S = \frac{E_{S1} + E_{S2}}{2} \qquad \textit{(2.1)}$$

Where:
E_{S1} : The secant modulus corresponding to stress in the tension flange.
E_{S2} : The secant modulus corresponding to stress in the compression flange.

Values of E_{S1} and E_{S2} for the corresponding serviceability design stress can be obtained from:

$$E_{S,i} = \frac{E}{1 + 0.002 \cdot \frac{E}{\sigma_{i,ED,ser}} \cdot (\frac{\sigma_{i,ED,ser}}{f_y})^n} \qquad \textit{(2.2)}$$

Where:
$\sigma_{i,ED,ser}$: The serviceability design stress in the tension or compression flange

E: The modulus of elastici$= 200 \cdot 10^3\ N/mm^2$
n: The Ramberg Osgood Parameter.

Noteworthy, n is a measure of the non-linearity of the stress-strain curve with lower values indicating a grater degree of non-linearity.

3 Design of Composite bridges

3.1 Basis of Design

During the design life of the bridge, it should follow certain basic requirements regarding structural resistance, serviceability, and durability (Vayas & Iliopoulos, 2014).

The design will be based on consideration of ultimate and serviceability limit states. The ultimate limit states are related to the safety of people and of the structure. That includes the loss of static equilibrium of the structure, failure by collapse or large deformations, failure caused by fatigue, and deformation of the foundation and the ground. Furthermore, serviceability limit states are associated with the function of the structure, for instance, deformation, and cracking of concrete. However, the area of this thesis aims to study the ultimate strength of composite bridges.

Durability is the aspect that ensures the fulfilment of the basic requirements of safety and serviceability all over the design life. The most important aspect influencing durability is the corrosion of steel that is affected by the environment. Steel reinforcement is covered with concrete. On the other hand, a coating system should be used to protect the structural steel (Vayas & Iliopoulos, 2014).

3.2 Design codes

In general, the design of a new bridge refers to several regulations that concern materials, loads, cross-sections, capacity verifications, etc. There are several standards in Eurocode that provide regulations and guidelines to design different types of bridges (EN 1994-2, 2005) (Vayas & Iliopoulos, 2014). Through every country has a specific document, called *National Annex,* which considers several factors that affect the design requirements, for instance, climate conditions. Krav Brobyggnad is the national annex that is used in Sweden, and it provides design values of several parameters (Krona, 2019). A list of the Eurocodes that are used in the design of composite bridges are shown in Table 3.1.

Table 3.1: list of Eurocode standards that are used in the design of composite bridges

Eurocode	Standard	Part
EN-1990	Basis of structural design	
EN-1991	Actions on structures	EN-1991-1-1: General actions EN-1991-1-4: Wind actions EN-1991-1-5: Thermal actions EN-1991-2: Traffic loads on bridges
EN-1992	Design of concrete structures	EN-1992-1-1: General rules. EN-1992-2: Concrete bridges

EN-1993	Design of steel structures	EN-1993-1-1: General rules EN-1993-1-4: Stainless steel EN-1993-1-5: Plate structural element EN-1993-1-8: Design of joints EN-1993-1-9: Fatigue EN-1993-2: Steel bridges
EN-1994	Design of composite steel and concrete structures	EN-1994-2: General roles for bridges.

3.3 Structural Materials

Materials used in composite bridges are presented in this section. According to Eurocode EN 1990, the design values for the strength properties of the material should be used.

3.3.1 Concrete

According to Eurocode 4 (EN 1994-2, 2005), the recommended concrete classes that are used for composite bridges are between C20/25-C60/75. The most usual strength class of the concrete is C35/45 to obtain a suitable cross-section for the concrete deck, but it can be more beneficial to use concrete classes C30/37 or C40/50 in some design models. Properties of concrete are listed in Table 3.2.

Table 3.2:Material Properties of Concrete (units in MPa)

Grade	f_{ck}	f_{cm}	f_{ctm}	$f_{ctk,0.05}$	$f_{ctk,0.95}$	E_{cm} x10^3
C20/25	20	28	2.2	1.5	2.9	30
C25/30	25	33	2.6	1.8	3.3	31
C30/35	30	38	2.9	2.0	3.8	33
C35/45	35	43	3.2	2.2	4.2	34
C40/50	40	48	3.5	2.5	4.6	35
C45/55	45	53	3.8	2.7	4.9	36
C50/60	50	58	4.1	2.9	5.3	37
C55/67	55	63	4.2	3.0	5.5	38
C60/75	60	68	4.4	3.1	5.7	39

According to Eurocode 2 (EN 1992-1-1, 2005),the compressive design strength of concrete is obtained from Equation **(3.1).**

$$f_{cd} = \alpha_{cc} * \frac{f_{ck}}{\gamma_c} \quad \textbf{(3.1)}$$

Where:
f_{ck}: The characteristic value of the compressive stress.
γ_c: The resistance factor for permanent and load variable that has value of 1.5.
α_{cc}: Reduction factor that considers the long-term effects on the compressive strength.
α_T: Coefficient of Thermal expansion that has value of 10*10^-6 [Per C]

3.3.1.1 Modular ratio of concrete due to creep

The creep coefficient is a time-dependent coefficient that can be determined in the expression according to (EN 1992-1-1, 2005), Annex B. the creep coefficient can be obtained from equation **(3.2).**

$$\varphi(t, t_0) = \varphi_0 * \beta_c(t, t_0) \quad \textbf{(3.2)}$$

According to EN1994-2 (EN 1994-2, 2005), the modular ratio of concrete is the ratio between the modulus of elasticity of steel to the modulus of elasticity of concrete. The modular ratio of concrete depends on time. Therefore, the modular ratio for short-term loading is n_0 and for, long-term loading is n_L. Moreover, the modular ratio depends on the type of loading for instance permanent loads, shrinkage, or imposed deformation Whereupon the effect of creep in the composite bridge can be considered for long-term loading in the equation **(3.3)**.

$$n_L = n_0[1 + \varphi_L(t, t_0)] \quad \textbf{(3.3)}$$

Where:
$\varphi(t, t_0)$ is the creep coefficient of the concrete slab.
n_0 is the modular ratio of concrete for short-term loading, for instance, for traffic loads, wind loads, temperature loads, and earthquakes.

The modular ratio of concrete is given by equation **(3.4)**:

$$n_0 = \frac{E_s}{E_{cm}} \quad \textbf{(3.4)}$$

Where:
E_s The modulus ratio of steel.

$E_{cm}$is the modulus ratio of concrete for short-term loading.
φ_L : the creep multiplier depending on the type of loading, which is taken 1.1 for permanent loads, 0.55 for the primary and secondary effect of shrinkage, and 1.5 for prestressing by imposed deformations.

Due to creep, redistribution of tension stresses occurs from concrete to steel, where concrete stresses decrease while steel stresses increase with time. Furthermore, the stiffness of the concrete slab will be reduced in the long term whereas stiffness of steel girders. Thus,

3.3.1.2 Shrinkage

According to Eurocode (EN 1992-1-1, 2005), total shrinkage has two components, dry shrinkage strain that is time-dependent and develops slowly as a function of migration of the water through hardened concrete, whereas autogenous shrinkage strain is a linear function of concrete strength that develops at the early age of new casted concrete. Total shrinkage strain can be obtained in the equation **(3.5)**.

$$\varepsilon_{cs} = \varepsilon_{cd} + \varepsilon_{ca} \qquad \textbf{(3.5)}$$

Where:
ε_{cs} :The total shrinkage strain.
ε_{cd} : The drying shrinkage strain.
ε_{ca} : The autogenous shrinkage strains.

3.3.2 Carbon Steel

3.3.2.1 Structural steel

Grades and properties of steel are described in the European Standard (EN10025, 2014). Table 3.3 presents the grades of steel, the yield strength, and the tensile strength of the steels produced to (EN10025, 2014) in accordance with (EN 1993-1-1, 2005). The grade of the structural steel is symbolled with the letter S followed by a number referring to the strength of steel with a thickness that is less than 16mm in MPa and one or two symbols specifying the material toughness. A sufficient material toughness will be needed to guarantee a ductile failure under tension and to avoid brittle failure (Vayas & Iliopoulos, 2014).

Table 3.3:Yield strength of carbon steel grades

	Nominal thickness of the element in mm			
	$t \leq 40mm$		$40mm < t \leq 80mm$	
Steel grade to EN 10025	f_y in MPa	f_u in MPa	f_y in MPa	f_u in MPa
S235	355	510	335	470

S275	275	390	255	370
S355 N/NL	355	490	335	470
S420 N/NL	420	520	390	520
S460 N/NL	460	540	430	540
S275 M/ML	275	370	255	360
S355 M/ML	355	470	335	450
S420 M/ML	420	520	390	500
S460 M/ML	460	540	430	530

Table 3.4: shows other material properties of structural steel.

Specific weight	$\gamma_a = \frac{78.5kN}{m^3}$
Modulus of elasticity	$E_a = 210GPa$
Passion ratio	$v_a = 0.3$
Shear modulus	$G_a = \frac{E_a}{2.(1+v_a)}$
Coefficient of thermal expansion	$a_t = 10.10^6$ [per C]

The partial factors for structural steel are given in (EN 1993-1-1, 2005) and listed in Table 3.5.

Table 3.5: Partial factors for structural steel

Partial factor	description	Value
γ_{M0}	Resistance of cross-section whatever the class is	1
γ_{M1}	Resistance of members to instability assessed by member checks	1
γ_{M2}	Resistance of cross-section in tension to fracture	1.25

3.3.2.2 Reinforcement steel

Steel grades for reinforcement steel is characterized with two letters and a number between them for instance B500B (Vayas & Iliopoulos, 2014). The first letter B refers to weldable high-bond bars that are used in composite bridges. The number 500 refers to the characteristic value (5% fractile) of the yield strength f_{sk}. The recommended value of the characteristic yield strength in composite bridges is between 400 and 600. The third letter refers to the ratio between tensile and yield strength. In composite bridges, it is recommended to use class B with a ratio between 1.08 and 1.15 or class C with a ratio that equals or larger than 1.15 but smaller than 1.35. That recommendation is to ensure a sufficient ductility. Although, the modulus of elasticity for reinforcement steel is $E_s = 200\ GPa$ according to (EN 1992-1-1, 2005), It can be taken as $E_s = 210\ GPa$ to make it the same as the modulus of elasticity of the structural steel (Vayas & Iliopoulos, 2014).

The partial factor for reinforcement steel can be taken as $\gamma_s = 1.15$ According to Eurocode (EN 1992-1-1, 2005).

3.3.2.3 Shear connectors

Strength classes for shear connectors are prescribed in Eurocode (EN 1993-1-8, 2005) and given in list of Eurocode standards that are used in the design of composite bridges. The height of the connector should follow the requirements of sufficient concrete cover and fulfil the condition $h \geq 3d$

Nominal values of the yield strength f_{yb} and the ultimate tensile strength f_{ub} for bolts are listed in Table 3.6.

Table 3.6:Nominal values of the yield strength and the ultimate tensile strength for bolts.

Bolt Class	4.6	4.8	5.6	5.8	6.8	8.8	10.9
$f_{yb}\ \frac{N}{mm^2}$	240	320	300	400	480	640	900
$f_{ub}\ \frac{N}{mm^2}$	400	400	500	500	600	800	1000

Note: the national Annex may exclude certain bolt classes.

The partial factor for shear connectors can be taken as $\gamma_{m2} = 1.25$ According to (EN 1993-1-8, 2005).

3.3.3 Stainless steel

Grades and properties of stainless steel are described in the European Standard EN10088. Table 3.7 presents several grades of Duplex stainless steel, the yield strength, and the tensile strength of the Duplex stainless steels produced to EN 10088 in accordance with (EN 1993-1-4, 2020). The grade of the structural stainless steel is symbolled with the Numbers followed by a number referring to the strength of stainless steel in MPa with a thickness limitation. 1,2 and 4 symbols specify the material toughness.

Table 3.7 Yield and ultimate strength of different grades of stainless steel from (EN 1993-1-4, 2020)

Nominal thickness of the element in mm						
Duplex	$t \leq 8mm$		$8mm < t \leq 13.5mm$		$13.5mm < t \leq 75mm$	
Steel grade to EN 10088	f_y in MPa	f_u in MPa	f_y in MPa	f_u in MPa	f_y in MPa	f_u in MPa
1.4062	530	700	480	680	450	650
1.4162	530	700	480	680	450	650
1.4362	450	650	400	650	400	630
1.4462	500	700	460	700	460	640
1.4482	500[1]	700[1]	480[2]	660[2]	450	650
1.4662	550[1]	750[1]	550[4]	750[4]	480	680

3.4 Structural Analysis

According to (EN 1994-2, 2005), action effects can be calculated by elastic global analysis. This section reviews some important parameters that affect the structural analysis of composite bridges.

3.4.1 Effective Width of concrete

According to (EN 1994-2, 2005),5.4.1.2, the effects of shear lag of global analysis are considered by the effective width of the concrete slab that is used in the composite cross-section where the effective width is smaller at support regions because of the higher magnitude of shear forces at these regions. The effective width differs at the mid-span region with one in the support region as shown in Figure 3.1.In the case of

using elastic analysis, the uniform effective width b_{eff1} is used at mid-span for spans that are supported at both ends as illustrated in Figure 3.1.

The effective width at mid-span or internal support is determined as:

$$b_{eff} = b_0 + \sum b_{ei} \qquad \textbf{(3.6)}$$

b_0 : The distance between the centres of the outstand shear connectors
b_{ei}: The value of the effective width of the concrete flange on each side of the web and taken as $\frac{L_e}{8}$ but not greater than the geometric width b_i.
L_e : The approximate distance between points of zero bending moment but not greater than geometry width b_i
b_i The distance from the outstand shear connector to a point midway between adjacent webs or distance to the free edge.

The effective width at the end support region is determined as:

$$b_{eff} = b_0 + \sum \beta_i * b_{ei}\text{i} \qquad \textbf{(3.7)}$$

With: $\beta_i = \left(0.55 + 0.025 * \frac{L_e}{b_{ei}}\right) \leq 1.0$
b_{ei} : The effective width of the end span at mid-span.

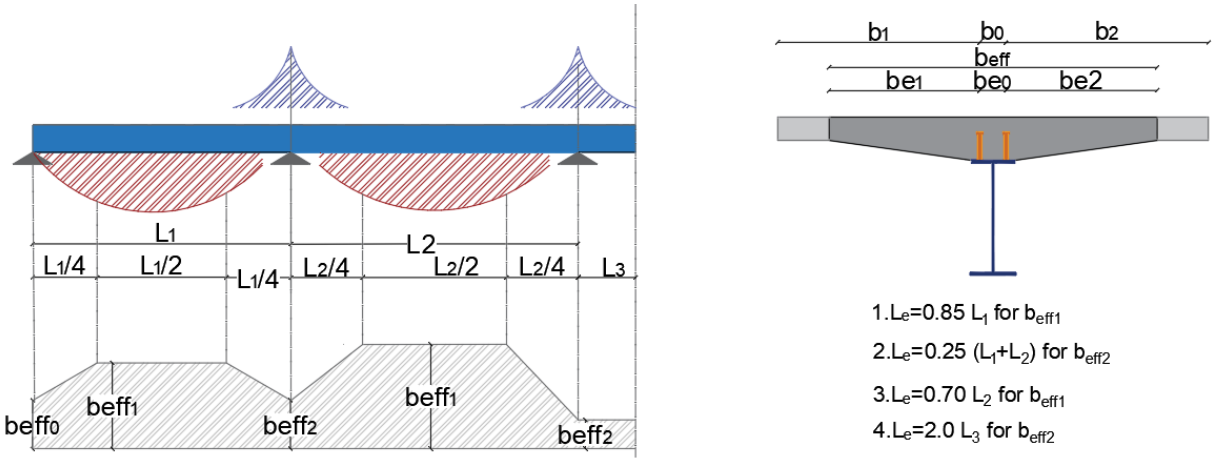

Figure 3.1 Equivalent spans for effective width of concrete flange, redrawn from EN1994-2

3.4.2 Cross-section classification

To check if the bending resistance will be determined by elastic or plastic analysis, cross-sectional classification is needed. Moreover, cross-sectional classification is important to determine if the cross-section is subjected to local buckling. If the section is class 1, the section can develop a plastic bending resistance and the section will have a sufficient rotational capacity. On the other hand, class 2 can develop plastic bending

capacity, but it has a limited rotation capacity. However, class 3 can only develop an elastic bending capacity and class 4 will have a resistance lower than the elastic capacity due to local buckling (Vayas & Iliopoulos, 2014).

According to Eurocode (EN 1994-2, 2005), 5.5, the classification that is defined in (EN 1993-1-1, 2005), 5.5.2 applies for composite beams. The cross section should be classified according to the least favorable class of its steel elements in compression. However, a steel compression element restraint by attaching it to a reinforced concrete element may be placed in a more favorable class. For composite sections with structural stainless steel, (EN 1993-1-4, 2020) can be used for classification of sections.

The classification of the cross section in composite bridges and the corresponding verifications are listed in Table 3.8.

Table 3.8:most usual bridge section classes from (Vayas & Iliopoulos, 2014)

Bridge section	Top flange	Bottom flange	Web	Plate buckling verifications	Cross section	verifications
Plate girder	1 or 2	1 or 2	1 or 2	___	1 or 2	(3.8)
	1 or 2	1 or 2	3	___	3	(3.8)
	1 or 2	1 or 2	4	reduced stress method	Treated as class 3	(3.11)

$$N_{c,Rd} = \frac{A.f_y}{\gamma_{M0}} \qquad \text{for classes 1,2, and 3 cross-sections} \qquad \textbf{(3.8)}$$

$$N_{c,Rd} = \frac{A_{eff}.f_y}{\gamma_{M1}} \qquad \text{for class 4 cross sections} \qquad \textbf{(3.9)}$$

Where:
A: The area of the gross cross section not allowing for fasteners hole
A_{eff}: The area of the effective cross section allowing for local buckling.

The buckling resistance of steel members can be obtained from equations **(3.10**),

$$\mathrm{N_{b,Rd}} = \frac{\chi \cdot \mathrm{A} \cdot f_y}{\gamma_{M1}} \qquad \text{for classes 1, 2, and 3 cross sections} \qquad \textbf{(3.10)}$$

$$N_{b,Rd} = \frac{\chi.A_{eff}.f_y}{\gamma_{M1}} \qquad \text{for class 4 cross section} \qquad \textbf{(3.11)}$$

Where:
χ : Reduction factor for flexural buckling that can be determined from Eurocode 3 for carbon steel or Eurocode 4 for stainless steel.

3.4.3 Sectional constants

The cross-section of a composite bridge consists of the steel girders and the concrete slab within its effective width. The composite cross-section will be transferred to an equivalent cross-section of only steel material by reducing the area of the concrete slab the modular ratio n_0 for the short term and n_L for the long term; see section 3.3.1.1.

For uncracked composite cross-section (state I), the area of the composite section is determined based on the modular ratio of concrete that differs depending on terms of loading according to (Vayas & Iliopoulos, 2014).Whereas in the case of using the corrugated web in the composite section, the contribution of the web to the area and the moment of inertia will be neglected for both cracked and uncracked cross-sections. The area of the composite cross section will be determined from Equation **(3.12)**.

$$A1_L = A_a + \frac{A_c}{n_L} \qquad \textbf{(3.12)}$$

Where:
$A_{1,L}$: The composite cross-section area.
A_a : The steel cross-section area.
A_c : The concrete cross-section area.
n_L : The modular ratio of concrete that is determined in Section 3.3.1.1

The distance of the centre of gravity of the composite cross-section from the centre of the concrete slab is determined by the Equation **(3.13)***:*

$$\bar{Z}_{1,L} = \frac{A_a * \bar{Z}_a}{A_{1,L}} \qquad \textbf{(3.13)}$$

Where:
$\bar{Z}_a$: The distance of the centre of gravity for steel cross-section from the centre of the concrete slab.

The static moment of composite cross-section is determined as:

$$S_{1,L} = A_{c,L} * \bar{Z}_{1,L} \qquad \textbf{(3.14)}$$

Where:
$A_{c,L}$: The transformed area of concrete cross-section depending on the loading term.

$$A_{c,L} = \frac{A_c}{n_L}$$

$\bar{Z}_{1,L}$: The centre of gravity of composite cross-section from the centre of concrete slab depending on loading term.

The moment of inertia of composite cross-section is obtained by the equation **(3.15)**:

$$I_{1,L} = I_{c,L} + I_a + S_{1,L} * \bar{Z}_a \qquad \textbf{(3.15)}$$

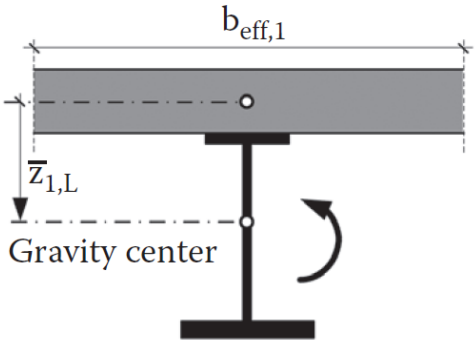

Figure 3.2 Uncracked composite section, from (Vayas & Iliopoulos, 2014)

$G.C$: Gravity centre.

$I_{c,L}$: Th transfomed moment of inertia of concrete cross-section.

Where: $I_{c,L} = \frac{I_c}{n_L}$

I_a : The moment of inertia of structural steel cross-section.

In cracked composite section (state II), the concrete slab is considered as cracked. Thus, the reinforcement steel within the effective width of concrete cross-section is included to calculate the area and the moment of inertia. They are obetained from the following equations **(3.16), (3.17)**, respectively.

$$A_{2,sa} = A_a + A_{s,tot} \qquad \textbf{(3.16)}$$

$$I_{2,sa} = I_a + A_a * \left(\bar{Z}_{2,sa} - \bar{Z}_a\right)^2 + A_{s,tot} * \bar{Z}_{2,sa}{}^2 \qquad \textbf{(3.17)}$$

Where:

$A_{s,tot}$: The total area of reinforcement steel.

The centre of gravity for the cracked composite section from the center of reinforcement is determined by equation **(3.18)**:

$$\bar{Z}_{2,sa} = \frac{A_a * \bar{Z}_a}{A_{2,sa}} \qquad \textbf{(3.18)}$$

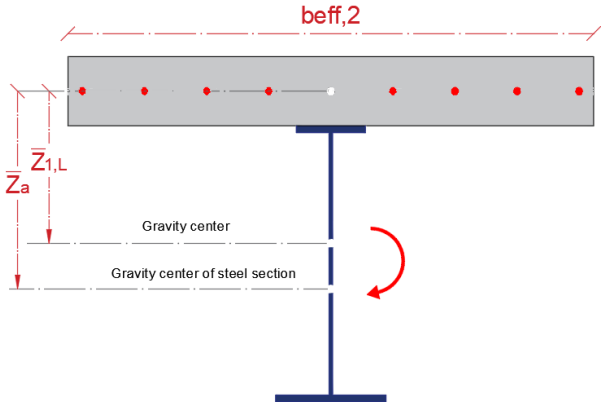

Figure 3.3 Fully cracked composite section, redrawn from (Vayas & Iliopoulos, 2014)

The web will not contribute for corrugated

In support regions, the section can also be considered as 'semi-cracked' where the cross sectional area of the beam is equal the amount area of reinforcement steel that is located in the centre of slab section for simplicity. The tension stiffening of uncracked concrete parts between reinforcement bars is taken into account by using an increased area for the effective beam (Vayas & Iliopoulos, 2014).

$$A_{t,i} = \frac{A_{s,i}}{\frac{1-(0.5 * f_{ctm})}{(\rho_{s,tot} * f_{sk})}} \qquad \textbf{(3.19)}$$

where:

$A_{s,i}$: The total amount of reinforcement in the slab

$\rho_{s,tot}$:The total reinforcement ratio.

f_{ctm} : The mean tensile strength of concrete , see Table 3.2

f_{sk} : The characterstic yield strength of reinforcement steel.

3.4.4 Effects of creep and shrinkage

3.4.4.1 Creep

Creep in composite members will cause a reduction in the bending stiffness that should be considered using the long-term modular ratio n_L (Vayas & Iliopoulos, 2014).The modular ratio depends on the type of loading that could be permanent, temporary or shrinkage see Section 3.3.1.1.

In statically determined structures, the reduction in stiffness will result in an increased deflection and a stress redistribution in the cross section increasing the stresses in steel girder and decreasing the stresses in concrete see Figure 3.4. Since the concrete is under compression and the bending stiffness is calculated based on the uncracked section, no

change in the internal forces will occur, and the secondary effects due to creep will not be considered.

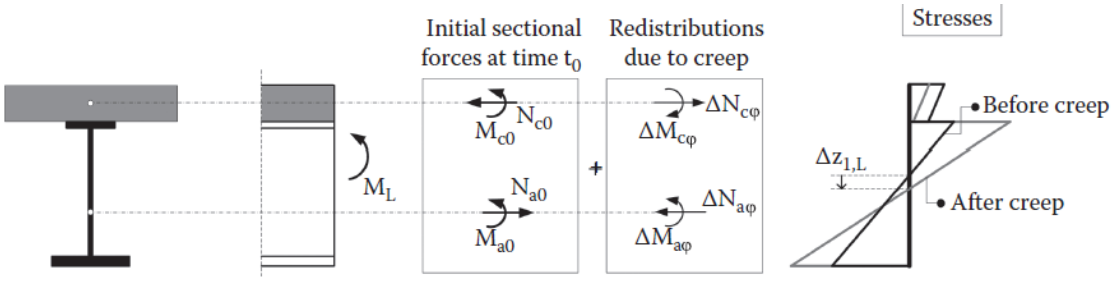

Figure 3.4 The effect of creep on stresses of a composite girder, from (Vayas & Iliopoulos, 2014)

3.4.4.2 Shrinkage

Shrinkage will cause a shortening in the concrete slab. Shear connection with the steel girder will restrain that shortening developing a tension force in the concrete N_{sh}. An equal compression force will act on the composite section and a moment M_{sh} will make the two forces in equilibrium (Vayas & Iliopoulos, 2014), see Figure 3.5

$$N_{sh} = -\varepsilon_{cs} \cdot \frac{n_0}{n_s} \cdot E_{cm} \cdot A_c \qquad \textbf{(3.20)}$$

$$M_{sh} = N_{sh} \cdot \bar{z}_{1,s} \qquad \textbf{(3.21)}$$

Where

n_0 the short-term modular ratio, see Section 3.3.1.1

n_s the long-term modular ratio for shrinkage, section 3.3.1.1.

$\bar{z}_{1,s}$ the gravity centre of the equivalent section calculated with n_s, section 3.4.4.

E_{cm} the concrete's modulus of elasticity.

A_c the sectional area of the concrete slab.

ε_{cs} the shrinkage strain according to section 3.3.1.2.

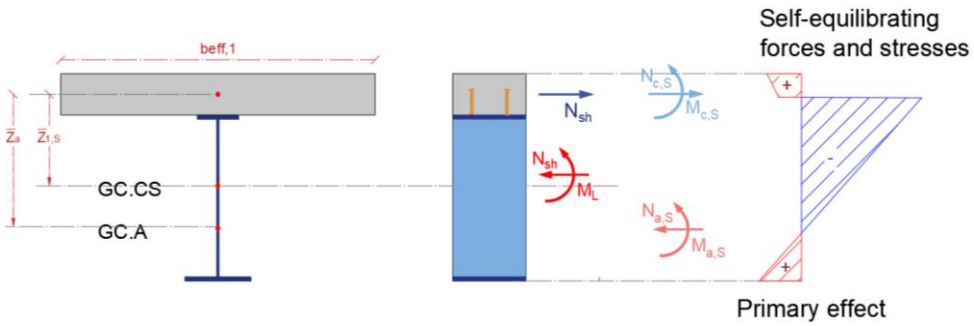

Figure 3.5 Primary effect due to shrinkage, redrawn from (Vayas & Iliopoulos, 2014)

The mentioned forces and the equilibrating moment from the primary effects will result in non-negligible values of stresses and deflections in statically determinate systems (*Vayas and Iliopoulos, 2014*). On the other hand, secondary effects due to shrinkage will not be considered because no change of the internal forces will take place in statically determined structures.

3.5 Design models

3.5.1 Design of shear connections

3.5.1.1 Dimensions of headed studs and detailing of shear connections

There are various types of headed studs that can be used as a full connection between concrete slab and structural steel girders in composite bridges. According to EN1994-2 Section 6.6.5.7, there are a wide number of requirements shall be fulfilled to ensure that the headed studs are appropriate for a specific composite section. Nevertheless, a requirement of a sufficient thickness of top steel flange shall be provided to permit well-proper welding with the studs and smooth transferring of loads from connectors to the plate without local failure or excessive deformation (EN1994-2.6.6.5.7). A typical headed stud is illustrated in the Figure 3.6 where dimensions of the stud are presented according to the standard conditions.

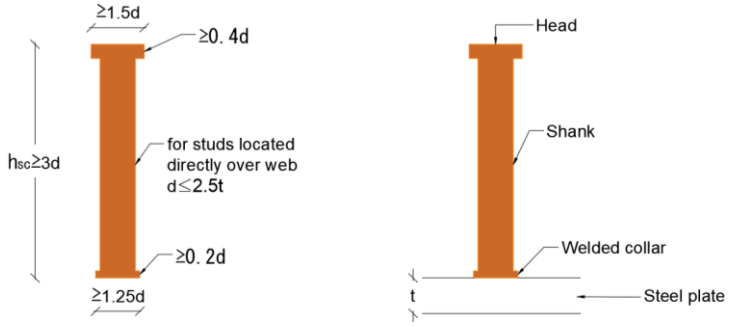

Figure 3.6 Dimensions of headed studs, redrawn from (Vayas & Iliopoulos, 2014)

The arrangement of the spacing between headed studs has demands according to EN-1994-2.6.6.5.5. The spacing between connectors is important to be sufficiently close to ensure the assumed of the stability of concrete slab and structural steel. Therefore, several requirements are presented in Table 3.9 that presents the case of using solid slab. In addition, the connectors can be placed as groups without losing sight of the group spacing is greater than the individual spacing between two connectors, this requires considering some risks in design such as, the non-uniform of longitudinal shear flow, buckling of steel flange and local resistance of the slab to the concentrated forces from connectors (EN 1994-2, 2005), 2.6.6.5.5. (4).

Table 3.9 Detailing of shear connectors from (Vayas & Iliopoulos, 2014)

Condition		Limitations
Spacing in longitudinal direction e_L	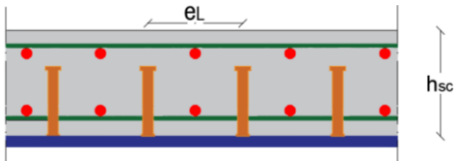	$5d \leq e_L \leq min\{5h_{sc}, 800mm\}$
Spacing in transverse direction e_T and clear distance between edge of studs and edge of flange e_D	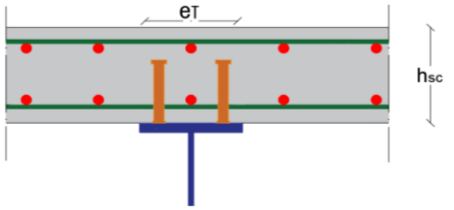	$e_{D\geq 25mm}$ for solid slab $e_T \geq 2.5 * d$
Distance between downside of head and lower transverse slab reinforcements	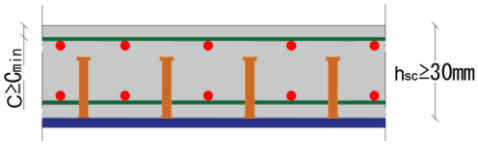	$\geq 30mm$ for flat slabs
Studs on compression flanges would be class 3 or 4 but are classified due to shear connection as 1 or 2	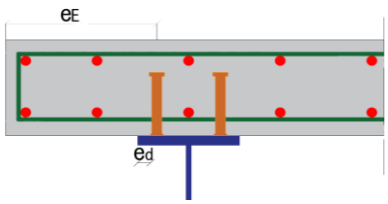	$e_L \leq 22.\varepsilon.t_{ao}$ $e_D \leq 9.\varepsilon.t_{ao}$ For solid slab
Preventing of longitudinal splitting of concrete in edge girders. If the distance of the edge of the concrete flange and the nearest row of shear connectors $e_E \leq 300mm$	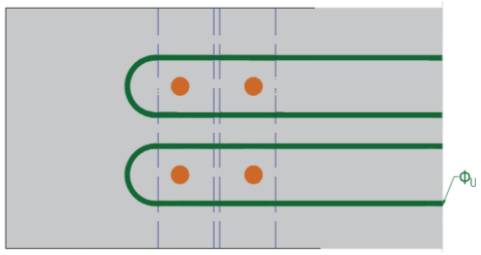	Additional U-bars passing around shear connectors of the edge girders should be provided. $e_E \geq 6 * d$ $\emptyset_U \geq 0.5 * d$

3.5.1.2 Shear resistance of headed studs

According to (EN 1994-2, 2005), the resistance of headed stud can be obtained as the minimum value from equations **(3.22)** and **(3.23)**. Equation **(3.22)**correspond to the shear failure at stud shank toe ($P_{Rd,1}$) and equation **(3.23)** determines the shear resistance from the crushing of concrete around the shank.

$$P_{Rd} = \frac{0.8\, f_u \pi \frac{d^2}{4}}{\gamma_V} \qquad \textbf{(3.22)}$$

Or

$$P_{Rd} = \frac{0.29\ \alpha\ d^2\sqrt{f_{ck}\ E_{cm}}}{\gamma_V} \qquad \textbf{(3.23)}$$

With:

$$\alpha = 0.2\left(\frac{h_{sc}}{d} + 1\right) \quad \text{for } 3 \le \frac{h_{sc}}{d} \le 4 \qquad \textbf{(3.24)}$$

$$\alpha = 1 \qquad \text{for } \frac{h_{sc}}{d} > 4 \qquad \textbf{(3.25)}$$

Where:

γ_V : The partial safety factor that has a recommended value of 1.25.

d : The diameter of the shank of the stud, $16mm \le d \le 25\ mm$.

f_u : The specified ultimate tensile strength of the material of the stud but greater than 500 N/mm^2.

f_{ck} : The characteristic cylinder compressive strength of the concrete at the age considered of density not less than 1750 kg/m^3.

h_{sc} : The overall nominal height of the s

To face any possible inelastic redistribution of shear, the shear connectors shall have sufficient deformation capacity. In addition, the shear connectors with sufficient deformation capacity are considered as ductile type if the characteristic slip capacity δ_{uk} greater than 6mm (EN 1994-1-1, 2005), Annex E where the ductility of connectors is important to justify the assumed plastic behavior of shear connectors.

3.5.1.3 Design of headed studs against longitudinal shear

The shear connectors shall be able to transmit the longitudinal shear at the interface between concrete slab and structural steel according to EN1994-2, 6.6.1.1. The longitudinal shear develops from the vertical shear forces. The horizontal shear flow for elastic behavior can be determined from the equation **(3.26)**.

$$V_{L,ED} = \frac{V_{ED} \cdot S}{I} \qquad \textbf{(3.26)}$$

Where

V_{ED} is the design vertical shear force

$S = S_{1,L}$ is the first moment of inertia of the concrete slab in respect to the centre of gravidity of the composite section for the considered time and load case section 3.4.3.

$I = I_{1,L}$ is the second moment of area of the composite cross section for the considered time and load case section 3.4.3.

Equation **(3.26)** shows that the longitudinal shear follows the vertical shear forces. However, for load combination, the longitudinal shear should be calculated separately

for each load case and then combined since the cross-sectional constants used in equation **(3.26)** are different for the various load cases (Vayas & Iliopoulos, 2014).

The direction of the longitudinal shear is associated with sign of vertical shear as shown in Figure 3.7. That should be considered in the combination of actions in a way that the longitudinal shears in the same directions will be added and in different directions will be subtracted (Vayas & Iliopoulos, 2014).

The longitudinal shear resistance provided by headed studs at ULS and SLS are given with equation **(3.27)** and **(3.28)**.

$$V_{L,Rd} = \frac{P_{Rd} \cdot n}{e_L} \qquad \textbf{(3.27)}$$

and

$$V_{L,Rd,ser} = \frac{P_{Rd,ser} \cdot n}{e_L} \qquad \textbf{(3.28)}$$

Where
P_{Rd} : the shear resistance at ULS.
$P_{Rd,ser}$ The shear resistance at SLS.
n : The number of shear connectors at one cross section.
e_L: The longitudinal spacing of connectors.

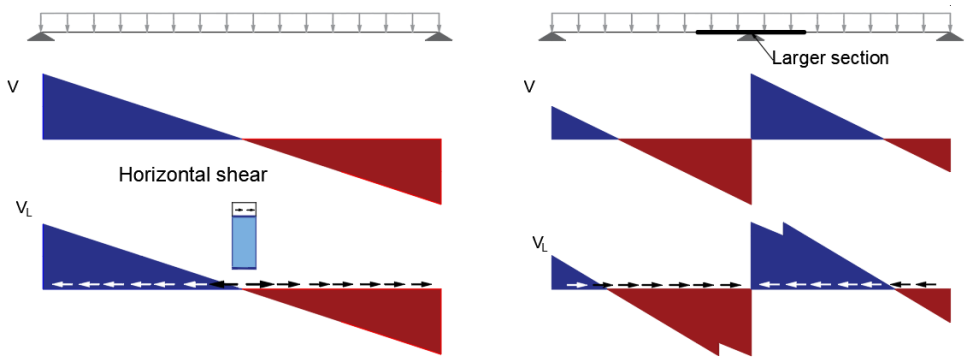

Figure 3.7 Shear forces and horizontal shear, redrawn from (Vayas & Iliopoulos, 2014)

As illustrated in Figure 3.8, the diagram of longitudinal shear $V_{L,Ed}$ should be covered by an appropriate shear resistance $V_{L,Rd}$ by choosing the size of shear connectors, the number of shear connectors in the cross section, and the longitudinal spacing of the shear connectors. Those parameters are usually kept constants over a certain distance to achieve a constant shear resistance over the mentioned distance. The design shear $V_{L,Ed}$ could exceed the shear resistance $V_{L,Rd}$ by 10% at a specific point, but the total resistance force should be larger than the design force (Vayas & Iliopoulos, 2014).

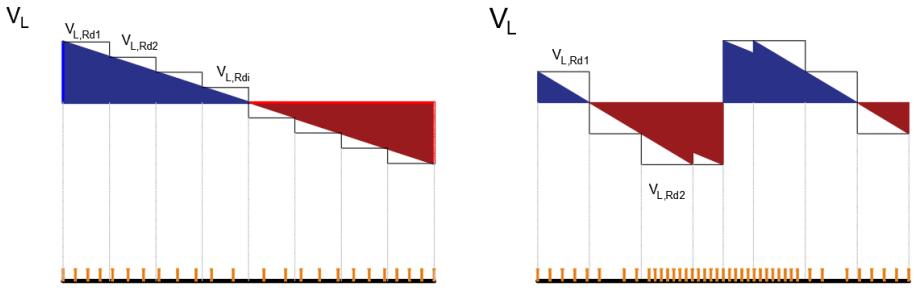

Figure 3.8 Cover of the diagram of longitudinal shear along the bridge, redrawn from (Vayas & Iliopoulos, 2014)

The longitudinal shear for an inelastic behavior is possible at ULS for class section 1 or 2 when it's possible to make use of the plastic bending resistance. The design longitudinal shear $V_{L,Ed}$ will be determined from the difference of the design axial forces on the slab at adjacent cross section, see Figure 3.9.

$$V_{L,Ed} = \frac{\Delta N_{c,Ed}}{\Delta x} \qquad \textbf{(3.29)}$$

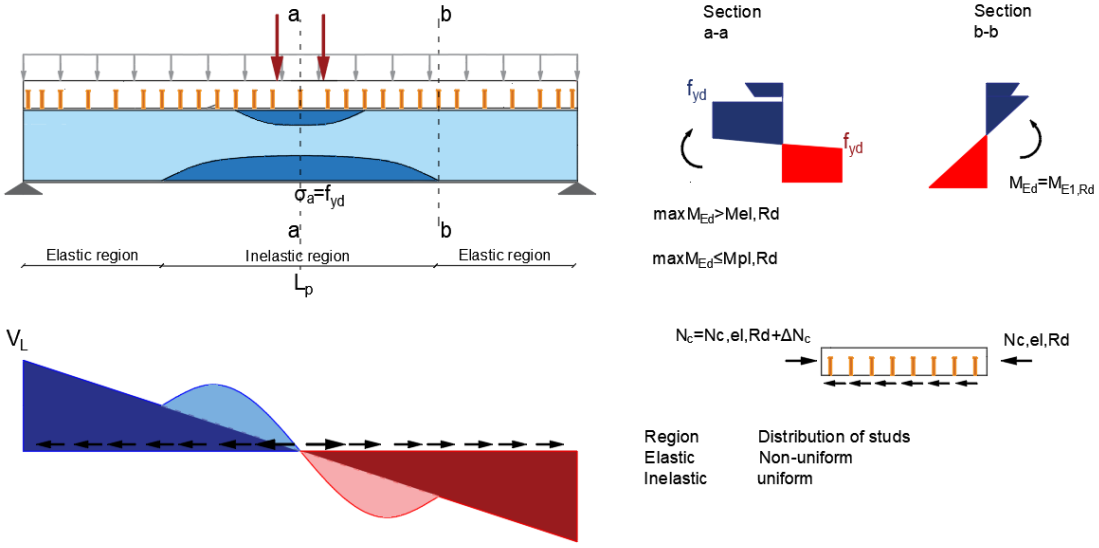

Figure 3.9 longitudinal shear in inelastic region, redrawn from (Vayas & Iliopoulos, 2014)

Longitudinal shear develops due to concentrated longitudinal forces for instance primary effects of shrinkage N_{cs}. As shown in Figure 3.10, the longitudinal shear develops at the ends of the bridge when the force N_{cs} is transferred to the beam by shear connectors over a length equal to $b_{eff,0}$. The longitudinal shear is given by Equation **(3.30)**.

$$V_{L,Ed,max} = \frac{2 \cdot N_{c,s}}{b_{eff,0}} \qquad (3.30)$$

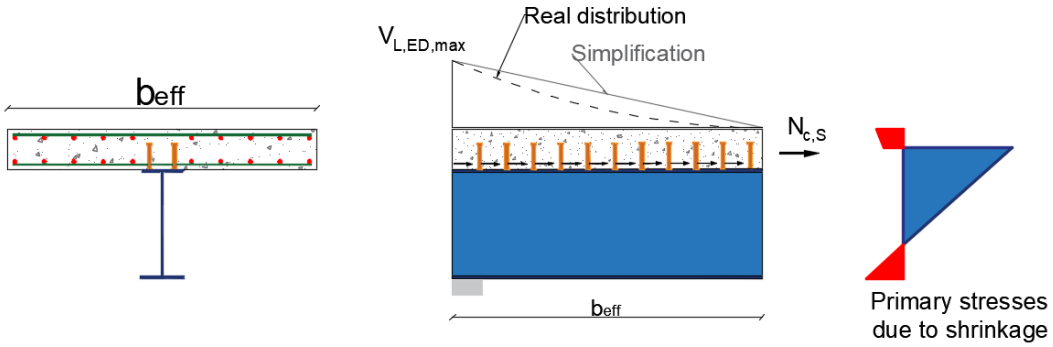

Figure 3.10 Distribution of end shear due to shrinkage at an edge support, redrawn from (Vayas & Iliopoulos, 2014)

3.5.1.4 Design of concrete slab against longitudinal shear

The longitudinal shear at the steel-concrete interface will be transferred from the concrete slab to the shear connectors and then to the structural steel. A sufficient transverse reinforcement is important to allow this transfer and to prevent shear failure or longitudinal splitting. Finally, the shear will be transferred by a struts and ties as illustrated in Figure 3.11.

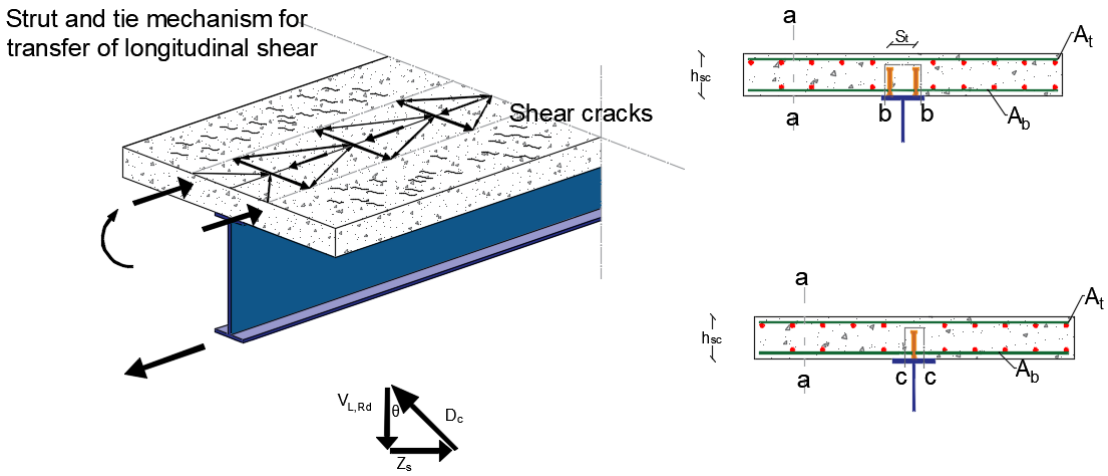

Figure 3.11 Failure mechanism and typical sections for checking shear failure, redrawn from (Vayas & Iliopoulos, 2014)

Those ties and struts need to be checked at ULS at different sections with the possibility of shear failure as shown in Figure 3.12.

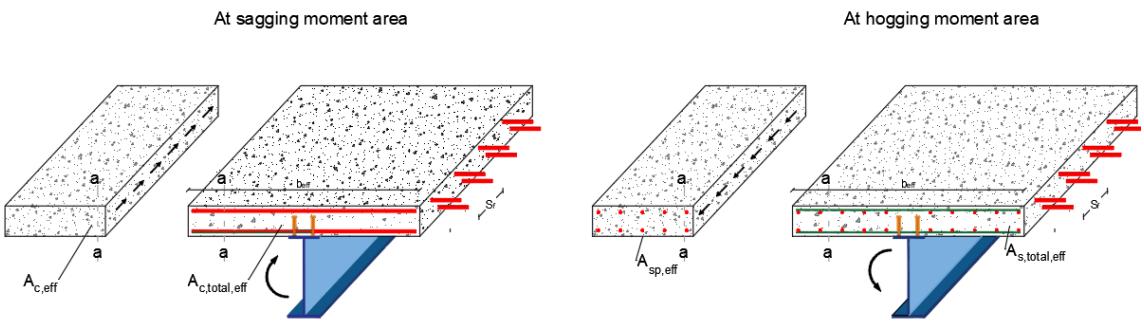

Figure 3.12 Design shear flow at section a-a, redrawn from (Vayas & Iliopoulos, 2014)

The design shear flow for various sections can be determined from Equation **(3.31)** and **(3.32)**.

For sagging bending:

$$V_{Lc,Ed} = V_{L,Ed}\frac{A_{cp,eff}}{A_{c,tot,eff}} \qquad \textbf{(3.31)}$$

For hogging bending, the crushing resistance of the struts can be obtained from Equation **(3.32)**.

$$V_{C,Rd} = v \cdot f_{cd} \cdot L_v \cdot sin\theta \cdot cos\theta = v \cdot f_{cd} \cdot L_v \cdot \frac{1}{cot\theta + cot\theta^{-1}} \qquad \textbf{(3.32)}$$

Where:

$$v = 0.6 \cdot \left(1 - \frac{f_{ck}\,MPa}{250}\right) \qquad \textbf{(3.33)}$$

The shear resistance of the ties is obtained from Equation **(3.34)**.

$$V_{s,Rd} = \frac{A_{sf}}{s_f} \cdot f_{sd} \cdot cot\theta \qquad \textbf{(3.34)}$$

Where

$\frac{A_{sf}}{s_f}$ is the area of transverse reinforcement divided by spacing as listed in Table 3.10.

Table 3.10: ratios of $\frac{A_{sf}}{s_f}$ from (Vayas & Iliopoulos, 2014)

Type of section for shear failure	a-a	b-b	c-c	d-d
$\frac{A_{sf}}{s_f}$	$A_b + A_t$	$2A_b$	$2A_b$	$2A_{bh}$

Where:
A_b: area of bottom transverse reinforcement.A_t: area of top transverse reinforcement.
A_{bh}: area of bottom transverse haunch reinforcement.

The minimum transverse reinforcement ratio is given by Equation **(3.35)**.

$$\min \frac{A_{sf}}{s_f \cdot h_c} = \frac{0.08 \cdot \sqrt{f_{ck}}}{f_{sk}} \qquad \textit{(3.35)}$$

3.5.2 Bending Capacity

According to (EN 1994-2, 2005), the design bending resistance shall be determined by rigid-plastic theory when the effective composite cross-section is in Class 1 or Class 2. Furthermore, elastic bending resistance of a composite cross section should be used if the cross section is in Class 3 or Class 4. However, elastic analysis and non-linear theory can be used to determine bending resistance to cross section of any class. The three methods are reviewed in this section.

3.5.2.1 Plastic Bending Capacity

In the case of using Class 1 or 2 for an effective composite cross-section, the moment due to the applied loads shall be checked by comparing them with the design bending resistance that is determined based on the rigid-plastic theory (EN1994-2.6.2.1).

To determine plastic bending resistance of a composite cross-section considering the plastic theory, full interaction between structural steel, reinforcement steel and concrete shall be assumed. In addition, the stresses in both structural steel and reinforcement steel are assumed to reach to their design yield strength f_{yd} and f_{sd} respectively in tension or compression. The contribution of reinforcement can be neglected in sagging areas. Meanwhile, the compressive stress in the effective area of concrete flange is taken as 0.85 of the design cylinder compressive strength f_{cd} of the concrete (EN1994-2.6.2.2).

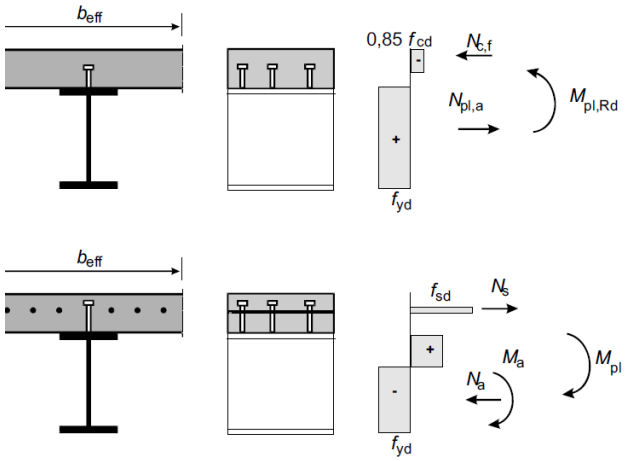

Figure 3.13 Examples of plastic stress distribution for a composite beam with a solid slab and full shear connection in sagging and hogging bending, from (EN 1994-2, 2005)

In hogging moment area where the concrete is exposed to tension stresses, the concrete has not contribution to resist bending moment. Thereby, the composite cross-section will consider the contribution from the reinforcement and the steel girders. Therefore, there is a condition of minimum ratio of reinforcement in the effective area of concrete flange that shall be determined from equation **(3.36)***:*

$$\rho_s = \frac{A_s}{A_c} \geq min\rho_s = \delta \frac{f_y}{235} . \frac{f_{ctm}}{f_{sk}} . \sqrt{k_c} \qquad \textbf{(3.36)}$$

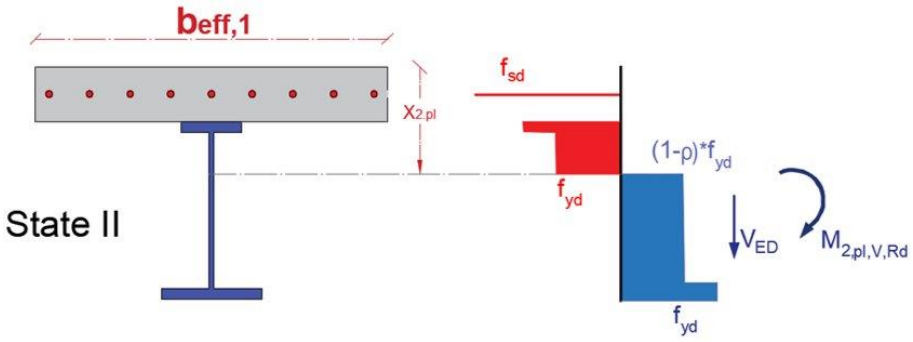

Figure 3.14 Minimum reinforcement ratio in hogging moment area, redrawn from (Vayas & Iliopoulos, 2014)

Where:

δ : equal 1.0 or 1.1 for cross sectional Class 1 or 2 correspondingly.

k_c : a coefficient equal 1.0 conservatively.

f_{sk} : The characterstic yield strength of reinforcement steel.

f_y : The yield strength of structural steel.

f_{ctm} : The mean tensile strength of concrete.
A_s : The area of tension reinforcement of ductility class B or C.
A_c : The area of the concrete flange within the effective width b_{eff}.

To prevent crushing of concrete, if the distance between plastic neutral axis and the extreme fibre of the concrete slab x_{pl} is greater than 0.15 of overall depth h of the composite cross-section, the design moment resistance $M_{pl,Rd}$ shall be reduced by factor β. The value of β shall be obtained from graph in Figure 3.15. Nevertheless, if the ratio of $\frac{x_{pl}}{h}$ is greater than 0.4 the bending resistance of moment shall be determined by non-linear method that considers the stress-strain relation of the materials as in (EN1994-2.6.2.1.4) or as elastic resistance from elastic method (EN1994-2.6.2.1.5). This reduction of design moment occurs when using of high strength steels S420 or S460 where the strain limitation of concrete is smaller than the strain limitations of structural steel and reinforcing steel of ductility classes B and C. Thereby, there is a risk that the concrete flange excess its ultimate strain while steels components have sufficient higher ultimate strain.

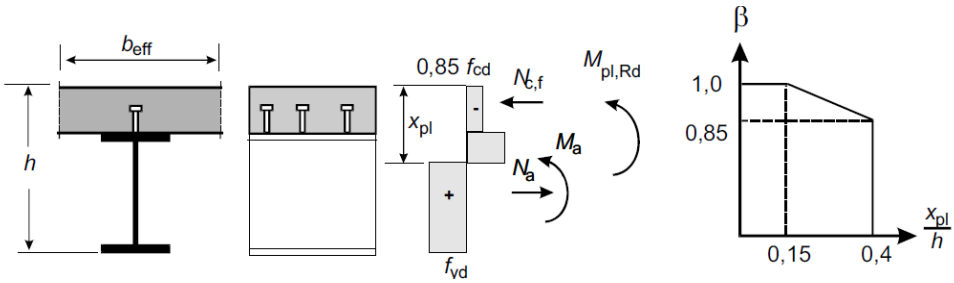

Figure 3.15 Reduction factor β for $M_{pl,Rd}$, from (EN 1994-2, 2005)

In the case when the acting design shear is greater than half of the shear resistance (EN 1993.1.5, 5.1) for carbon steel, (1993.1.4 for stainless steel) and (1993.1.5 Appendix D corrugated), a part of structural steel resistance can be of use to resist the shear forces. Thus, the design strength of structural steel shall be reduced accordance to equation **(3.37)** (Vayas & Iliopoulos, 2014).

$$f_{y,red} = (1 - \rho).f_{yd} \qquad \textbf{(3.37)}$$

Where
f_{yd} : The design strength of steel.

$$\rho = \left(\frac{2.V_{Ed}}{V_{Rd}} - 1\right)^2 \qquad \textbf{(3.38)}$$

V_{Ed} : The design shear force of the relevant wall resulting from vertical shear and torsion

V_{Rd} : The design shear of the wall, either the plastic resistance $V_{pl,Rd}$ or shear buckling resistance $V_{bw,Rd}$

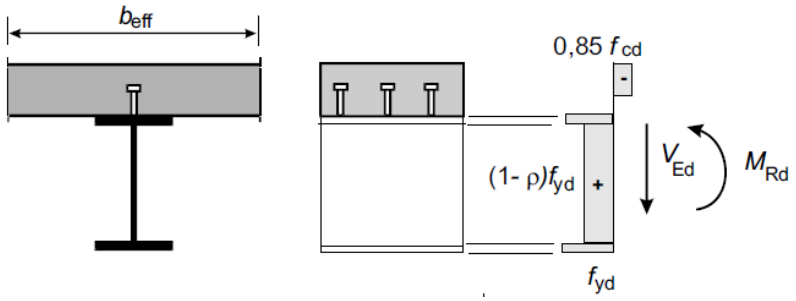

Figure 3.16 Plastic stress distribution allowing for the interaction with shear, from (EN 1994-2, 2005)

In global analysis for a continuous composite bridge, some inelastic rotation with moment redistribution in the internal support regions are required to develop the plastic moment resistance in the mid-span regions in cross-section Class 1 or 2. The bending moment from the elastic global analysis cannot overreach 90% of the plastic bending resistance in cross-section Class 1 or 2 if the cross-section in the internal support regions is classified as Class 3 or 4, and if the ratio of lengths between spans (shorter/longer) is less than 0.6. In fact, unequal lengths require higher plastic rotation and larger moment redistribution. Otherwise, the global analysis of inelastic behavior shall be exploited where the inelastic resistance in support regions in Class 3 or 4 is limited (EN1994-2.6.2.1.3). The limitations of moment resistance for a continuous beam are illustrated in Figure 3.17.

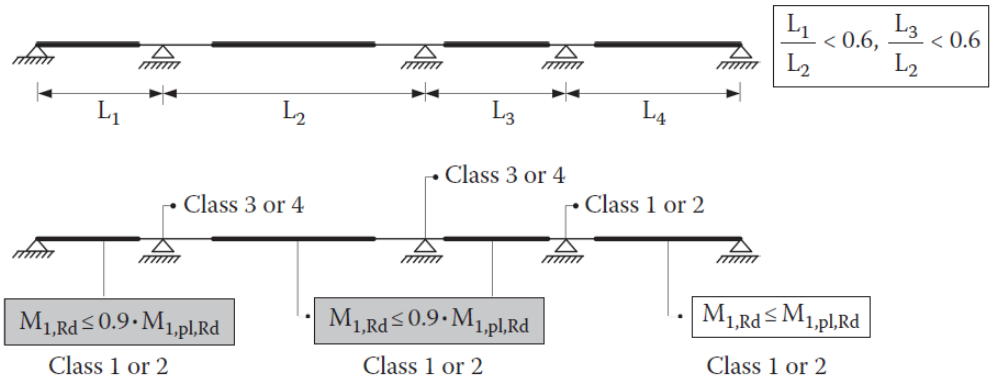

Figure 3.17 Moment resistance limitation for spans of continuous beams, from (Vayas & Iliopoulos, 2014)

Table 3.11:Verifications of class 1 or 2 cross sections for bending moment and shear from (Vayas & Iliopoulos, 2014)

Field of application	Shear	Bending moment
Spans of simple or continuous beams in general	$V_{Ed} \leq 0.5V_{Rd}$ $V_{Ed} > 0.5V_{Rd}$	$M_{Ed} \leq \beta * M_{1,pl,Rd}$ $M_{Ed} \leq \beta * M_{1,pl,V,Rd}$
Internal supports of continuous beams	$V_{Ed} \leq 0.5V_{Rd}$ $V_{Ed} > 0.5V_{Rd}$	$M_{Ed} \leq \beta * M_{2,pl,Rd}$ $M_{Ed} \leq \beta * M_{2,pl,V,Rd}$
Spans of continuous beams with cross sections at adjacent supports class 3 or 4 and ratios of adjacent spans$\leq$ 0.6	$V_{Ed} \leq 0.5V_{Rd}$ $V_{Ed} > 0.5V_{Rd}$	$M_{Ed} \leq 0.9 * \beta * M_{1,pl,Rd}$ $M_{Ed} \leq 0.9 * \beta * M_{1,pl,V,Rd}$

Where:
V_{Ed}: is the plastic resistance or the shear buckling resistance
$M_{1,pl,Rd}$ and $M_{2,pl,Rd}$: are the plastic moments for sagging and hogging bending
$M_{1,pl,V,Rd}$ and $M_{2,pl,V,Rd}$: are the reduced plastic moments for sagging and hogging due to shear.

The web will not contribute for corrugated

3.5.2.2 Non-Linear Resistance to Bending

The non-linear theory could be used to determine the bending resistance for composite cross section of any class (EN 1994-2, 2005).The composite cross section is supposed to keep plane and the strain in bonded reinforcement is deemed to be the same as the mean strain in the surrounding concrete both in tension and compression (EN 1994-2, 2005), 6.2.1.4. Stress-strain relation shall be considered. The stress in the concrete and the reinforcement are obtained from stress-strain curves in (EN 1992-1-1, 2005), 3.1.7 and (EN 1992-1-1, 2005), 3.2.7 respectively. For the structural steel, the bi-linear diagram in (EN 1993-1-1, 2005), 5.4.3(4) should be used.

For composite cross-sections class 1 or class 2 with the concrete flange in compression, the non-linear bending resistance to bending M_{Rd} is given as a function of the compressive force in the concrete N_c by the following simplified equations as illustrated in Figure 3.18.

$$M_{Rd} = M_{a,Ed} + \left(M_{el,Rd} - M_{a,Ed}\right) \cdot \frac{N_c}{N_{c,el}} \qquad for \;\; N_c \leq N_{c,el} \qquad \textbf{(3.39)}$$

$$M_{Rd} = M_{el,rd} + \left(M_{pl,Rd} - M_{el,Rd}\right) \cdot \frac{N_c - N_{c,el}}{N_{c,el} - N_{c,el}} for N_{c,el} \leq N_c \leq N_{c,f} \quad \textbf{(3.40)}$$

With:

$$M_{el,rd} = M_{a,Ed} + k \cdot M_{c,Ed} \quad \textbf{(3.41)}$$

Where:
$M_{a,Ed}$ is the design bending moment applied to the structural steel before composite behaviour.
$M_{c,Ed}$ is the part of the design bending moment acting on the composite section.
k : the lowest factor that a stress limit in (EN 1994-2, 6.2.1.5(2)) is reached.
$N_{c,el}$ is the compressive force in the concrete flange associated with $M_{el,Rd}$.

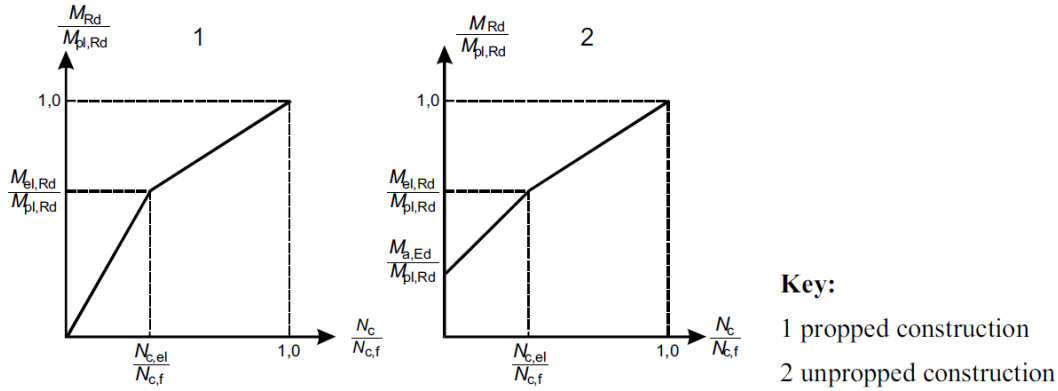

Figure 3.18 Simplified relationship between M_{RD} and N_c for sections with concrete slab in compression, from (EN 1994-2, 2005)

3.5.2.3 Elastic Bending Capacity

To determine the composite cross-section bending resistance, stresses should be calculated using the elastic theory. The effective width of concrete flange shall be determined accordance to section-3.4.1. The effective cross-section is calculated accordance to (EN1993-1-5.4.3) for cross-section in Class 4 and 1993.1.4 for stainless steel. The elastic bending resistance is calculated based on the limiting stresses as mentioned in (EN 1994-2, 6.2.1.5(2)).

Stresses acting on structural steels at the construction phase shall be considered and added to stresses due to actions on the composite member. The effect of creep shall be considered in term of usage of the modular ratio of concrete. The primary effects of shrinkage should be considered for the concrete in sagging bending areas and neglected for concrete in hogging areas. However, secondary effects of creep and shrinkage are neglected for the case of simply supported beams.

Stresses shall be verified to load combination for short-term and long-term loading. Where the short-term design indicates to the early age of the bridge, it's based on the modular ratio of concrete n_0. Consequently, the primary effects of creep and shrinkage can be neglected at that stage. Bending moments acting on the composite cross-section with short-term properties can be combined and stresses acting on structural steels at the construction phase shall be added. Stresses will be combined and compared with the limits. The short-term design is important for stresses in concrete. The combination of stresses acting on a composite cross-section that are included in elastic bending capacity are summarized in Figure 3.19.

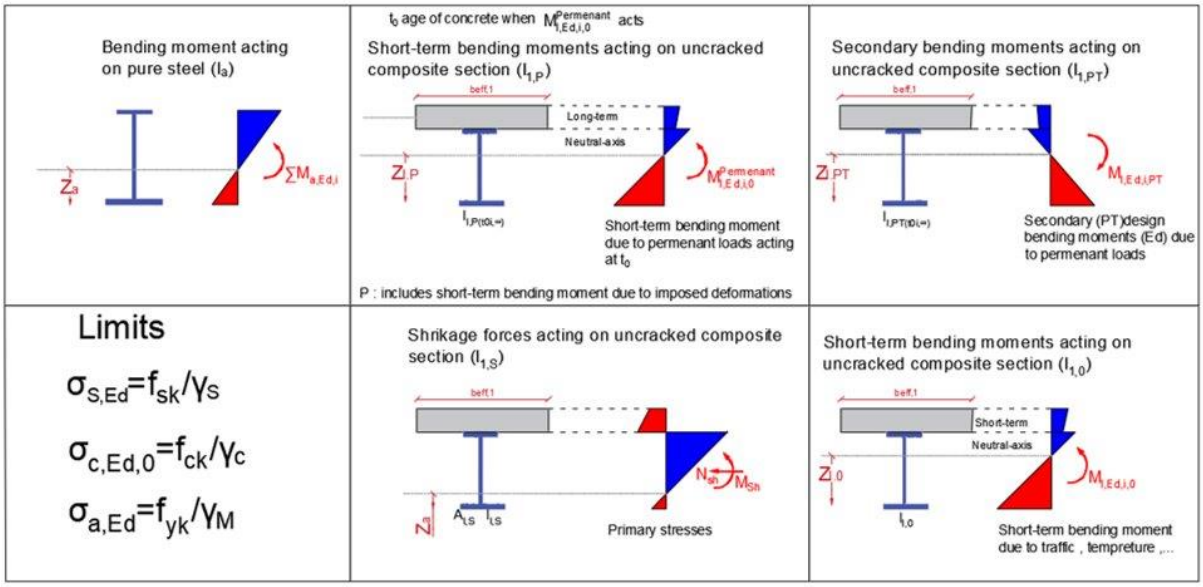

Figure 3.19 Stress distribution for cross section in Class 3 considering loading history, redrawn from (Vayas & Iliopoulos, 2014)

3.5.2.4 Lateral torsional buckling

A steel flange that is attached to a concrete slab by shear connection may be assumed to be laterally stable. However, all other steel flanges in compression "indeterminate structure" should be checked for lateral stability (EN 1994-2, 2005). In addition, general methods for checking lateral stability are provided by Eurocode 3. Consequently, Applicable to the steel section on the basis of the cross-sectional forces on the composite section, taking into account effect of sequence of construction the lateral and elastic torsional restraint at the level of the shear connection to the concrete slab may be taken into account by reducing the moment resistance with χ_{LT} where values for χ_{LT} can be obtained from (EN 1993-1-1, 2005).

At the level of the top steel flange, a rotational stiffness k_s per unit length of the steel beam may be adopted to represent the U-frame model as illustrated in Figure 3.20.

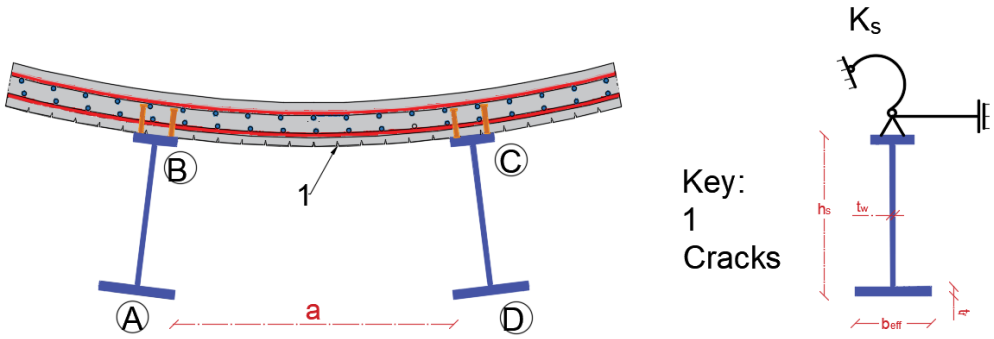

Figure 3.20 U-frame model from EN-1994-2(2005)

$$k_s = \frac{k_1 \cdot k_2}{k_1 + k_2}$$

Where:
k_1: The flexural stiffness of the cracked concrete slab in the direction transverse to the steel beam. It can be taken as:

$$k_1 = \alpha \cdot E_a \cdot I_2 / a$$

a: The spacing between the parallel beams.
$E_a \cdot I_2$: The cracked flexural stiffness per unit length (EN 1994-2, 2005), 1.5.2.12.
k_1: The flexural stiffness of the steel web, to be taken as:

$$k_2 = \frac{E_a \cdot t_w^3}{4 \cdot (1 - v_a^2) \cdot h_s}$$

Where $v_a$is Poisson's ratio for steel and $h_s$and $t_w$are defined in Figure 3.20.

4 State of the art

The concept of composite bridges with stainless steel corrugated I-girders has been noteworthy because of its economic and environmental advantages. The important references related to the effect of using corrugated webs and stainless steel on the flexural capacity of the composite bridges will be reviewed in this section.

4.1 Corrugated I-girders bridges

I-girders with the corrugated web have higher shear buckling strength than that in flat web girders (Jun , Yuqing, Airong , & Teruhiko, 2012).Therefore, smaller web thicknesses can be used, and the material needed is reduced (Henrysson & Yman , 2020).

The flexural behavior of corrugated web girders is different from that of flat web girders. Figure 4.1 shows the longitudinal stress distribution in a corrugated profile obtained from an analytical model. It can be noted that stress intensity in the longitudinal folds is much higher than stress distribution in the inclined folds. Consequently, stress extension is much higher in corrugated profiles compared with in-plane webs due to the lower axial stiffness of the corrugated profile which is usually called the accordion effect of the corrugated web (Inaam & Upadhyay , 2022).The accordion effect allows corrugated webs to stretch or contract easily.

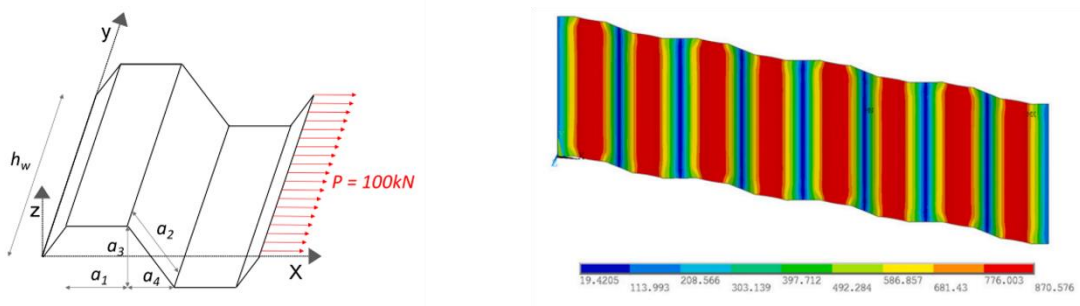

Figure 4.1 Axial load and stress intensity of a corrugated profile (Inaam. Q and Upadhyay. A,2022)

(ELgaaly & Seshadri, 1997) conducted an experimental study to verify the flexural capacity of corrugated web beams and suggested that the ultimate moment capacity can be obtained with the yield stress of the flanges ignoring any contribution from the web.

(Elammary, Saddek, & Alwetaishi, 2017) conducted an experimental, analytical, and numerical study to define the flexural capacity of conventional steel I beam, and I beam with corrugated webs. The study concluded that the flexural capacity of a steel beam with the corrugated web is less than that for the conventional steel I beam in a range between 10 to 20%**.** The study was extended to include the flexural capacity of two steel-concrete composite beams with corrugated webs. The results of the test were listed in the Table 4.1. The failure mode of the two specimens is a flexural failure with a ductile behavior as stated in the table.

Table 4.1 Test results of composite concrete-steel beams, from (Elammary, Saddek, & Alwetaishi, 2017)

Beam No	f_{cu} N/mm^2	P_{cr} kN	P_u kN	P_u/P_{cr}	M_U kN.m	Mode of failure
B1	27.5	62	170	2.12	89.25	Flex Comp ductile
B2	27.5	60	170	2.12	89.25	Flex Comp ductile

The load-displacement relation of the two beams is illustrated in the Figure 4.2. The results were compared with the nominal design moment capacity that found to be equal to 84.3 kN ∗ m. This value is 95% form the maximum moment that the beam resisted. The study conducted that the flexural capacity of composite beams could be decreased by 10 to 20% in case of using the corrugated web instead of the flat web.

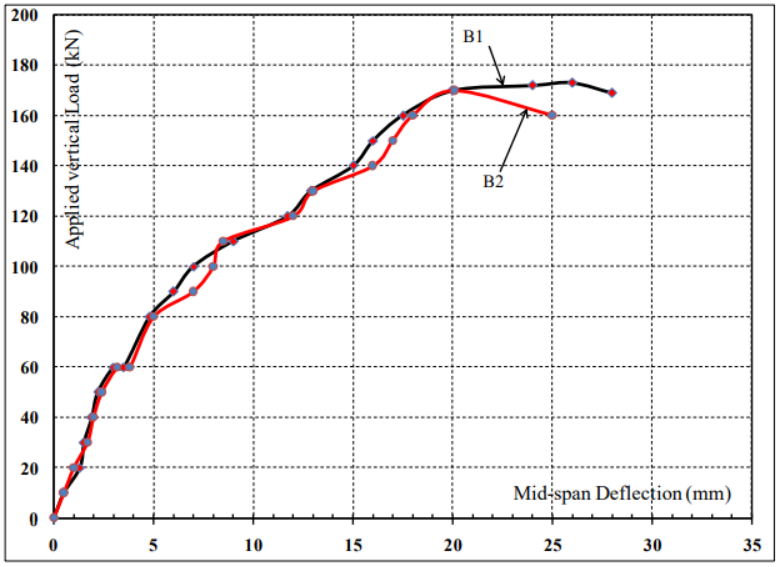

Figure 4.2 Load-mid-span deflection curve for B1 and B2, from (Elammary, Saddek, & Alwetaishi, 2017)

(Inaam & Upadhyay , 2022) conducted a numerical parametric study to evaluate the accordion effect in bridge girders with corrugated webs. The Figure 4.3 shows the longitudinal stress distribution in a corrugated profile. The longitudinal folds resist longitudinal stresses, and the inclined folds create discrete discontinuities. Since the inclined fold varies by changing corrugation angle and fold width, the accordion effect has a high sensitivity to geometrical parameters.

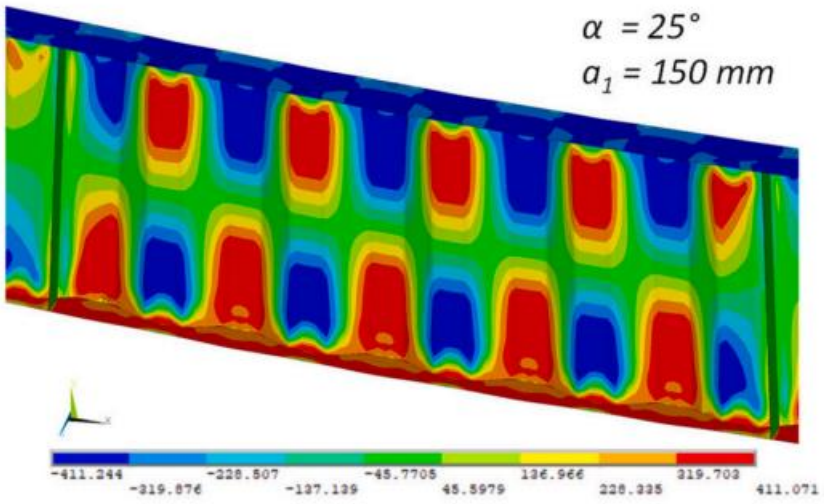

Figure 4.3 Longitudinal stress distribution for a corrugated profile, from (Inaam & Upadhyay , 2022)

A minimum web contribution of 10%,20% or 30% can be used for the determination of bending resistance if the conditions of the three key parameters listed in Table 4.2 are satisfied (Inaam & Upadhyay , 2022).

Table 4.2 Conditions required for web utilization, from (Inaam & Upadhyay , 2022)

$\frac{t_{w,eff}}{t_w}$	$\frac{h_w}{t_w}$	$R = \frac{(a_1 + a_4)}{(a_1 + 2a_4)b_f}$	$O = \frac{b_f + a_3}{b_f - a_3}$
0.1	≤ 150	< 0.18	≤ 1.6
0.2	≤ 125	< 0.13	≤ 1.2
0.3	≤ 90	< 0.09	≤ 1.1

Dense corrugation has more axial stiffness than coarse corrugation. Compact webs have a better ability to contribute to the flexural capacity. Using unequal corrugation folds (a1>a2) results in higher web participation.

4.2 Stainless steel

Stainless steel has very good corrosion and fire resistance, high strength, and ductility as well as improved durability (Zhou, o.a., 2021). It does not require coatings to be applied. Therefore, it has a lower life cycle cost compared with carbon steel (Shammas & Cashell, 2019).Therefore, stainless steel attracted researchers.

(EN 1993-1-4, 2020), use the concept of cross-section classification to treat local buckling in order to determine the bending resistance of stainless-steel elements.

However, the concept of cross-section classification used in Eurocode is suitable for materials with the stress-strain response with an idealized elastic-perfectly plastic model which is not the case for stainless steel (Afshan & Gardner, 2013).

Stainless steel has a non-linear stress-strain relation from an early stage and a remarkable strain hardening prior to failure as shown in Figure 4.4 (Shammas & Cashell, 2019)

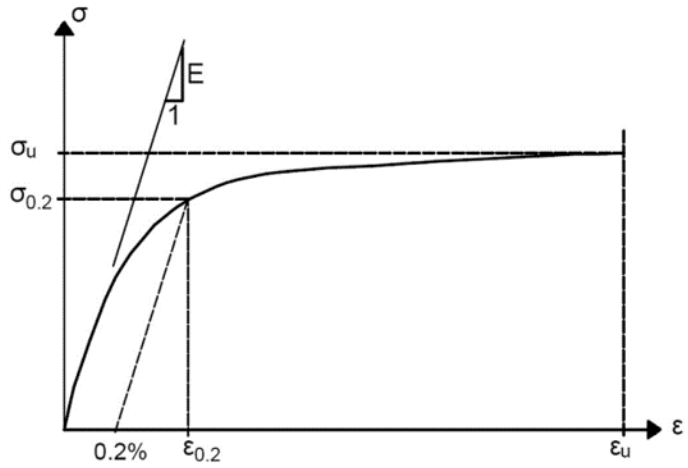

Figure 4.4 Stress-strain relation for stainless steel, from (Shammas & Cashell, 2019)

The results from 65 bending test of stainless-steel beams were compared. The ultimate bending resistance M_u from the test is normalized with M_{pl} and plotted against the cross-section slenderness (Afshan & Gardner, 2013) as shown in Figure 4.5.

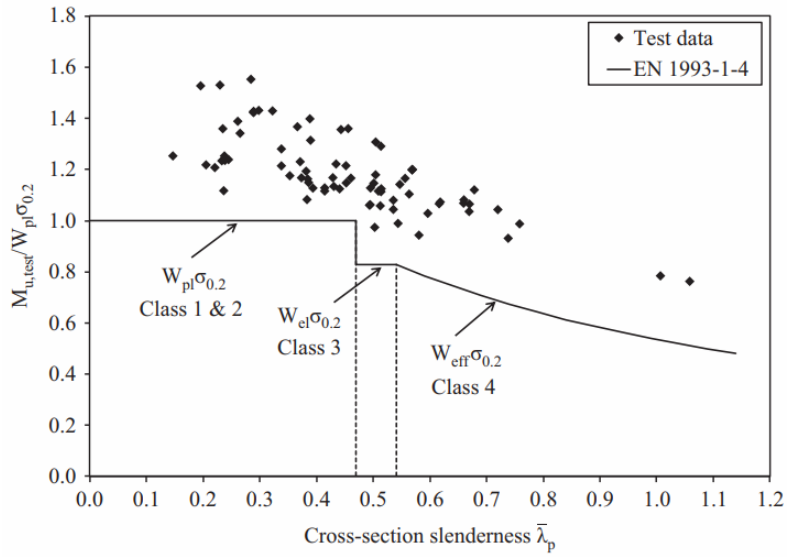

Figure 4.5 comparison of 65 beam test results with EN1993-4-1 provisions, from (Afshan & Gardner, 2013)

This comparison shows the relationship between cross-section slenderness and the increase of the bending resistance due to strain hardening. The slenderest is the cross section, the more considerable is the increase of the bending capacity due to strain hardening. This increase is related to the increase of cross-section deformation capacity (Afshan & Gardner, 2013).

(Afshan & Gardner, 2013) proposed a new design method called the continues strength method (CSM) to predict the effect of strain hardening. The CSM replaces the concept of cross-section classification with a non-dimensional measure of cross-section deformation capacity.

(EN 1993-1-4, 2020) Annex B presents the continues strength method that consider strain hardening effect to calculate the resistance of stainless-steel elements. The linear hardening material model introduced by Eurocode is illustrated in Figure 4.6.

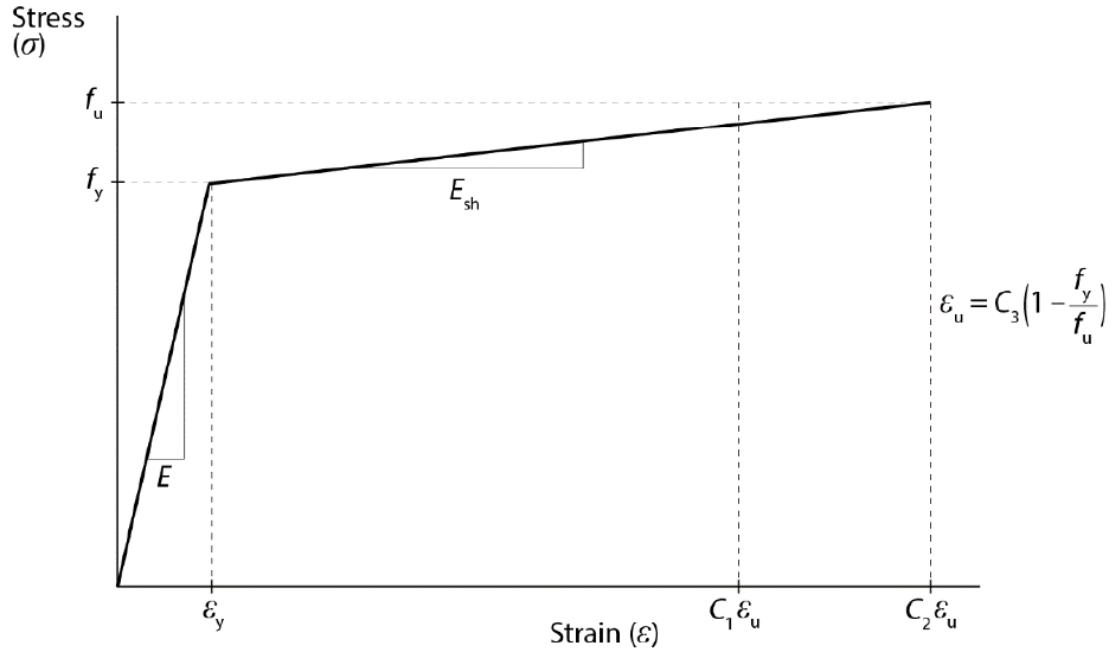

Figure 4.6 CSM bi-linear elastic, linear hardening material model, from (EN 1993-1-4, 2020), Annex(B)

The bending resistance of the steel-concrete composite section is determined according to (EN 1994-2, 2005) by the rigid plastic theory that is reasonable for carbon steel. However, that assumption could be incorrect for stainless steel where strain hardening develops in the lower flange of a ductile cross section before the collapse moment is reached (Shammas & Cashell, 2019).

Eurocode (EN 1994-2, 2005) limits the bending resistance to the plastic bending resistance and uses cross-section classification that is suitable for materials with the stress-strain response with an idealized elastic-perfectly plastic model.

Furthermore, the overall cross-section classification is determined depending on the slenderest element in which neglects the element interaction. However, the interaction

between elements enables a flange of class 2 to reach its plastic capacity even though the web is in class 3.

Then, (Shammas & Cashell, 2019) suggested an analytical solution based on the continuous strength method to estimate the bending resistance of stainless-steel concrete composite beams considering the effect of strain hardening. They presented two models to predict bending resistance, a detailed model and a simplified model.

Figure 4.7 shows the strain distribution through the depth of the cross-section and the corresponding stress distribution obtained by the detailed model.

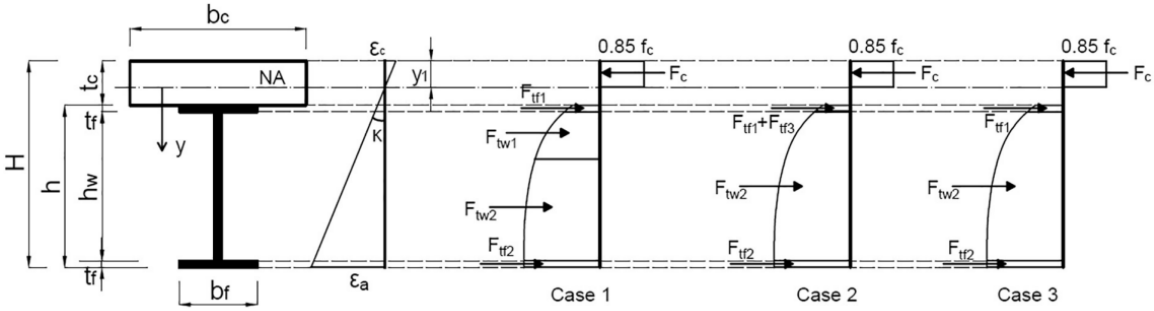

Figure 4.7 The stress- strain distribution diagrams for composite beam with full connection, (Shammas & Cashell, 2019)

There are three possible cases for stress distribution as presented in Figure 4.7. In case 1, the location $y_{0.2}$ where the strain in the stainless-steel section equals yielding strain is within the web of the stainless-steel as described in the expression **(4.1**):

$$y_{0.2} \geq t_c - y_1 + t_f \qquad \textbf{(4.1)}$$

where:
y_1: The depth of compressive area of the concrete slab
t_c : The total thickness of concrete slab
t_f : The thickness of top flange of structural stainless steel

Case 2 corresponds to situation where the mentioned location is within the top steel flange, as described in expression **(4.2)**:

$$t_c - y_1 \leq y_{0.2} \leq t_c + t_f \qquad \textbf{(4.2)}$$

Case 3 is when the location lies within the concrete slab as described in the following expression:

$$0 \leq y_{0.2} \leq t_c - y_1 \qquad \textbf{(4.3)}$$

The internal axial forces and the corresponding moments can be calculated for all cases as presented in Table 4.3.

Table 4.3 Expression for the internal forces and bending moments in the cross-sections for the three cases from (Shammas & Cashell, 2019).

	$Case\ 1$	$Case2$	$Case3$
F_c	$0.85f_c.b_c.y_1$	$0.85f_c.b_c.y_1$	$0.85f_c.b_c.y_1$
M_c	$0.85f_c.b_c.\frac{y_1^2}{2}$	$0.85f_c.b_c.\frac{y_1^2}{2}$	$0.85f_c.b_c.\frac{y_1^2}{2}$
F_{tf1}	$\int t_c - y_1{}^{t_c-y_1} + t_f b_f \sigma_{1(\varepsilon)}.d_y$	$\int t_c - y_1{}^{y_{0.2}} b_f \sigma_{1(\varepsilon)}.d_y$	$\int t_c - y_1{}^{t_c-y_1} + t_f b_f \sigma_{2(\varepsilon)}.d_y$
M_{tf1}	$\int t_c - y_1{}^{t_c-y_1} + t_f b_f \sigma_{1(\varepsilon)} y.d_y$	$\int t_c - y_1{}^{y_{0.2}} b_f \sigma_{1(\varepsilon)} y.d_y$	$\int t_c - y_1{}^{t_c-y_1} + t_f b_f \sigma_{2(\varepsilon)} y.d_y$
F_{tf2}	$\int H - t_f - y_1{}^{H-y_1} b_f \sigma_{1(\varepsilon)}.d_y$	$\int H - t_f - y_1{}^{H-y_1} b_f \sigma_{2(\varepsilon)}.d_y$	$\int H - t_f - y_1{}^{H-y_1} b_f \sigma_{2(\varepsilon)}.d_y$
M_{tf2}	$\int H - t_f - y_1{}^{H-y_1} b_f \sigma_{1(\varepsilon)} y.d_y$	$\int H - t_f - y_1{}^{H-y_1} b_f \sigma_{2(\varepsilon)} y.d_y$	$\int H - t_f - y_1{}^{H-y_1} b_f \sigma_{2(\varepsilon)} y.d_y$
F_{tf3}	----------	$\int y_{0.2}{}^{t_c-y_1} + t_f t_w \sigma_{2(\varepsilon)}.d_y$	----------
M_{tf2}	----------	$\int y_{0.2}{}^{t_c-y_1} + t_f t_w \sigma_{2(\varepsilon)} y.d_y$	----------
F_{tw1}	$\int t_c - y_1 + t_f{}^{y_{0.2}} t_w \sigma_{1(\varepsilon)}.d_y$	----------	----------
M_{tw1}	$\int t_c - y_1 + t_f{}^{y_{0.2}} t_w \sigma_{1(\varepsilon)}.y.d_y$	----------	----------
F_{tw2}	$\int y_{0.2}{}^{H-t_f-y_1} t_w \sigma_{2(\varepsilon)}.d_y$	$\int t_c - y_1 + t_f{}^{H-t_c-y_1} t_w \sigma_{2(\varepsilon)}.d_y$	$\int t_c - y_1 + t_f{}^{H-t_c-y_1} t_w \sigma_{2(\varepsilon)}.d_y$
M_{tw2}	$\int y_{0.2}{}^{H-t_f-y_1} t_w \sigma_{2(\varepsilon)}.y.d_y$	$\int t_c - y_1 + t_f{}^{H-t_c-y_1} t_w \sigma_{2(\varepsilon)}.y.d_y$	$\int t_c - y_1 + t_f{}^{H-t_c-y_1} t_w \sigma_{2(\varepsilon)}.y.d_y$

The detailed analytical solution to obtain the plastic bending moment requires numerical integrations to obtain the internal forces and moments that make the analytical calculation of plastic bending capacity complicated. Therefore, a simplified analytical model has been proposed to make the calculations easier.

The main assumption of simplified analytical method is that the effective area of structural steel section is stressed to constant stress value σ_m where σ_m is defined as the stress at 60% of the steel beam height. as illustrated in Figure 4.8. Noteworthy, in case

of using carbon steel in composite cross -section, Eurocode 4 recommends stressing the effective area of the structural steel to its yield strength.

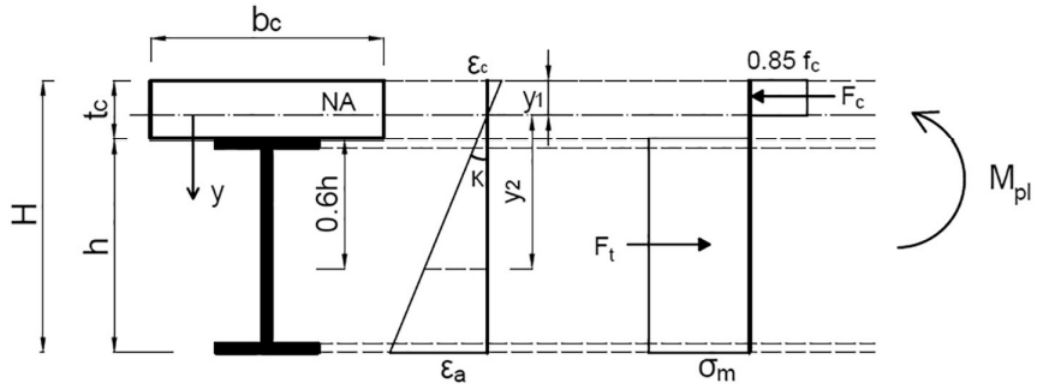

Figure 4.8 The stress and strain distribution diagrams for composite beams with full shear connection based on the simplified approach from (Shammas & Cashell, 2019).

As illustrated in Figure 4.8, the distance between the neutral axis and the location for σ_m can be determined as:

$$y_2 = t_c + 0.6h - y_1 \quad \textbf{(4.4)}$$

Where:
y_1 : The height of compressive area of the concrete slab
t_c : The total height of concrete slab
h: The total height of structural steel section.

From the horizontal equilibrium of the internal forces:

$$F_c = F_t \rightarrow 0.85\, F_c\, y_1\, b_c = A_s\, \sigma_m \quad \textbf{(4.5)}$$

Or

$$y_1 = \frac{A_s}{0.85\, f_c\, b_c}\sigma_m \quad \textbf{(4.6)}$$

Where*:*
A_s : The cross-sectional area of the stainless steel

It is assumed that $y_2 \geq y_{0.2}$, therefore stresses value σ_m can be determined by equation

$$\sigma_m = \sigma_{0.2}\left[1 + \frac{r_2\left[\frac{\varepsilon_2}{\varepsilon_{0.2}} - 1\right]}{1 + (r^* - 1).\left(\frac{\frac{\varepsilon_2}{\varepsilon_{0.2}} - 1}{\frac{\varepsilon_u}{\varepsilon_{0.2}} - 1}\right)}\right]^{p^*} \quad \textit{(4.7)}$$

In which ε_2 is the strain in the steel section at $y_2$given by equation **(4.8)** and k is the cross-sectional curvature determined from equation **(4.9).**

$$\varepsilon_2 = k.y_2 = k.(t_c + 0.6h - y_1) \quad \textit{(4.8)}$$

$$\kappa = \min(\kappa_c, \kappa_a) \quad \textit{(4.9)}$$

Where:

$\kappa_c = \frac{\varepsilon_{cu}}{y_1}$ and $\kappa_a = \frac{\varepsilon_u}{H - y_1}$

Where the material parameters used in equation **(4.7)** can be obtained from equations **(4.10)** to equation **(4.14)**.

$$\varepsilon_{0.2} = \frac{\sigma_{0.2}}{E} + 0.002 \quad \textit{(4.10)}$$

$$\sigma_u = \sigma_{0.2}.\frac{1 - 0.00375(n - 5)}{0.2 + 185e} \quad \textit{(4.11)}$$

Where*:*

$e = \frac{\sigma_{0.2}}{E}$

$$E_u = \frac{E_2}{1 + (r^* - 1).m} \quad \textbf{(4.12)}$$

Where

$$E_2 = \frac{E}{1 + 0.002\ {}^{n}/_{e}}$$

$$r^* = \frac{E_2(\varepsilon_u - \varepsilon_{0.2})}{\sigma_u - \sigma_{0.2}}$$

$$m = 1 + 3.5.\frac{\sigma_{0.2}}{\sigma_u}$$

$$r_2 = \frac{E_2.\varepsilon_{0.2}}{\sigma_{0.2}} \quad \textbf{(4.13)}$$

$$p^* = r^* \frac{1 - r_u}{r^* - 1} \quad \textbf{(4.14)}$$

Where:

$$r_u = \frac{E_u(\varepsilon_u - \varepsilon_{0.2})}{(\sigma_{u-}\sigma_{0.2})}$$

$$\varepsilon_u = \min\,(1 - \frac{\sigma_{0.2}}{\sigma_u}.A)$$

The plastic bending capacity of the composite beam can be calculated as:

$$M_{pl} = \sigma_m\, A_s[H - {}^{h}/_{2} - {}^{y_1}/_{2}] \quad \textbf{(4.15)}$$

Where, ε_u is the ultimate tensile strain, A is the stainless-steel elongation, E_2 and E_u are the slope of stress-strain curve at $\varepsilon_{0.2}$ and ε_u, respectively. The parameters r, r_2, r^*, r_u, p, p^*need also to be determined.

(Zhou, et al., 2021) presented an experimental, numerical and analytical study of the behavior of stainless-steel concrete composite beams subjected to bending. A total of eighteen full- scale stainless steel-concrete composite beams having various shear spans and different degree of interaction as listed in *Table 4.4* were tested under bending, shear and combined bending and shear. Eight of them were tested in bending under a simply support condition as illustrated in *Figure 4.9*. The geometry and the instruments for the test are shown in *Figure 4.10*.

Figure 4.9 Number of bending, shear, and combined bending and shear tests that were carried out by (Zhou, et.al, 2021).

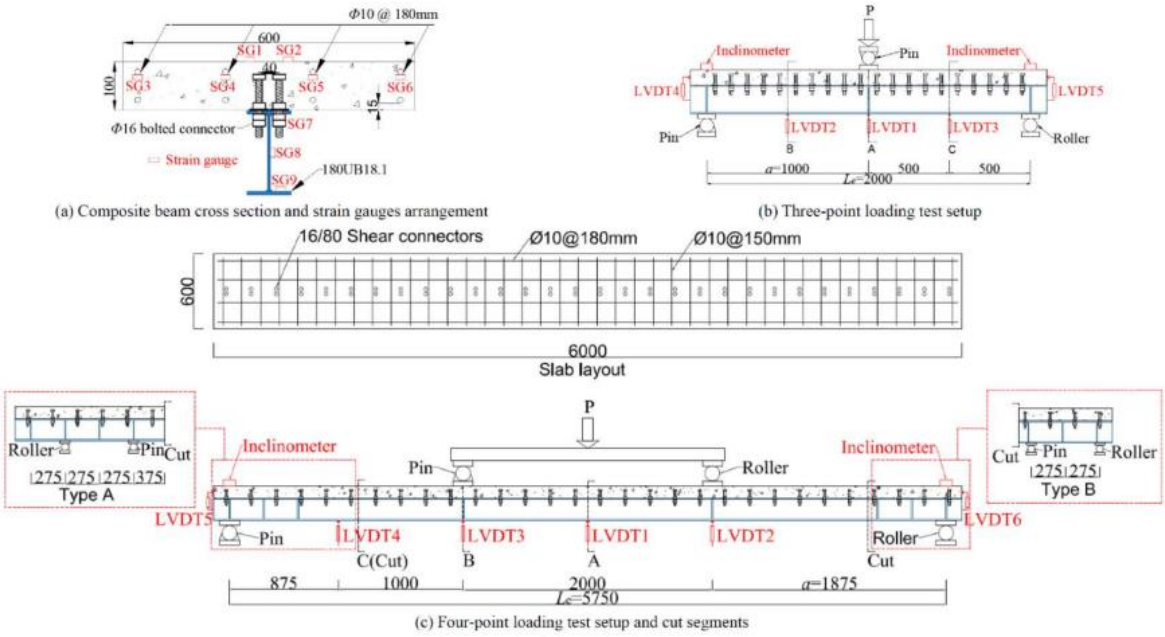

Fig. 3. Configuration of geometry and instrument setup for stainless steel-concrete composite beam tests.

Figure 4.10 Configuration of geometry and instrument setup for stainless steel-concrete composite beams tests, from (Zhou, et.al, 2021)

Table 4.4 Specimen details of stainless-steel composite beams (Zhou, et.al., 2021)

	Specimens	Beam materials	L_e mm	a mm	Loading method	Connector types	Connector materials	Connector spacing mm	β
Bending test	CSSB1-BF	LD2101	5800	2000	FPL	Bolt	D2205	200	1
	CSSB2-SF	LD2101	5800	2000	FPL	Stud	D2205	200	1
	CSSB3-BP	LD2101	5800	2000	FPL	Bolt	D2205	400	0.7
	CSSB4-SP	LD2101	5800	2000	FPL	Stud	D2205	400	0.6
	CSSB5-BF	A304	5800	2000	FPL	Bolt	A316L	200	1
	CSSB6-BF	D2205	5800	2000	FPL	Bolt	D2205	200	1
	CSSB7-BF	LD2101	2000	1000	TPL	Bolt	D2205	200	1
	CSSB8-SP	LD2101	2000	1000	TPL	Stud	D2205	200	1
Shear test	CSSB9-BF	LD2101	550	275	TPL	Bolt	D2205	100	1
	CSSB10-SF	LD2101	550	275	TPL	Stud	D2205	100	1
	CSSB11-BP	LD2101	550	275	TPL	Bolt	D2205	100	0.7
	CSSB12-SP	LD2101	550	275	TPL	Stud	D2205	100	0.6
	CSSB13-BF	A304	550	275	TPL	Bolt	A316L	100	1
	CSSB14-BF	D2205	550	275	TPL	Bolt	D2205	100	1
Combined bending and shear test	CSSB15-BF	LD2101	1600	800	TPL	Bolt	D2205	100	1
	CSSB16-BF	LD2101	800	400	TPL	Bolt	D2205	100	1
	CSSB17-SF	LD2101	1600	800	TPL	Stud	D2205	100	1
	CSSB18-SF	LD2101	800	400	TPL	Stud	D2205	100	1
FPL: four-point loading; TPL: three-point loading									

Comparing experimental results with design models of carbon steel, the ultimate bending resistance is 14% to 24% higher than M_{pl}. It's obvious that stainless steel–concrete composite beam could sustain higher flexural capacity due to its remarkable strain hardening effects.

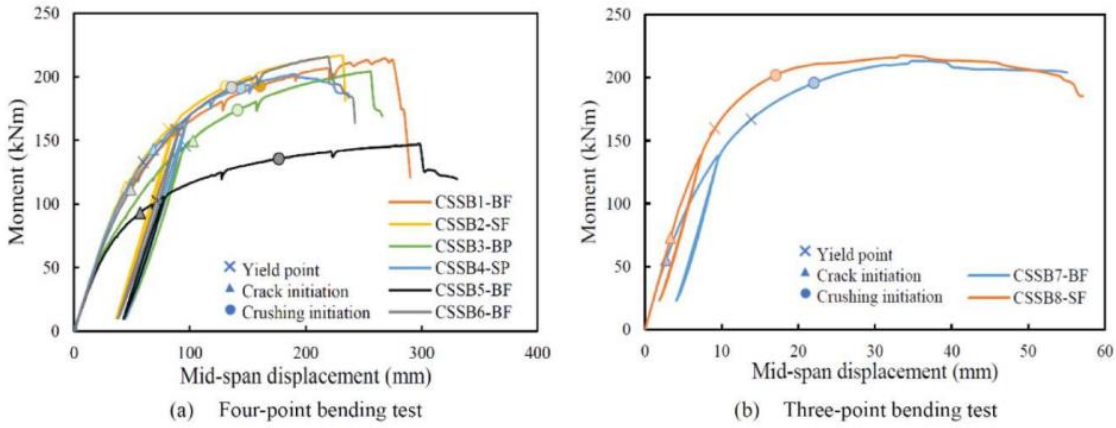

Figure 4.11 Moment- mid-span displacement curves for bending tests

Table 4.5 Results of stainless-steel composite beams from bending tests and analytical models from (Zhou, et.al, 2021)

Bending test	Specimens	V_u kN	M_U kN.m	$K_{I.M}$ kN.m/mm	M_{RPA} kN.m	M/M_{RPA}	M_{SHA} kN.m	M/M_{SHA}	$M_{SHA.S}$ kN.m	$M/M_{SHA.S}$
FPL	CSSB1-BF	107	204	2.86	177	1.15	190	1.07	190	1.08
	CSSB2-SF	108	206	2.89	177	1.16	190	1.09	190	1.09
	CSSB3-BP	102	194	2.45	170	1.14	175	1.11	175	1.11
	CSSB4-SP	101	192	2.73	165	1.16	170	1.13	170	1.13
TPL	CSSB5-BF	73	139	2.55	118	1.18	126	1.10	125	1.12
	CSSB6-BF	108	205	2.62	177	1.15	190	1.08	190	1.08
	CSSB7-BF	213	213	21.74	175	1.22	190	1.12	190	1.12
	CSSB8-SF	218	218	22.35	175	1.24	190	1.15	190	1.15

The study concluded that the stainless steel-concrete composite beam could sustain higher flexural capacity compared with the design codes due to its remarkable strain hardening effects.

5 Finite element studies

The purpose of this chapter is to develop parametric studies using the finite element modeling approach to evaluate the influence of stainless steel and corrugation in the web on the ultimate bending strength of composite sections with dimensions similar to those used in bridge construction. First, in section 5.1, the approach adopted for modeling and analysis by the finite element method in Abaqus software is described. The considered modeling approach is used to simulate a number of bending tests performed on composite sections by others, and the results are compared with the results of the tests with the aim of validation of the modeling approach. Later, in section 5.2, three composite beams with large dimensions were designed and studied using the described FEM and their bending behaviors when they have a flat web and are made of carbon steel were compared with other conditions, including stainless steel and corrugated web plates, with the aim of evaluating the effects of changing the material to stainless steel and the web configuration into corrugated on the ultimate bending strength.

5.1 Modelling method

5.1.1 FE element type

The composite steel-concrete bridges are usually modelled as assembled parts of structural steel and concrete slab. Those parts have individual properties and are modelled by using different element types. The concrete slab is modelled using 3D solid elements (C3D8R) available in ABAQUS element library with 8 nodes and reduced integration points as illustrated in Figure 5.1. This element type allows for simulating the interfaces accurately.

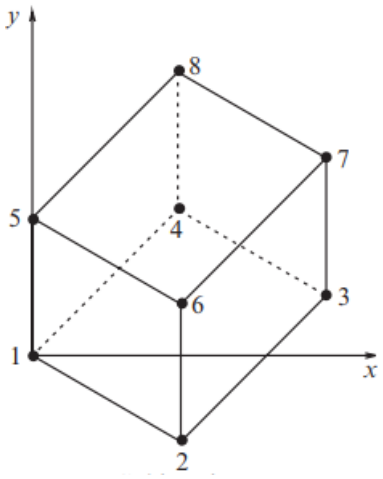

Figure 5.1 3D solid element (C3D8R), from (Ellobody, 2014)

On the other hand, structural steel plate elements were modelled using conventional shell element type S4R. If the cross section is classified as a compact section that has enough thickness to develop its plastic moment resistance without any possibility of

local buckling, then it can be modelled with solid elements with 8 nodes. But if the elements, such as the web and the flanges, are classified as non-compact that have thinner plate thickness than compact sections, then a conventional shell element with reduced integration points type S4R is suitable to model the structural steel section as illustrated in Figure 5.2. Reduced integration provides accurate results since the elements are not loaded in in-plane bending. Conventional shell elements normally have 5 or 6 degrees of freedom per node, which are S4R5 and S4R6 respectively. Using S4R5 instead of solid elements facilitates the modelling of metal structures and reduces the computational time.

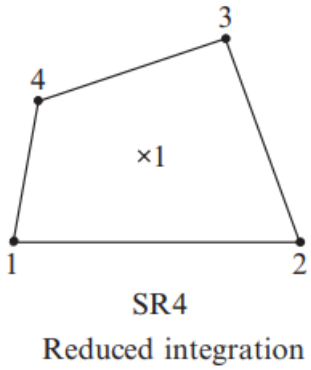

Figure 5.2 Conventional shell element SR4, from (Ellobody, 2014)

The steel rebars were modelled using truss elements T3D2, which are embedded in the concrete slab. The T3D2 element is shown in Figure 5.3.

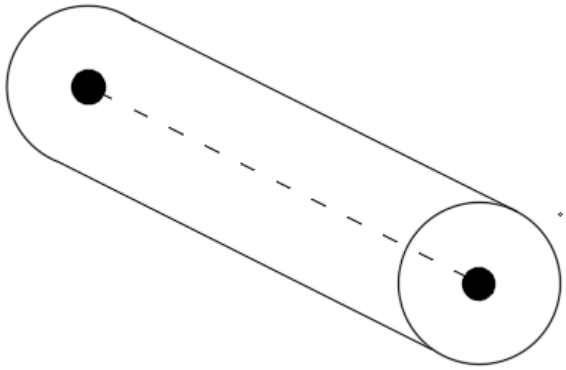

Figure 5.3 Truss element T3D2 redrawn from (Agampodi , Safat, & Ashraf, 2018)

5.1.2 Modelling the behaviour of carbon Steel

The carbon Structural steel and reinforcement were modeled using the stress-strain relation given in (EN 1993-1-5) as illustrated in Figure 5.4. The curve is linear until yielding, followed by bi-linear behavior after yielding until it reaches the ultimate tensile stress as shown in Figure 5.4.

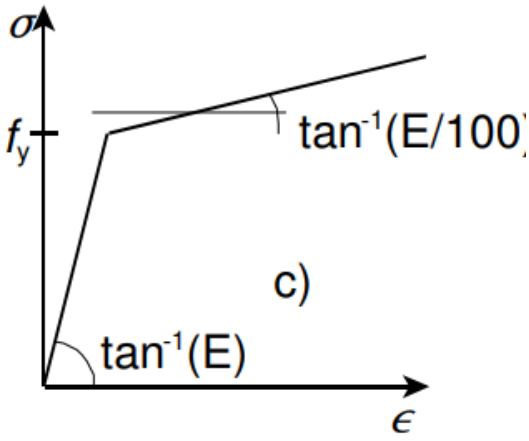

Figure 5.4: Stress-strain relation with strain hardening (EN 1993-1-5, 2005)

The material's yielding strength, f_y, and the ultimate strength, f_u, for the employed steel grad were obtained from Table 3.3 in section 3.2.2. Furthermore, the engineering value of yield strain ε and ultimate strain ε_u. are determined from equations ***(5.1),(5.2)***, respectively, where the equations are integrated from the stress-strain curve that is presented in Figure 5.4.

$$\varepsilon = \frac{f_y}{E_0} \qquad \textbf{(5.1)}$$

$$\varepsilon_u = \frac{f_y}{E_0} + \frac{f_u - f_y}{\frac{E_0}{100}} \qquad \textbf{(5.2)}$$

Where:
E_0 : Young's modulus of elasticity

The elastic part of the curve was introduced to ABAQUS with Young's modulus (E_0) and Poisson's ratio υ. The non-linear part should be introduced using the characteristic values according to the recommendations in EN 1993-1-5. Considering that the analysis of composite bridges is associated with large inelastic strains, the engineering stress-strain curves should be converted to true curves of stress and strain as illustrated in Figure 5.5. The true values of stress and strain can be determined from equations ***(5.3)*** and ***(5.4)*** respectively.

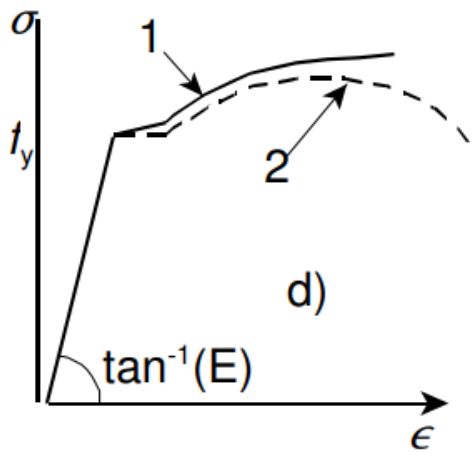

1 true stress-strain curve
2 stress-strain curve from tests

Figure 5.5 True stress-strain relation, from (EN 1993-1-5, 2005)

$$\sigma_{true} = \sigma * (1 + \varepsilon) \quad \textbf{(5.3)}$$

$$\varepsilon_{true} = ln * (1 + \varepsilon) \quad \textbf{(5.4)}$$

The plastic true strain will be calculated from equation ***(5.5)***.

$$\varepsilon_{true}^{pl} = ln * (1 + \varepsilon) - \frac{\sigma_{true}}{E_0} \quad \textbf{(5.5)}$$

In this study, Steel grades S355, S420, HPS-556, and HPS-583 were used for the modelling of steel plate elements. Additionally, the used reinforcement had a yield strength of 413.7 MPa and an ultimate tensile strength of 620.5 MPa. The material properties, including the true stress values, and the plastic true strain values for the used carbon steel in different strengths are presented in Table A.7 to Table A.11 in Appendix A. The implemented stress-strain curves are illustrated in Figure 5.6.

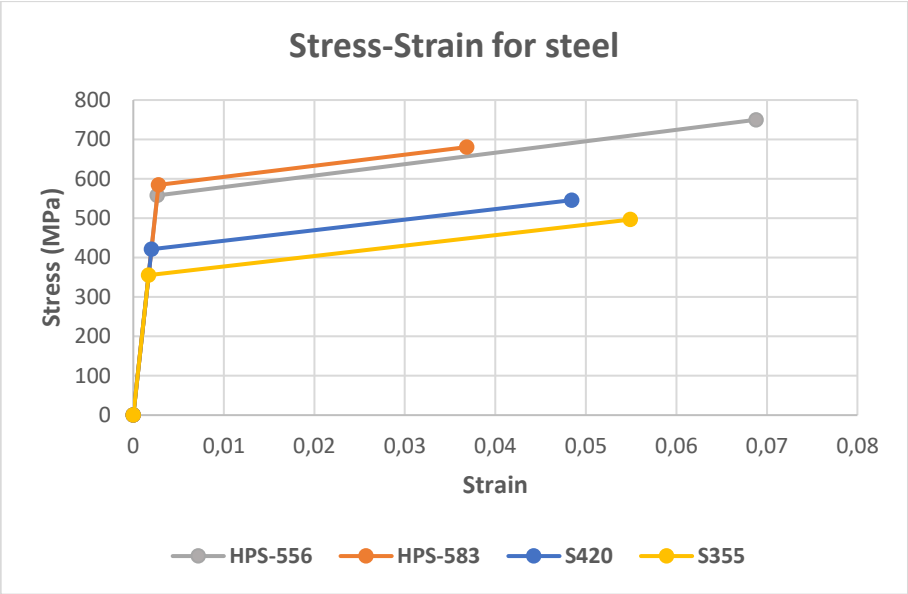

Figure 5.6 True Stress-strain curves for the used steel materials

5.1.3 Modelling the behaviour of stainless steel

The stainless steel was modeled using the stress-strain relation as given in (Design manual for structural stainless steel, 2018), Annex C. For stainless steel the stress-strain relation is different from that for carbon steel as mentioned in section 2.3.2. In stainless steel, the stress-strain curve shows a non-linear behavior from an early stage and is rounded without a specific yielding point (Design manual for structural stainless steel, 2018). Therefore, the yielding strength, f_y, of stainless steel is taken as 0.2% proof stress, $\sigma_{0.2}$. Furthermore, stainless steel has a remarkable strain hardening as illustrated in Figure 5.7. The engineering values of stress and strain for stainless steel can be determined for the cases before and after yielding from equations ***(5.6)***,***(5.7)***, respectively.

$$\varepsilon = \frac{\sigma}{E} + 0.002\left(\frac{\sigma}{f_y}\right)^n \quad for\ \sigma \leq f_y \qquad \textbf{(5.6)}$$

$$\varepsilon = 0.002 + \frac{f_y}{E} + \frac{\sigma - f_y}{E_y} + \varepsilon_u\left(\frac{\sigma - f_y}{f_u - f_y}\right)^m \quad for\ f_y < \sigma < f_u \qquad \textbf{(5.7)}$$

The parameters in the above mentioned equations are defined as follows:
σ : The engineering stress
ε : The engineering strain.
E,f_y, f_u are given in section 3.2.3
E_y : The tangent modulus of the stress-strain curve at the yielding point that can be determined from equation ***(5.8)***

$$E_y = \frac{E}{1 + 0.002n\,{}^{E}/_{f_y}} \qquad \textbf{(5.8)}$$

Where $n\ and\ m$ are coefficients that determine the grade of nonlinearity for different stainless-steel grades and should be calculated as follows:

$$m = 1 + 2.8 \cdot \frac{f_y}{f_u} \qquad \textbf{(5.9)}$$

$$n = \frac{\ln(4)}{\ln\left[\frac{f_y}{R_{p0,05}}\right]} \qquad \textbf{(5.10)}$$

Where
$R_{p0,05}$ is the 0.05% proof stress.

The true values of the stress and the logarithmic plastic strain can be calculated from equations ***(5.3)***,***(5.5)*** respectively.

In this study, duplex stainless-steel grade 1.4162 was used in the parametric studies. The stress-strain curve depends on the thickness of the element. Since three different thicknesses were used in this study, the material properties, the true stress values, and the plastic true strain values for stainless steel in different thicknesses are listed in Table A.12 to Table A.14 in Appendix A. The stress-strain for the employed stainless-steel plates in the current study are illustrated in Figure 5.7.

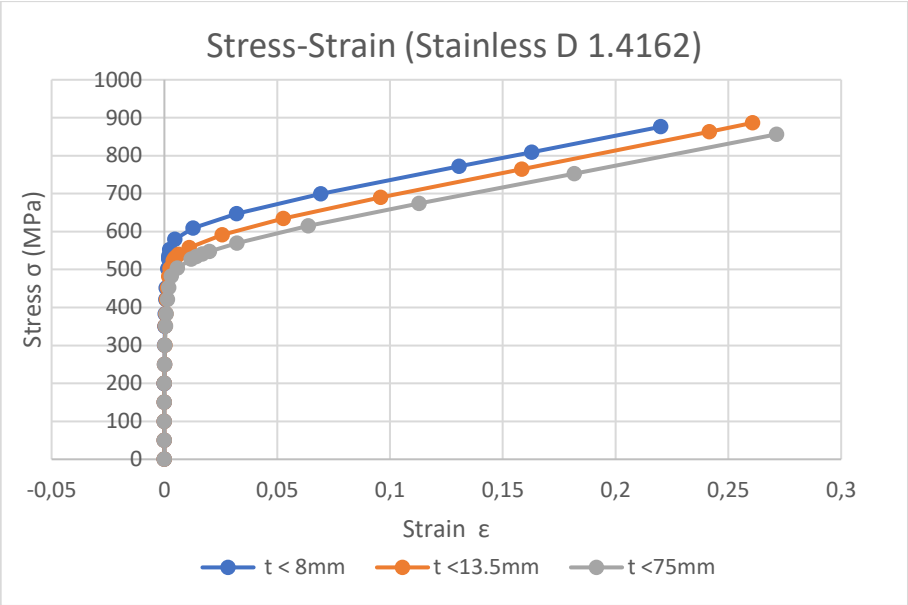

Figure 5.7 : True stress-strain curves for the used stainless-steel plates in the current study

5.1.4 Modelling the behaviour of the concrete material

In ABAQUS, concrete is modeled by using the concrete damage plasticity model. This model is able to model both plain and reinforced concrete. The damage plasticity model combines the concepts of isotropic damage of elasticity with isotropic tensile and compressive plasticity to introduce the inelastic behavior of concrete (Ellobody, 2014). The two main failure mechanisms that occur in damage plasticity model are tensile cracking and compressive crushing of concrete.

In this model, the uniaxial tensile and compressive responses of concrete are distinguished by damage plasticity as illustrated in Figure 5.8 and Figure 5.9. In the plasticity damage model, the stress-strain curves can be converted into stress versus plastic-strain curves. That conversion can be done automatically by ABAQUS. When the concrete specimen is unloaded from any point on the strain softening branch of the stress-strain curve, the unloading response is weakened, and the elastic stiffness of concrete seems to be degraded. The degradation of the elastic stiffness can be characterized by the plasticity damage variables d_t and d_c for the tensile and compressive stress-strain curve, respectively (Ellobody, 2014).

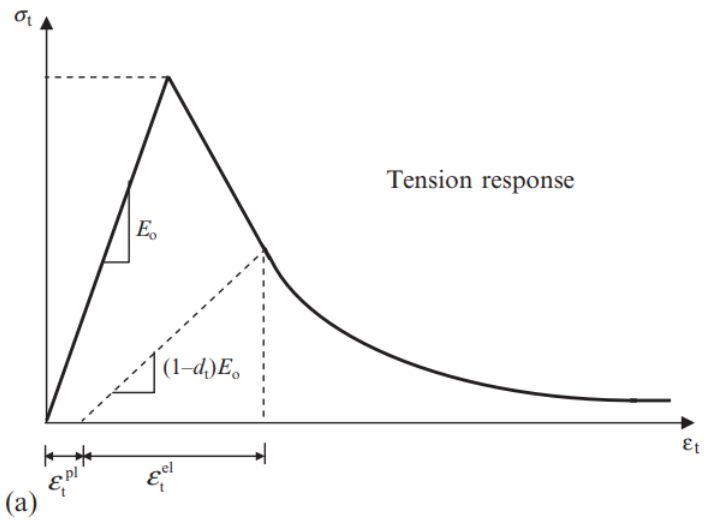

Figure 5.8 Response of concrete to uniaxial loading in tension (Ellobody, 2014)

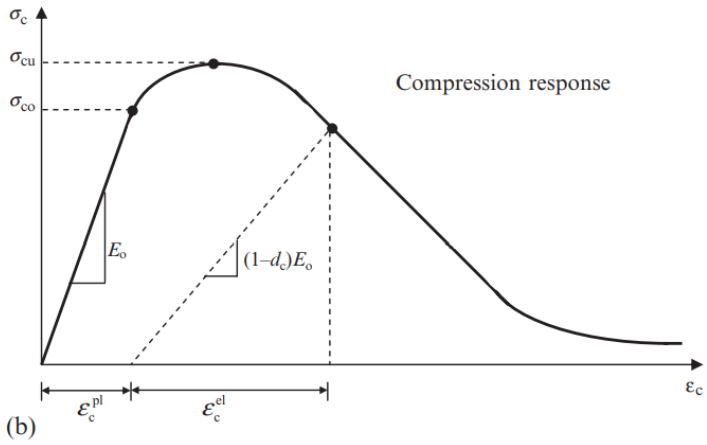

Figure 5.9 Response of concrete to uniaxial loading in compression, from (Ellobody,2014)

The variables d_t and d_c can be determined from equation **(5.11), (5.12),** respectively (Hafezolghorani, Hejazi, Vaghei, & Bin Jaafar, 2017)

$$d_t = 1 - \frac{\sigma_t}{\sigma_{t0}} \qquad \textbf{(5.11)}$$

$$d_c = 1 - \frac{\sigma_c}{\sigma_{cu}} \qquad \textbf{(5.12)}$$

The compressive response of concrete is obtained from the stress-strain relation for non-linear structural analysis given by EN 1992-1-1 as illustrated in Figure 5.10, the response is linear until the limit of $0.4 \cdot f_{cm}$. The non-linear part of the curve consists

of an ascending part until the compressive strength, f_c, followed by a descending part until reaching the ultimate compressive strain, ε_{cu1}.

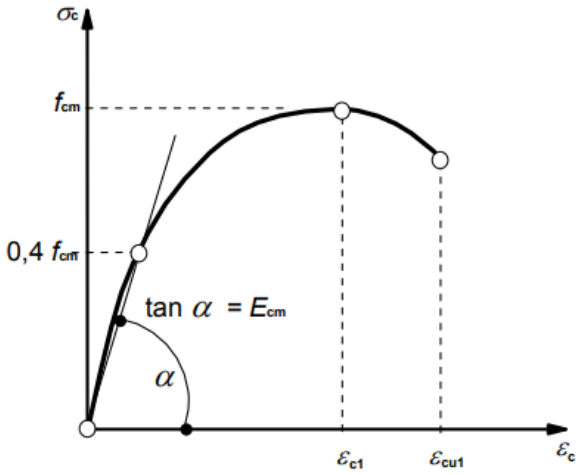

Figure 5.10 schematic representation of the stress-strain relation for structural analysis of concrete (the use of $0.4f_{cm}$ for the definition of E_{cm} is approximate) (EN 1992-1-1, 2005)

In this study, concrete classes C30/37, C35/45, and C50/60 were used in the parametric studies. The material properties, the true stress values, and the plastic true strain values for the used concrete in compression are listed in Table A.1 to Table A.3 in Appendix A. The stress-strain curves for the concrete in compression in the current study are illustrated in Figure 5.11.

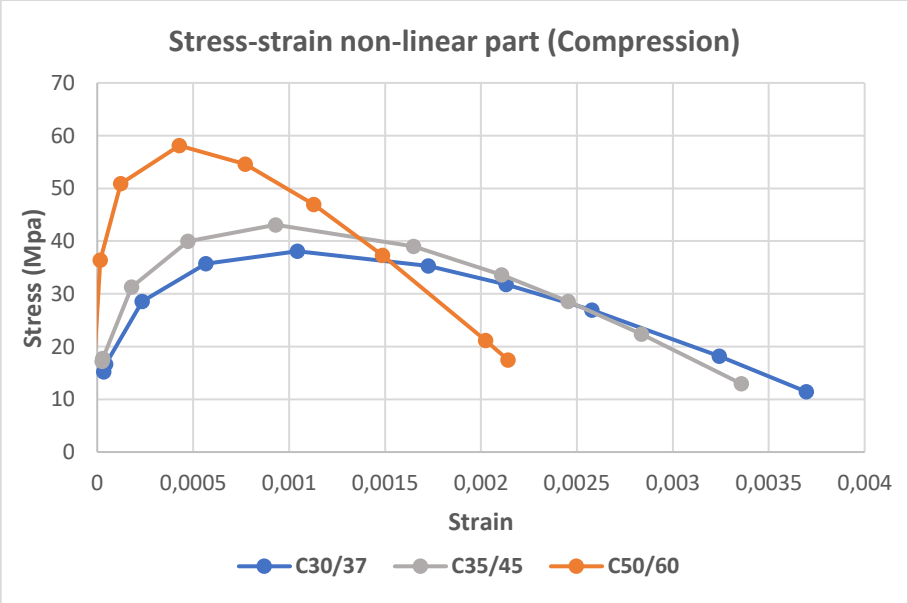

Figure 5.11 The nonlinear part of the stress-strain curve of the used concrete materials in compression in the current study.

In concrete specimens under uniaxial tensile test, cracks initiate and propagate when the tensile stress reaches the tensile strength, f_{ctm}, as illustrated in Figure Figure 5.12. The softening behavior of concrete can be described by the stress that can be transferred through the fracture zone. This transferred stress, $\sigma_{c(w)}$, is a function that depends on the crack opening width w. Furthermore, the area under the softening curve, $\sigma_{c(w)}$, is denoted as the fracture energy, G_F, that is an important concept in FE modelling of concrete cracks (Plus, Zandi, Johansson, & Shu, 2021).

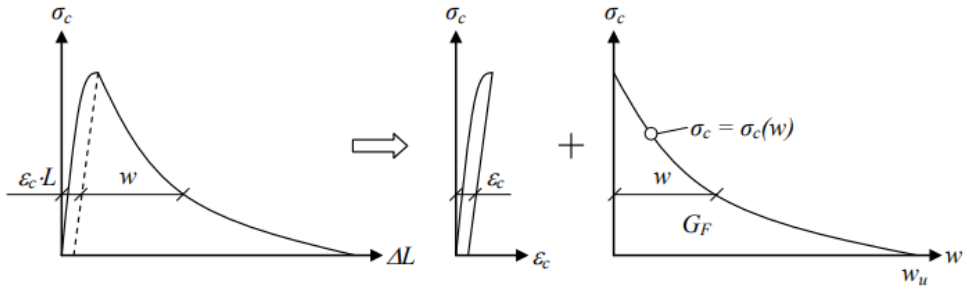

Figure 5.12 Stress-displacement relation for a uniaxial tensile test specimen. The displacement is separated into a stress-strain relation and a stress-crack opening relation. The area under the softening curve, $\sigma_{c(W)}$, represents the fracture energy, G_F. From (Plus, Zandi, Johansson, & Shu, 2021)

The tensile strength for different concrete classes can be obtained from Table 3.2 in section 3.3.1. The softening in the stress-strain response can be introduced as a linear line that can be determined by the fracture energy and the crack band width. The fracture energy divided by the crack band width (h) will be used to determine the area under the softening part of the tensile stress-strain curve. From this, the cracking strain can be obtained using equation (***5.13)***. The crack band width can be taken as the cubic root of the volume between integration points of a solid element. The fracture energy depends on the concrete class and can vary between $0.04\ N/mm$ for concrete with a compressive strength 20 MPa to $0.12\ N/mm$ for concrete with a compressive strength of 40 MPa (Ellobody, 2014).

$$\varepsilon_{su} = \frac{2G_F}{f_{ctm}} \cdot \frac{1}{h} \qquad \textbf{(5.13)}$$

The tension-stiffening effect in concrete need to be estimated effectively. This depends on the density of reinforcement, the bond between the rebars, the relative size of concrete aggregate compared to rebar diameter, and the mesh size. In plane concrete, mesh refinement causes a narrower crack band. Consequently, failure occurs only in localized regions and no additional cracks will be able to form. In that case, the analysis will not converge to a unique solution. In reinforced concrete, the interaction between the reinforcement bars and the concrete reduces the mesh sensitivity. However, a reasonable amount of tension stiffening needs to be introduced in the concrete model to simulate the interaction.

The tensile behavior of concrete classes C30/37, C35/45, and C50/60 is illustrated in Figure 5.13.The fracture energy, crack band width, tensile strength, and the ultimate cracking strain values for the used concrete in tension are listed in Table A.4 to Table A.6 in Appendix A.

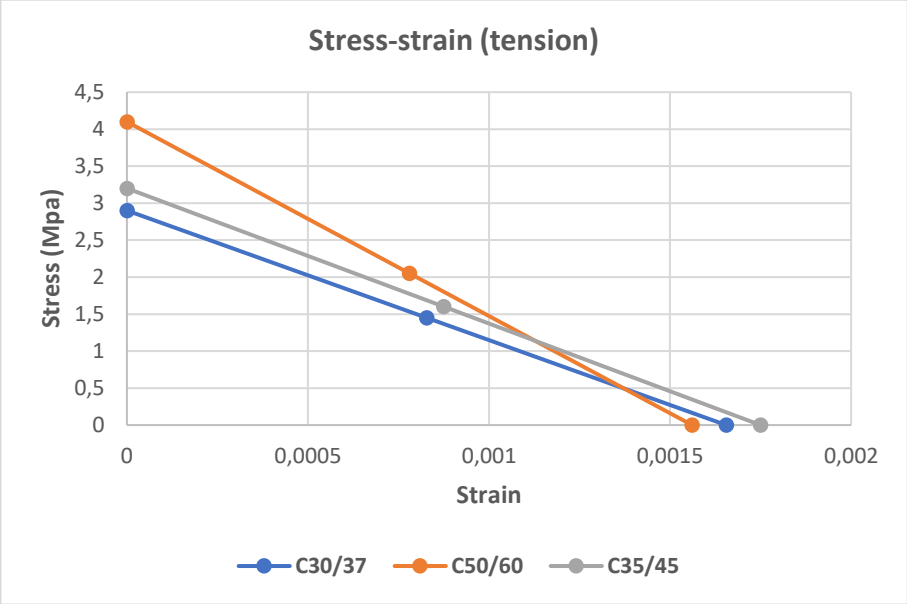

Figure 5.13 : Area under softening curve $\sigma_{c(W)}$ represents the fracture energy, G_F, for used concrete materials in tension behaviour in the current study.

There are other parameters that are included in damage plasticity model to define the yield surface in concrete. The first parameter is the dilation angle that equals the volume strain over shear strain. The dilation angle for concrete is usually 20° to 40°, which affect the material ductility. The flow potential eccentricity of 0.1 is usually used in concrete. The ratio of initial equiaxial compressive yield stress to initial uniaxial compressive yield stress was given by $fb0/fc0$ and its default value is 1.16. Viscosity parameter enhances the convergence rate of the model when the softening process occurred and ABAQUS uses a null default viscosity parameter (Hafezolghorani, Hejazi, Vaghei, & Bin Jaafar, 2017). However, the parameters used by (Jankowiak & Lodygowski, 2005) were adapted in this master thesis and are listed in Table 5.1:

Table 5.1 Parameters of concrete damage plasticity model (Jankowiak & Lodygowski, 2005)

Dilation angle	Eccentricity	f_{b0}/f_{c0}	k	Viscosity
38	1	1.12	0.667	0.003

5.1.5 Modelling of the shear connections

Figure 5.14 shows the load-slip behavior of a headed stud in a pushout test. This behavior can be modeled in ABAQUS using non-linear springs in the longitudinal direction by using a cartesian connection. Moreover, the vertical pressure between the concrete slab and the steel plate of the top flange can be transferred using vertical rigid springs with high stiffness.

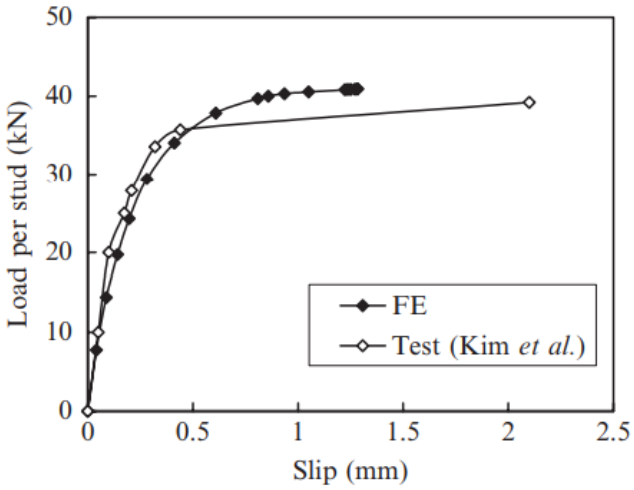

Figure 5.14 Load slip behavior for pushout specimen, from (Ellobody,2014).

A simplification in this master thesis has been done by using a Tie interaction between steel and concrete. The Tie connection fuses the two surfaces together and cancels any slip between them. However, real structures will always have a degree of slip between steel and concrete as discussed in section 2.1.2.

(A.Jaafer & L.Kareem, 2020) carried out a parametric study to determine the effect of the degree of interaction between steel and concrete in curved composite plate girders. The study showed that the slip between steel and concrete affects both the load capacity and ductility of the beam as illustrated in Figure 5.15. On the other hand, when the connection degree is higher than 0.9 which is the case for the beams with number of studs higher than 24, the models showed a close load capacity. However, the beam with 26 studs has 18% larger displacements than the beam with 30 studs.

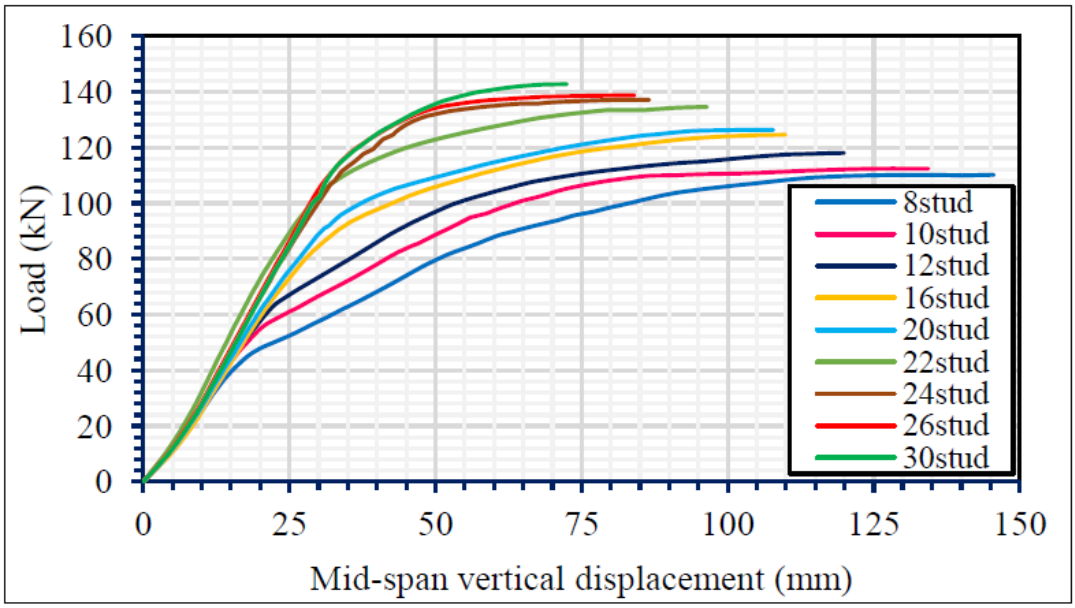

Figure 5.15 Partial interaction effect on the load-deflection relationship of the curved composite beam, redrawn from (A.Jaafer & L.Kareem, 2020)

Based on that, the simplification using tie connection will affect the deflection of the models about 20% less than the test. However, it will not affect the ultimate bending moment capacity, and that is why it can be a proper modeling technique in the current study.

5.1.6 Mesh type

The finite element mesh should have a reasonable size that can lead to convergence and reasonable results on the other hand, the larger the number of elements, the longer the computational time for the analysis. Therefore, a convergence study should be done to choose the best mesh size that provides an acceptable accuracy with reasonable time (Ellobody, 2014). The aspect ratio can be defined as the ratio of the longest dimension to the shortest dimension of a quadrilateral finite element. As shown in Figure 5.16, when the aspect ratio increases, the accuracy of the results decreases.

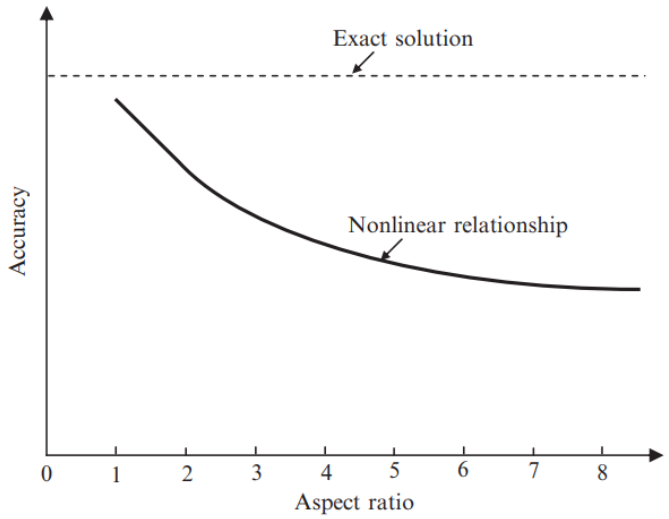

Figure 5.16 Effect of aspect of finite element on the accuracy of results (Ellobody, 2014)

A convergence study has been carried out on one of the models considered in the current study, G1 section 5.2.1.1, and the ultimate load was plotted against the mesh size as illustrated in Figure 5.17 . It was found that the exact solution for the ultimate load is attained with a mesh size of 50 mm and the analysis time was reasonable.

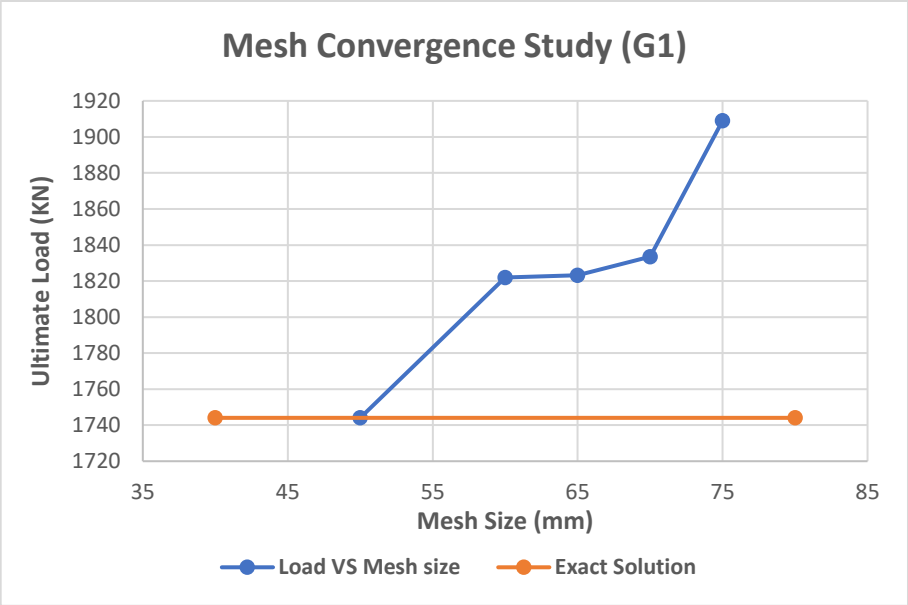

Figure 5.17 Mesh convergence study of bridge G1 in the current study.

5.1.7 Modelling of boundary conditions and loading

The application of boundary conditions in the FE modelling of composite bridges plays an important role since the analysis should account for geometrical and material non-linearities (Ellobody, 2014) at the same time

Boundary conditions can be applied by preventing translation or rotation at specific DOFs. For instance, applying a roller support can be implemented by preventing displacements in the vertical direction. This boundary condition can be applied to a reference point that has a rigid body constraint with the surface where the support should be applied, as shown in Figure 5.18. By using this method, the concentration of stresses in the area of the support can be avoided.

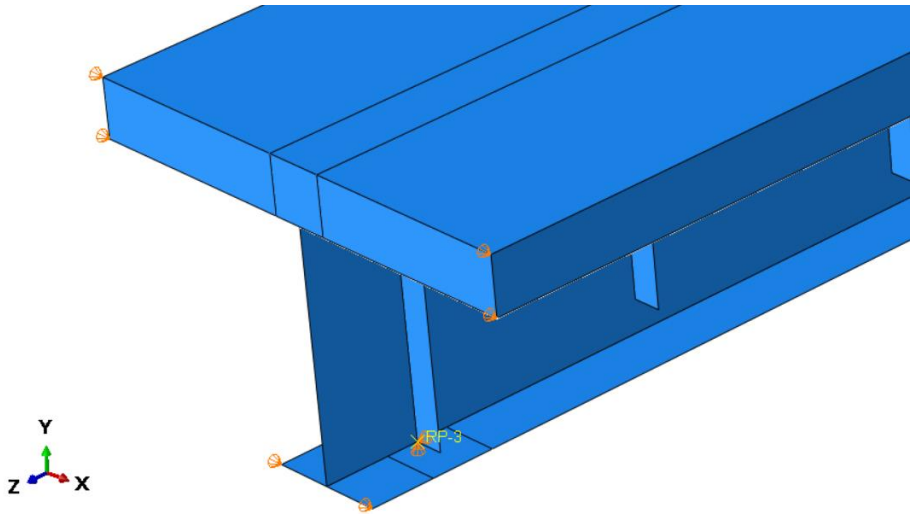

Figure 5.18 Boundary Conditions implemented in ABAQUS

The load was applied in increments as a static concentrated load that is applied to a reference point that is coupled with a specified surface area or a spreader plate by using a coupling constraint.

For the analysis, the Riks method was used to study the fully non-linear behavior due to geometrical, and material non-linearities. It's important to include the non-linear geometry option to deal with large displacements in the analysis.

It is worth mentioning that ABAQUS treats the load magnitude as an unknown when the Riks method is used, thus the load and displacement values in each increment are solved simultaneously. Therefore, the progress of solution must be checked and measured by using another quantity which is the arc length along the path of the static equilibrium in the load-displacement domain. In addition, Newton's method is used to solve the nonlinear equilibrium equations (Ellobody, 2014).

When a new step is defined, an initial increment of displacement in arc length along the static equilibrium path is provided. Subsequently, the initial load proportionality factor, LPF, is equal to the initial increment in a scheme that computes load magnitude by incremental steps automatically. If the convergence of increment fails, it is recommended to adjust the maximum and minimum values of arc length increment. The end of a solution can be determined either by specifying a maximum value of load or a maximum value of displacement at as specified degree of freedom "DOF" that is desired to be studied (Ellobody, 2014).

The configuration of the ABAQUS coordinate system is presented in Figure 5.19. This system has an important role in identifying the directions of the FE model. Thus, the

results can be taken in the desired direction to predict the failure mode that has occurred in the model. For instance, S33 shows the stress distribution in z-z-direction and U22 shows the displacements in the vertical direction y-y.

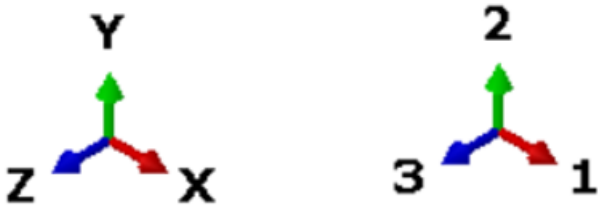

Figure 5.19 Configuration of the ABAQUS coordinate system used in the analysis in the current study.

5.2 Parametric studies

In the current finite element studies, different composite girder models were simulated with the aim of verifying their ultimate bending strength and the effects of changing the material to stainless steel and employing a corrugated web plate on the bending capacity of composite girders.

Before running the parametric studies, the finite element modeling approach described in the previous section is verified by simulating two previous bending tests on composite girders with flat webs and in carbon steel. Subsequently, 12 parametric models were designed with different geometric parameters, material and shape of the web in order to study the effects of employing stainless steel and corrugated webs on the bending behavior.

5.2.1 Verification of the finite element modelling approach

Two bridge girders with a composite girder tested by (Mans, Yakel, & Azizinamini, 2001) are simulated with the aim of verifying the finite element approach. The girders are called G1 and G2 in the original study. The experiments were a three-point bending test that had been carried out to evaluate the flexural behavior of the bridge and to predict the ultimate load and the corresponding displacement at the mid span of the bridge girder.

5.2.1.1 G1

The dimensions of G1 are presented in Figure 5.20 and the used materials are listed in Table 5.2

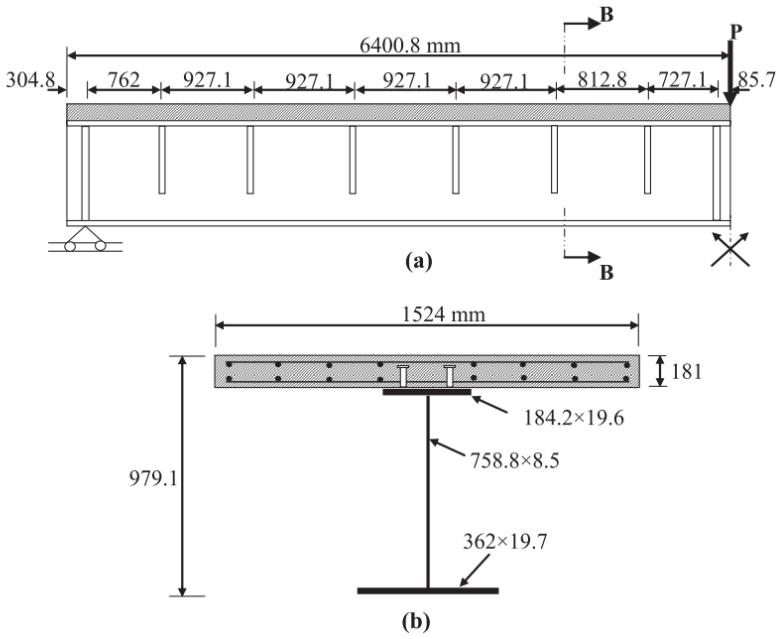

Figure 5.20 Composite steel-concrete girder G1 tested by (Mans, Yakel, & Azizinamini, 2001), redrawn from (Ellobody, 2014)

Table 5.2 Strength of materials used in G1 model in MPa

G1			
Concrete	Flanges	Web	Reinforcement
C30/37	HPS-556	HPS-583	413

G1 has been modelled using ABAQUS and the results are verified against the experimental test. Figure 5.21 shows the displacement of G1 in the vertical direction, and Figure 5.22 shows the von mises stresses in G1.

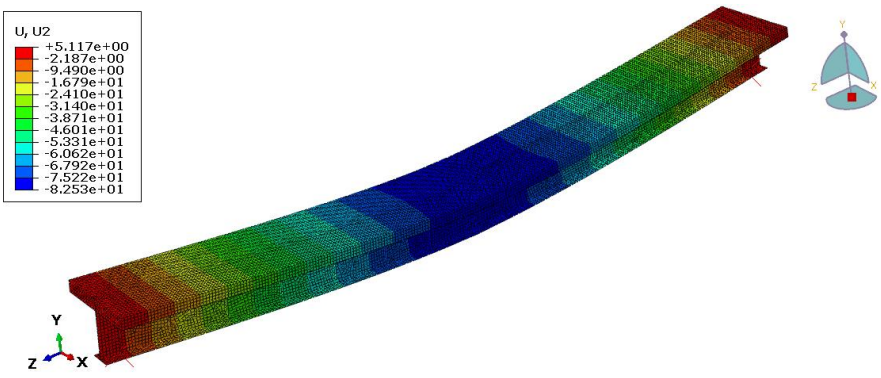

Figure 5.21 The vertical displacements along the span of G1.

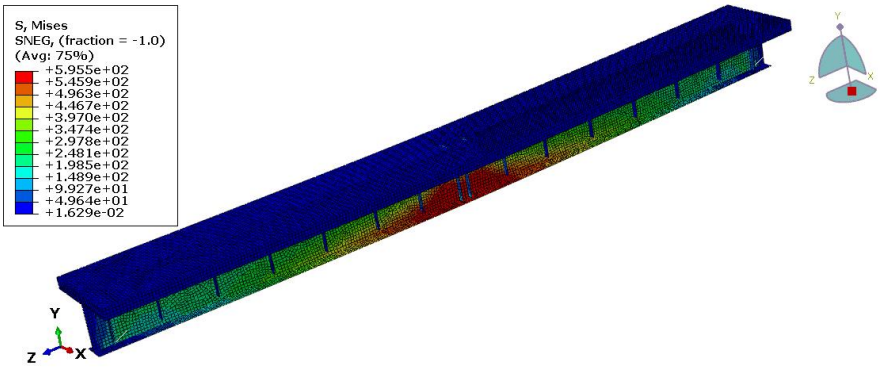

Figure 5.22 The Von Mises stress distribution along the span of G1

The failure mode of G1 was the simultaneous crushing of concrete and yielding of steel plates in tension. Figure 5.23 shows the crushing of concrete that is obvious because the strain in concrete exceeds the crushing strain of the concrete ($\varepsilon_{cu} = 3.5 \times 10^{-3}$). Furthermore, Figure 5.24 shows the yielding of the steel plate in the bottom flange at the failure (ultimate load).

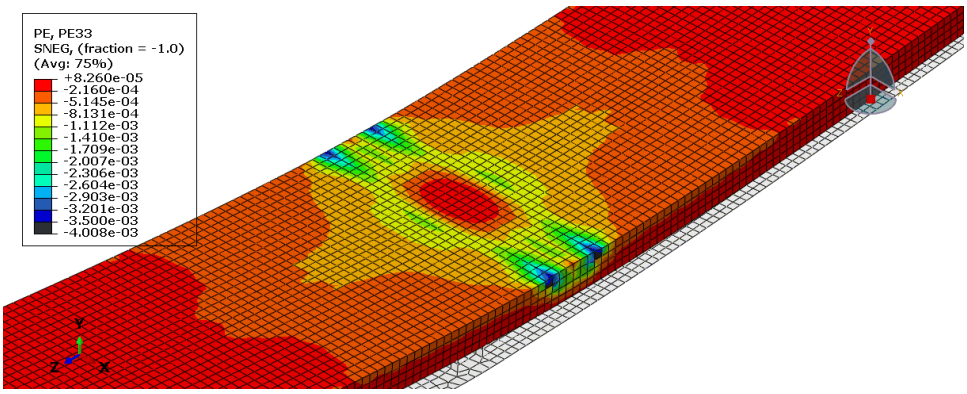

Figure 5.23 Crushing of concrete in G1

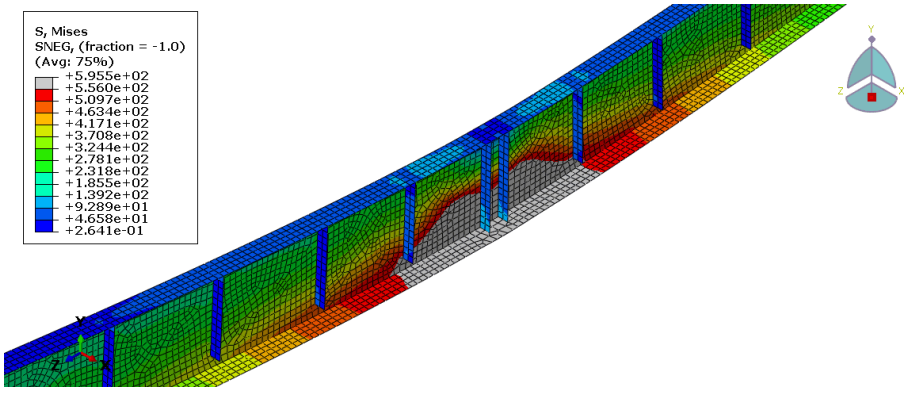

Figure 5.24 Yielding of the bottom flange in G1

The values of the total applied load and the displacement for G1 are listed in Table B.1in Appendix B. The load on G1 is plotted against the displacement as shown in Figure 5.25. The maximum load and the corresponding displacement in G1 are compared with the results from the test as listed in Table 5.3. The comparison showed that the difference in the total applied load is 0% and the difference in displacement is 16.3%.

Table 5.3 Comparison of results from test and FEM model for Bridge G1

	Total Applied load	Maximum displacement
G1 test results	1744.4 kN	98.6 mm
G1 FEM model results	1743.7 kN	82.53 mm
Difference	0%	16.3%

The relatively large difference in displacement (16.3%) is caused by using the tie connection as discussed in section 5.1.5. It will be accepted in this study since it does not affect the load capacity.

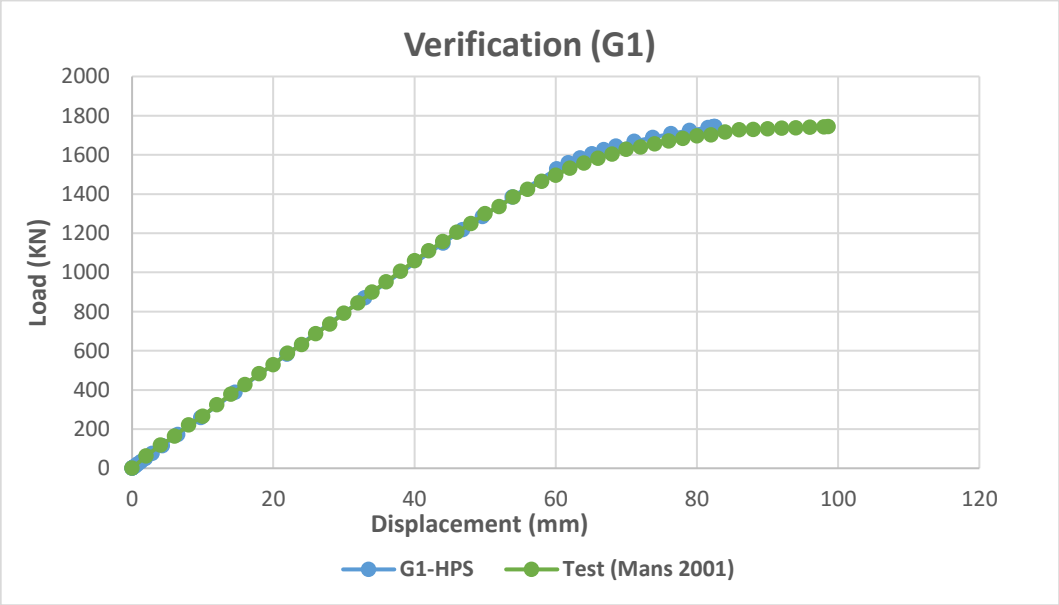

Figure 5.25 Load-displacement curve for G1

5.2.1.2 G2

The second simulated girder for the purpose of FEM verification is G2, a composite girder which was also tested by (Mans, Yakel, & Azizinamini, 2001). The experiment was a three-point bending test that was carried out to evaluate the flexural behavior of the girder and to predict the ultimate load and the corresponding displacement at the mid span. The dimensions of the girder are presented in Figure 5.26 and the used materials are listed in Table 5.4.

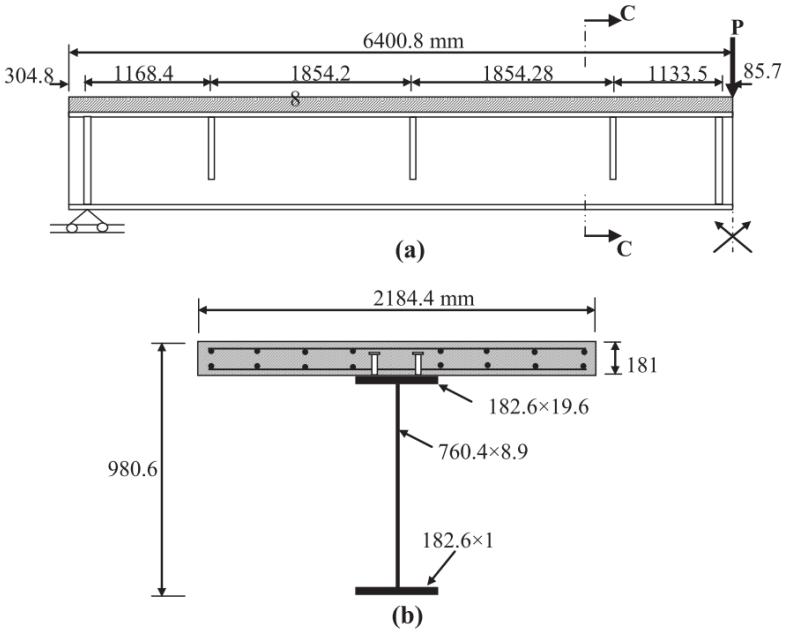

Figure 5.26 Composite steel-concrete girder G2 tested by (Mans, Yakel, & Azizinamini, 2001),redrawn from (Ellobody, 2014)

Table 5.4 Strength of materials used in G2 model in MPa

G2			
Concrete	Flanges	Web	Reinforcement
C50/60	HPS-556	HPS-583	413

The composite girder has been modelled using ABAQUS and verified against the experimental test. Figure 5.27 shows the displacement of G2 in the vertical direction. and Figure 5.28 shows the von mises stresses in G2.

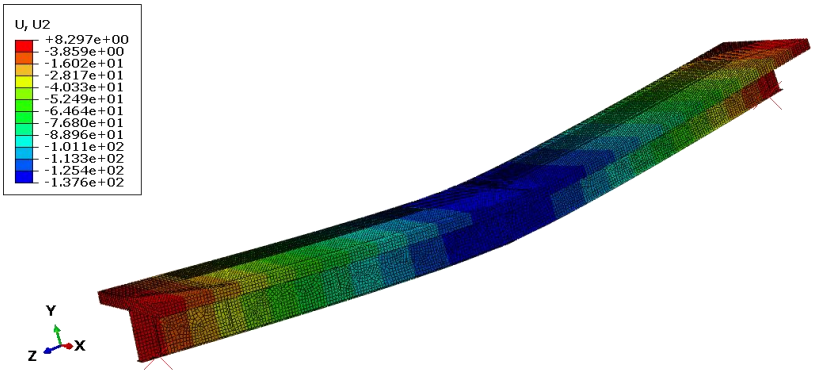

Figure 5.27 Vertical displacement (G2)

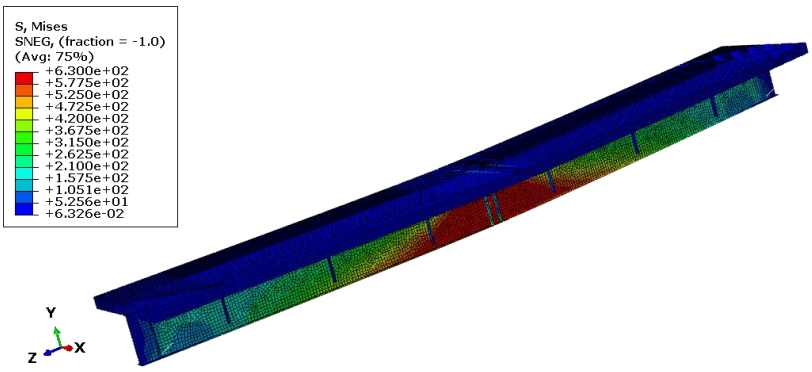

Figure 5.28 The Von mises stress distribution (G2)

The failure mode of in G2 was the yielding of the steel plate in tension as illustrated in Figure 5.29.

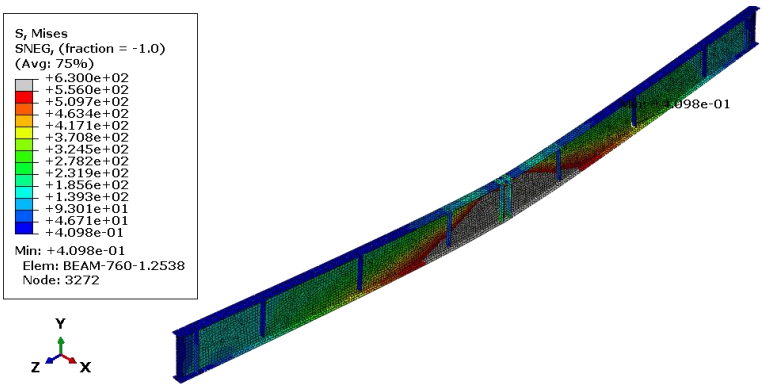

Figure 5.29 Yielding of structural steel (G2)

The values of the ultimate load and the displacement for G2 are listed in Table B.6 in Appendix B. The total applied load on G2 is plotted against the displacement as shown in Figure 5.30 and compared with the results from the test as listed in Table 5.5. The comparison showed that the difference in the ultimate load is 4.4% and the difference in displacement is 22.8%. As previously discussed, the difference in displacement is caused by using the tie connection as discussed in section 5.1.5. It is acceptable in this study since it doesn't affect the load capacity.

Table 5.5 Comparison of results from test and FEM model for Bridge G2

	Ultimate load	Maximum displacement
G2 test results	1432 kN	178.2 mm
G2 FEM model results	1438.8 kN	137.6 mm
Difference	4.4%	22.8%

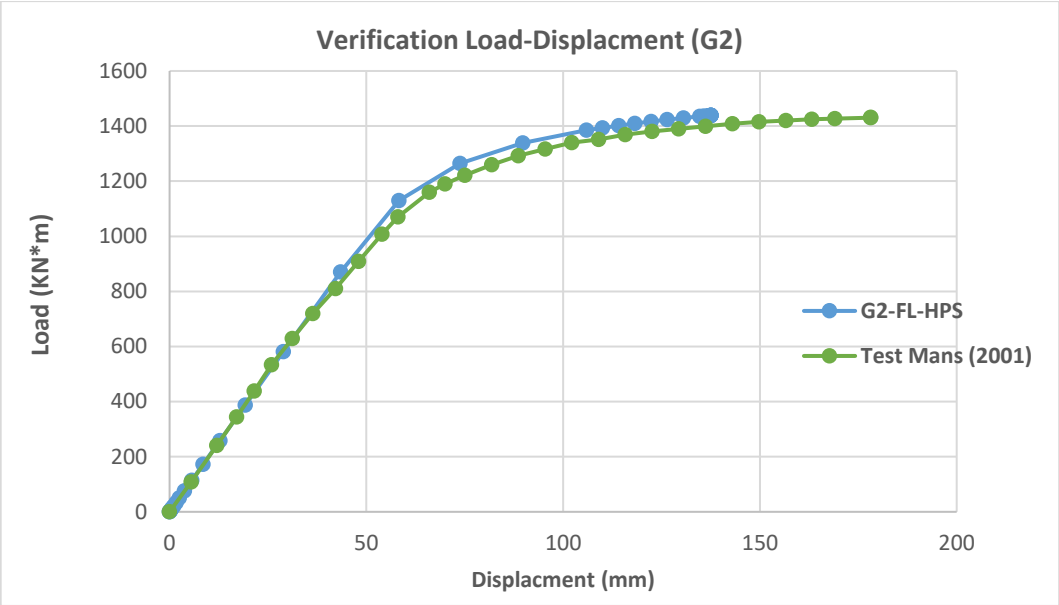

Figure 5.30 The load-displacement curve in G2

5.2.2. Design of the parametric models

The parametric models in the current study are developed based on the three different bridge girders geometries. The first two girders are G1 and G2 which are the tested girders by (Mans, Yakel, & Azizinamini, 2001) and their dimensions were presented in Figure 5.20 and Figure 5.26 respectively. The third girder selected from bridge 100-262-1 which is a composite bridge originally designed by WSP and redesigned in stainless steel having a corrugated web by (Henrysson & Yman , 2020). The dimensions of the bridge girder are shown in Figure 5.31 and listed in Table 5.6 and Table 5.7. Furthermore, the corrugation parameters are presented in Table 5.8 and the corrugated profile is illustrated in Figure D 1 in Appendix D.

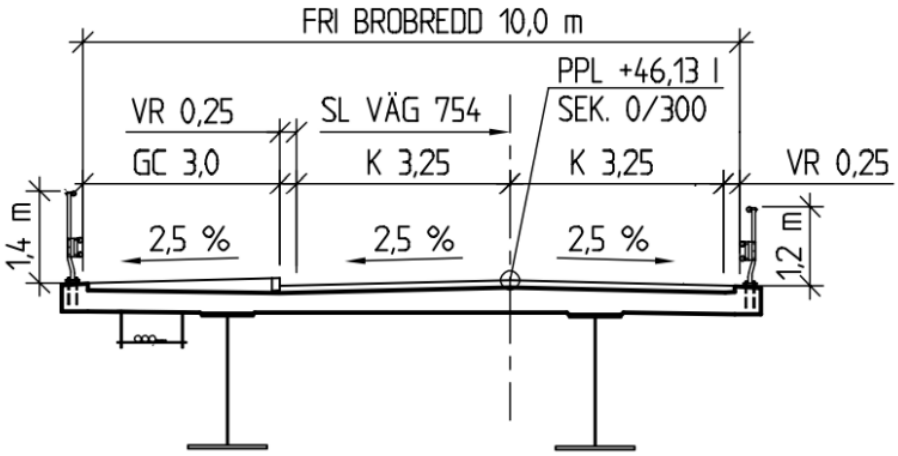

Figure 5.31 Dimensions of bridge 100-262-1 (Henrysson & Yman, 2020)

Table 5.6 The geometry of the bridge 100-262-1.

Bridge 100-262-1	Bridge length	Span length	Bridge width	Bridge height
	52 meters	51 meters	10 meters	2.37meters

Table 5.7 Sectional dimensions of Bridge 100-262-1 at different section.

Sectional constants	Sectional dimensions at x=0-10 meters near to support		Sectional dimensions at x=10-25.5 meters	
	Original design [mm]	New design [mm]	Original design [mm]	New design [mm]
b_{f_u}	800	850	800	850
t_{f_u}	42	45	42	45
b_{f_l}	1200	1225	1200	1225
t_{f_l}	55	50	55	50
t_w	17	6	17	6
h_w	1953	1955	1953	1955

Table 5.8 Corrugation shape of new design for Bridge 100-262-1

Corrugation Parameters	
a_1	120
a_2	119
a_3	70
a_4	96
α	36
w	216
s	239

For each of the bridge geometries, i.e., G1, G2, and 100-262-1, four different parametric models are developed including Flat web-Carbon Steel (FL-CS), Flat Web-Stainless Steel (FL-SS), Corrugated Web-Carbon Steel (CR-CS), and Corrugated Web-Stainless Steel (CR-SS) models. So, in total 12 parametric models were designed and their ultimate bending behavior were studied using the ABAQUS software package according to the approach that were verified in the previous section.

Material properties for G1 are presented in Table 5.9, and Table 5.10. Material properties for G2 are presented in Table 5.11 and Table 5.12. The used materials for 100-262-1 are listed in the Table 5.13. The classification of the cross section for the models and the ratio of the area of the corrugated web to the total steel area are presented in Table A 15 to Table A 17 in Appendix A.

Table 5.9 Material properties for G1 with flat web

Concrete	G1-FL-CS		G1-FL-SS	
C30/37	Flanges	Web	Flanges	Web
	S420	S355	Stainless steel D 1.4162	

Table 5.10 Material properties for G1 corrugated web

Concrete	G1-CR-CS		G1-CR-SS	
C30/37	Flanges	Web	Flanges	Web
	S420	S355	Stainless steel D 1.4162	

Table 5.11 Material properties for G2 with flat web

Concrete	G2-FL-CS		G2-FL-SS	
C50/60	Flanges	Web	Flanges	Web
	S420	S355	Stainless steel D 1.4162	

Table 5.12 Material properties for G2 corrugated web

Concrete	G2-CR-CS		G2-CR-SS	
C50/60	Flanges	Web	Flanges	Web
	S420	S355	Stainless steel D 1.4162	

Table 5.13 Material properties of bridge 100-262-1

Concrete	Original design (100-262-1-FL)		New design (100-262-1-CR)	
C35/45	Flanges	Web	Flanges	Web
	S420	S355	Stainless steel D 1.4162	

The results of the parametric studies for each of the girders will be presented in the subsequent sections for each of the girder geometries (G1, G2, and 100-262-1) and the results are compared with the base design in carbon steel and having a flat web.

5.2.1.3 The results of the parametric studies in G1

Load-displacement curves for the four models developed from the bridge G1 are shown in Figure 5.32 and the values of the ultimate load and the displacement for the developed models are listed in Table B.2 to Table B.5 in Appendix B.

By comparing the load-displacement curves in G1, it is obvious that the ultimate load for the models with stainless steel is higher than that for the models with carbon steel. Furthermore, the ultimate load for the models with the corrugated web is less than that for the models with the flat web. However, the models with the corrugated web have a more ductile behavior than those with the flat web and a larger displacement.

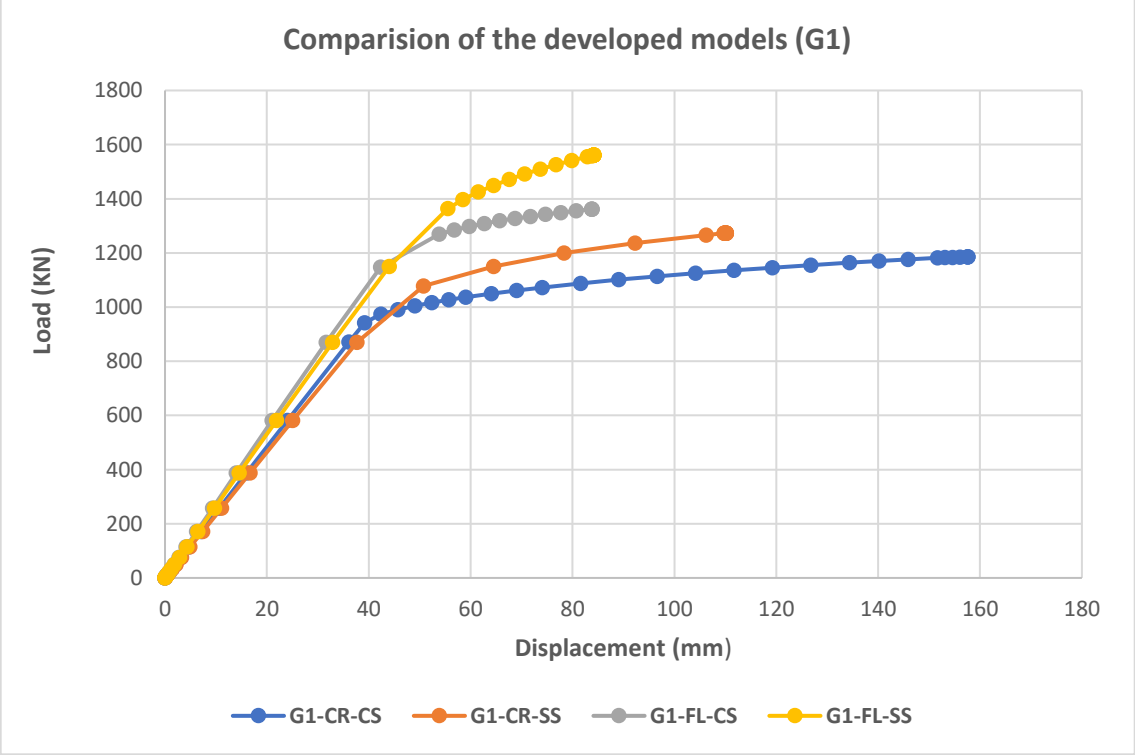

Figure 5.32 Comparison of the developed models from bridge (G1)

In order to investigate the effect of using stainless steel and corrugated web on the flexural capacity of composite bridges, a comparison has been done by normalizing the ultimate moment for each model with the ultimate moment for the model Flat web-Carbon Steel (FL-CS). The result was plotted as shown in Figure 5.33.

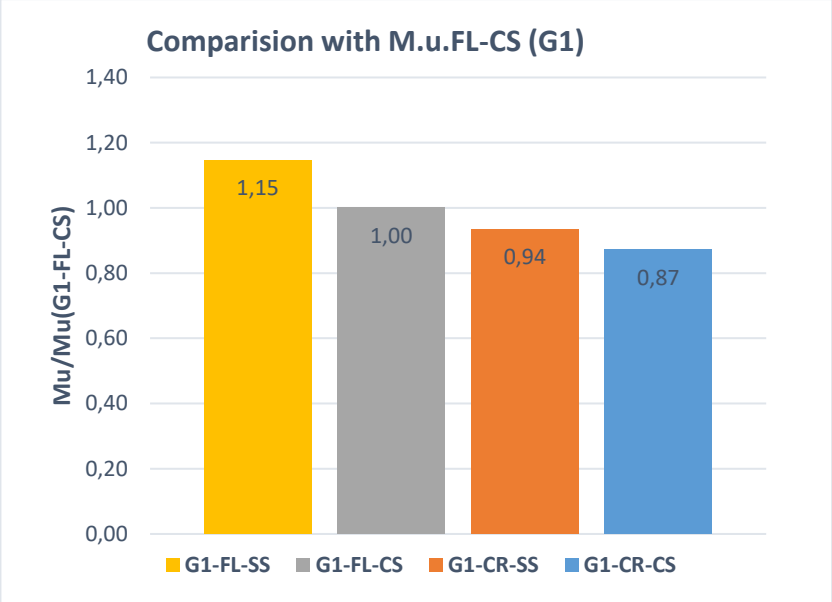

Figure 5.33 Comparison of ultimate bending moment of different models with ultimate bending moment of (G1-FL-CS).

The comparison shows that the model with flat web and stainless steel has 15% higher flexural capacity than the one with carbon steel. That agrees with what is discussed about the effect of strain hardening on the flexural capacity in section 4.2.

However, the model with corrugated web and carbon steel has 13% lower flexural capacity than the flat one. That agrees with the effect of corrugation on the flexural capacity explained in section 4.1. The web in a corrugated plate girder doesn't contribute to the flexural capacity due to the accordion effect. Based on that, the effective area of the steel will be reduced when using a corrugated web plate girder. Additionally, the height of the beam will affect the effect of corrugation on the flexural capacity since the corrugated area will be multiplied with its level arm when calculating the flexural capacity. Additionally, the model with corrugated web and stainless steel has 6% lower flexural capacity than the flat one. Therefore, using the concept of stainless-steel corrugated web will relieve the effect of corrugation on the flexural capacity.

The ultimate moment M_u for each model was also compared with the plastic bending capacity M_{pl} calculated according to Eurocode in order to evaluate the design models based on EN 1994-2. The bending capacity M_s according to the simplified model by (Shammas & Cashell, 2019) explained in Section 4.2 was also calculated for each model. Both M_{pl} and M_s are listed in Table 5.14 and the detailed calculations are presented in Appendix C.

Table 5.14 Plastic bending capacity for the developed models (G1)

Bridge	G1				
	X_{pl}/h	M_{pl}	M_s	M_u	M_u/M_{pl}
G1-FL-HS	0,21	4635		5315,956	1,146916
G1-FL-SS	0,204	3946	3982	4757,623	1,205682
G1-FL-CS	0,198	3512		4150,035	1,181673
G1-CR-SS	0,181	2969	3165	3881,872	1,303954
G1-CR-CA	0,175	2806		3614,715	1,288209

The ultimate moment M_u was normalized with the corresponding plastic bending capacity and plotted against the cross-section slenderness (X_{pl}/h) as illustrated in Figure 5.34.

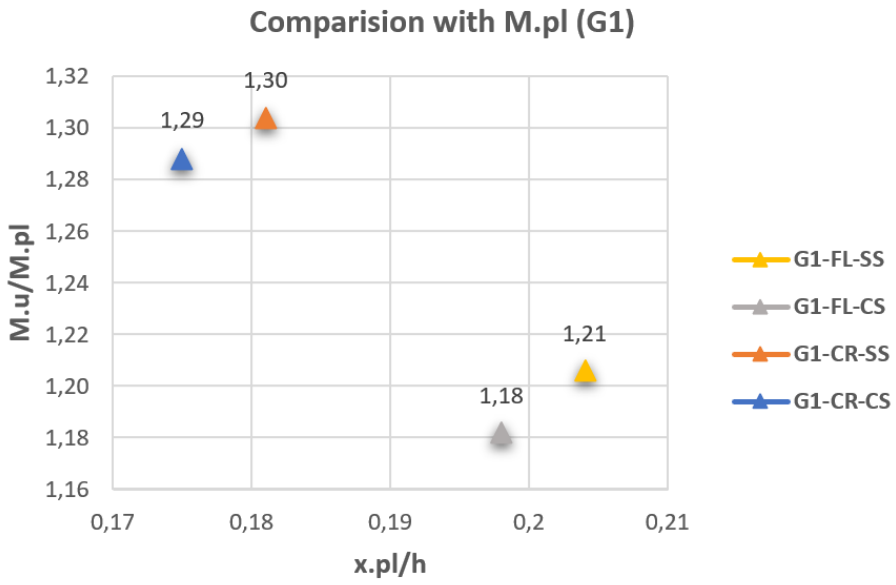

Figure 5.34 Ultimate bending moment normalized with plastic bending capacity against the ratio of the depth of the neutral axis to total depth.

The comparison shows that the ratio M_u/M_{pl} is larger than one for all models showing that the ultimate bending capacity is higher than the plastic bending capacity. This is because of strain hardening in stainless steel which is neglected when M_{pl} was calculated as discussed in section 4.2. Moreover, safety factors used by Eurocode to reduce the strength of the concrete when calculating M_{pl}, will contribute to a larger M_u/M_{pl} ratio.

The comparison also shows that the ratio for the models with stainless steel is higher than the ratio for the models with carbon steel since strain hardening in stainless steel is significantly remarkable as discussed in section 4.2. Furthermore, the ratio M_u/M_{pl}

for the models with corrugated web is larger than the ratio for the models with flat web due to the increased ductility caused by corrugation. Since the web in a corrugated plate girder doesn't contribute to the flexural capacity and the effective area of the steel will be reduced, the neutral axis will move upward causing a smaller x_{pl}/h and a slenderer cross-section. As a result, the beam will behave in a more ductile manner showing a more significant effect of strain hardening as discussed in 4.2, and the ratio M_u/M_{pl} will be larger also.

5.2.1.4 The results of the parametric studies in G2

The load-displacement curves for the four models developed based on G2 are shown in Figure 5.35. and the values of the ultimate load and the displacement are listed in Table B.7 to Table B.10 in Appendix B.

The load-displacement curves in G2 are similar to those in G1 having the ultimate load for models with stainless steel higher than that for models with carbon steel and the ultimate load for models with corrugated webs less than that for models with flat webs. Moreover, models with corrugated webs in G2 has also a ductile behavior and large displacement. However, models with corrugated webs show a more ductile behavior compared to those in G1 and the difference in the ultimate load because of corrugation is more notable in G2 compared to G1.

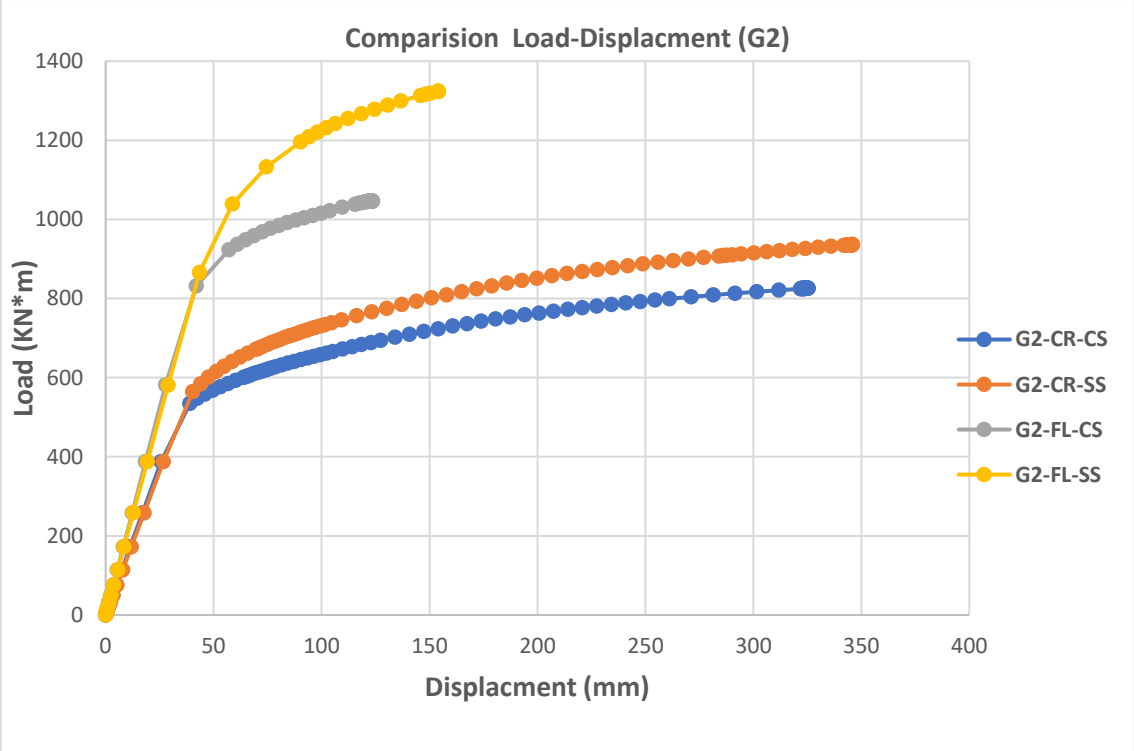

Figure 5.35 Load-displacement curves for the developed models (G2)

In order to investigate the effect of using stainless steel and corrugated web on the flexural capacity of composite bridges, a comparison has been done by normalizing the ultimate moment for each model with the ultimate moment for the model Flat web-Carbon Steel (FL-CS). The result was plotted as shown in Figure 5.36.

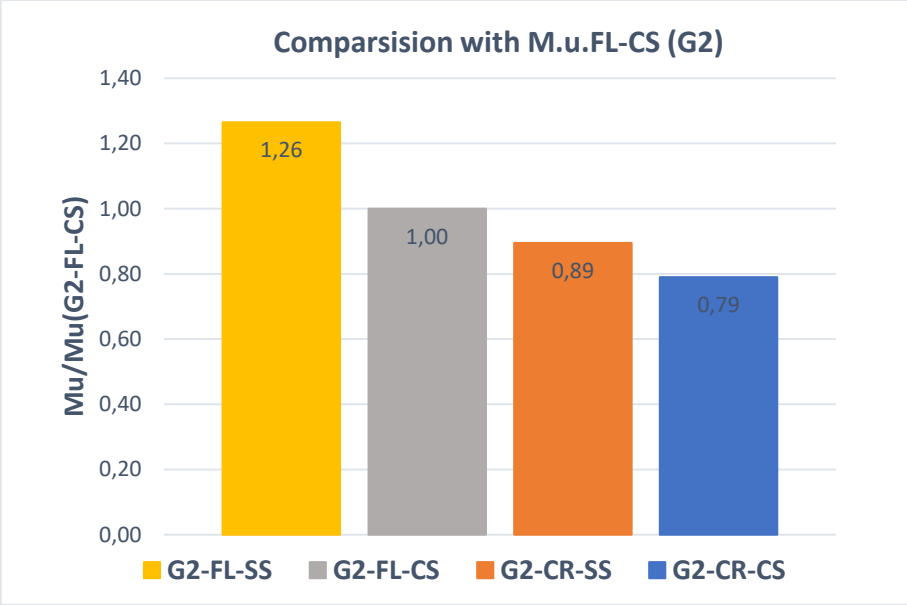

Figure 5.36 Comparison of ultimate bending resistance of different models with ultimate bending resistance of (G2-FL-CS).

The comparison in G2 shows that the model with flat web and stainless steel has 26% higher flexural capacity than the one with carbon steel. However, the model with corrugated web and carbon steel has 21% lower flexural capacity than the flat one. Using the concept of stainless-steel corrugated web in G2 resulted in 11% lower flexural capacity. The increase of the flexural capacity due to using stainless steel is more significant in G2 compared to G1. This is because G2 is slenderer than G1 and strain hardening is more significant as discussed in section 4.2. Moreover, the decrease caused by corrugation is more significant in G2 compared to G1. Since both beams has the same height, the larger corrugated area in G2 is the factor causing this significant decrease.

The ultimate moment M_u, the plastic bending capacity M_{pl}, and the bending capacity M.s for G2 are listed in Table 5.15 and the detailed calculations are presented in Appendix C.

Table 5.15 Plastic bending capacity for the developed models (G2)

Bridge	G2				
	X_{pl}/h	M_{pl}	M_s	M_u	M_u/M_{pl}
G2-FL-HS	0,168	4101		4383,908	1,0689
G2-FL-SS	0,106	3423	3810	4033,175	1,178257
G2-FL-CS	0,088	2907		3188,299	1,096766
G2-CR-SS	0,053	1788	2168	2852,428	1,595318

G2-CR-CA	0,049	1674		2517,514	1,503891

The ultimate load was normalized with the corresponding plastic bending capacity and plotted against the cross-section slenderness ($x_{.pl}/h$) as illustrated in Figure 5.37.

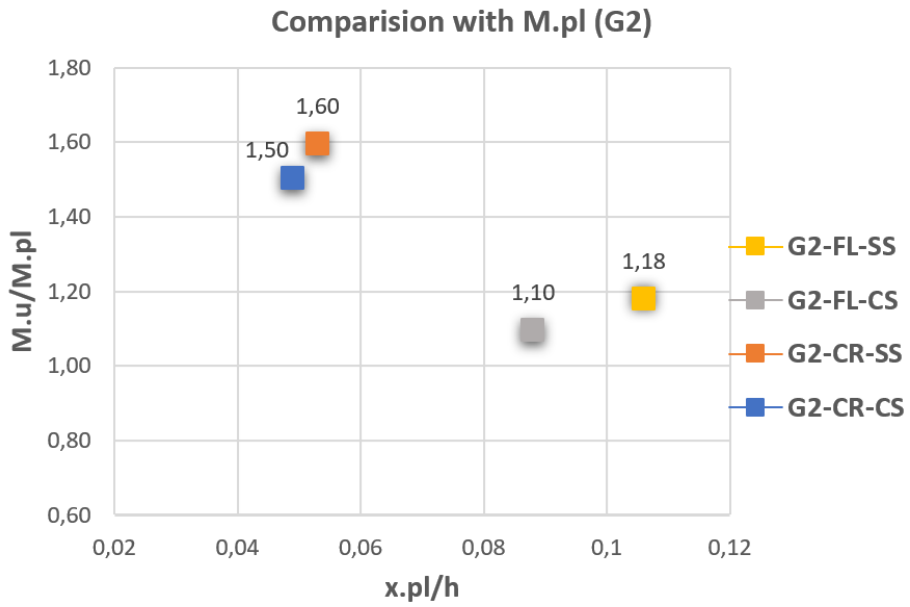

Figure 5.37 Ultimate bending moment normalized with plastic bending capacity against the ratio of the depth of the neutral axis to total depth

An analogous result to G1, ratios M_u/M_{pl} obtained from G2 are also larger than one. Furthermore, models with stainless steel have higher ratios than models with carbon steel since strain hardening in stainless steel is significantly remarkable. However, the difference of the ratio M_u/M_{pl} between stainless steel and carbon steel in G2 is about 8% for flat web models and 10% for corrugated web models compared to 3% for flat web models and 1% for corrugated web models in G1. This is because G2 has a slenderer cross section. This comparison shows how the slenderness of the cross section is important to exploit the effect of strain hardening as discussed in 4.2.

An analogous result to G1, the ratio for the models with corrugated web is larger than the ratio for the models with flat web. However, the difference of the ratio M_u/M_{pl} between flat models and corrugated models in G2 is about 40% compared to 10% in G1. The ratio of the area of the corrugated web to the total steel area is 49% in G2 compared to a ratio of 38% in G1 as listed in Table A 15 to Table A 17 in Appendix A. Consequently, the effect of the corrugation on the slenderness of the cross section is more significant in G2. That agrees with the discussion in 5.2.1.3.

5.2.1.5 The results of the parametric studies in 100-262-1

The 100-262-1 bridge girders have been also modelled using ABAQUS. The first model is the original design with Flat web-Carbon Steel (FL-CS), the second is with Flat Web-Stainless Steel (FL-SS), the third is Corrugated Web-Carbon Steel (CR-CS), and the fourth is the new design with Corrugated Web-Stainless Steel (CR-SS). The values of the ultimate load and the displacement for the models (bridge 100-262-1) are listed in Table B.11to Table B.14in Appendix B. Figure 5.38shows the vertical displacement of the Corrugated Web-Stainless Steel (CR-SS) model and Figure 5.39 shows the von mises stresses. The largest vertical displacement in the middle of the span is about 188 mm and the tensile stress of the stainless steel has exceeded its yielding stress of 450 MPa to reach up to 582 MPa.

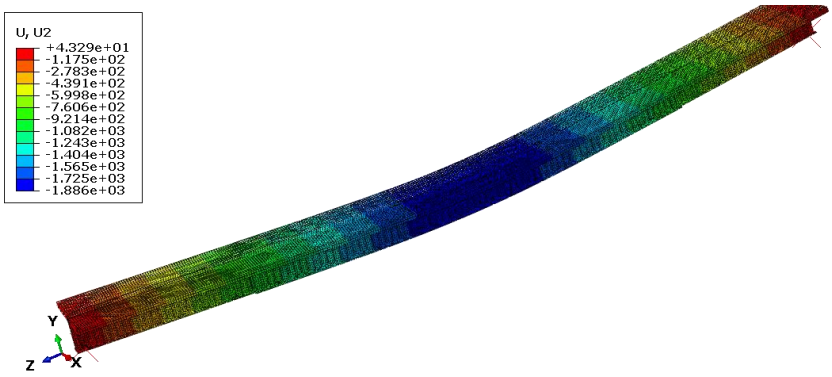

Figure 5.38 Vertical displacement (Bridge 100-262-1- CR-SS)

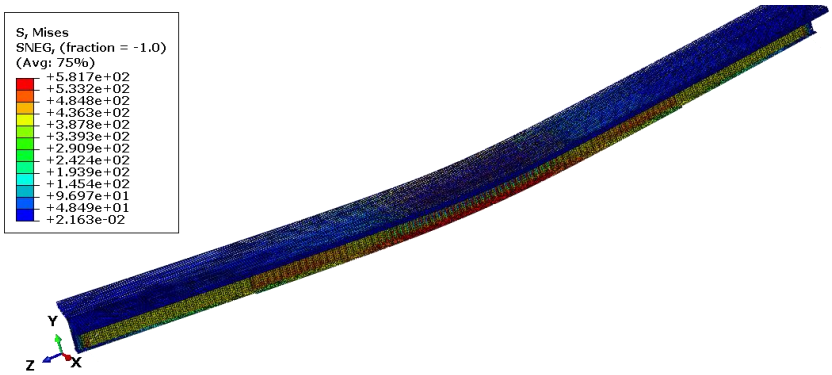

Figure 5.39 Von mises stress distribution (Bridge 100-262-1- CR-SS)

The failure modes of the model (262-CR-SS) were the crushing of concrete and yielding of steel plates. Figure 5.40 shows the crushing of concrete that is obvious since the strain in concrete exceeds the crushing strain of the concrete of 0,0037 for concrete class C35 as given in table (1) in Appendix A. Furthermore, Figure 5.41 shows the yielding of the steel plates at the ultimate load.

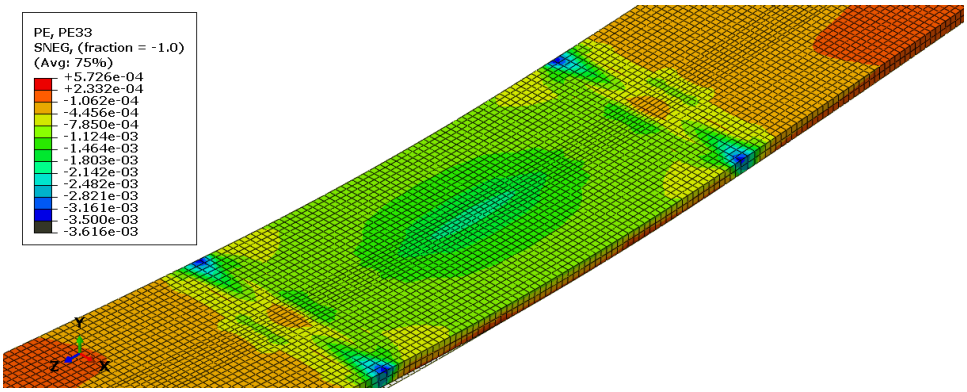

Figure 5.40 Crushing of concrete (Bridge 100-262-1- CR-SS)

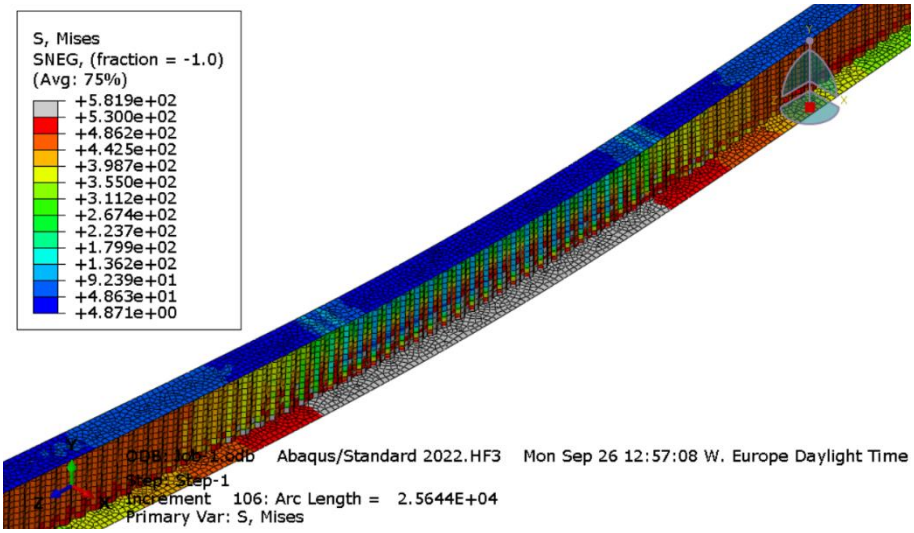

Figure 5.41 Yielding of steel plates (Bridge 100-262-1- CR-SS)

The load-displacement curves for the four models of the bridge 100-262-1 are shown in Figure 5.42.

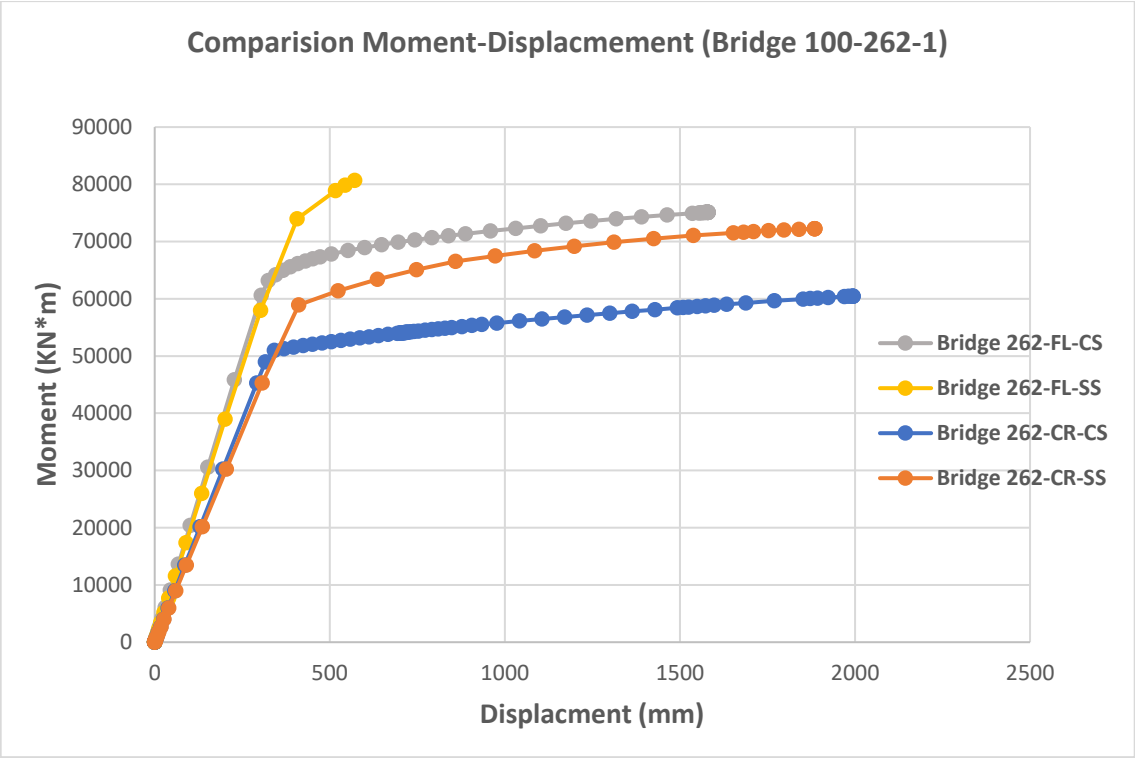

Figure 5.42 Comparison of load-displacement curves in 100-262-1 models

The load-displacement curves in 100-262-1 behave similar to those in G1 and G2 having the ultimate load for models with stainless steel higher than that for models with carbon steel and the ultimate load for models with corrugated webs less than that for models with flat webs. Moreover, models with corrugated webs in 100-262-1 has also a ductile behaviour and larger displacements. However, the increase in ductility caused by using a corrugated web is the least in 100-262-1 compared to that G1 and G2 and the difference in the ultimate load because the effect of corrugation is the least compared to G1 and G2.

In order to investigate the effect of using stainless steel and corrugated web on the flexural capacity of composite bridges, a comparison has been done by normalizing the ultimate moment for each model with the ultimate moment for the model Flat web-Carbon Steel (FL-CS). The result was plotted as shown in Figure 5.43.

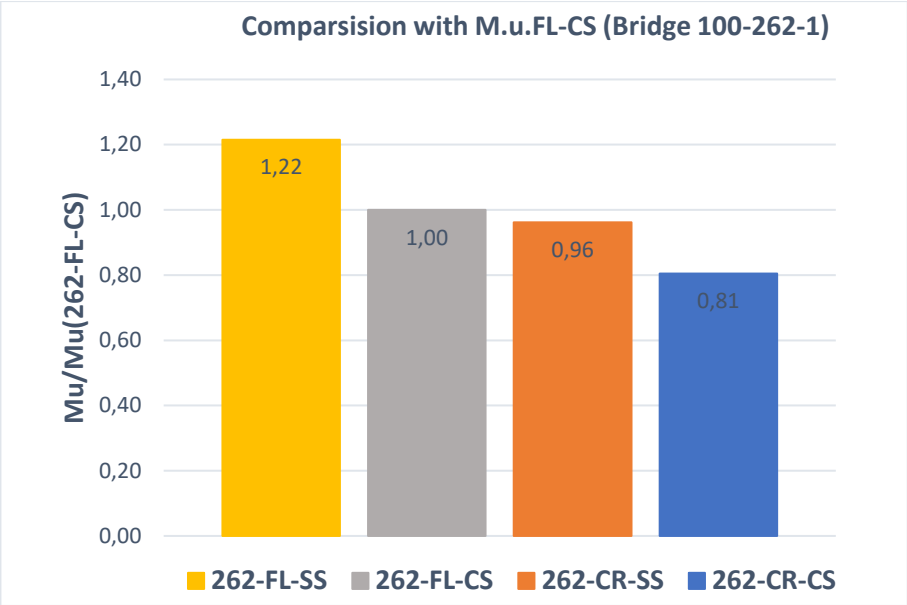

Figure 5.43 Comparison of ultimate bending resistance of different models with ultimate bending resistance of (100-262-1 -FL-CS).

The comparison in 100-262-1 shows that the model with flat web and stainless steel has 22% higher flexural capacity than the one with carbon steel. However, the model with corrugated web and carbon steel has 19% lower flexural capacity than the flat one. Using the concept of stainless-steel corrugated web in 100-262-1 resulted in 4% lower flexural capacity. The reduction in flexural capacity of 100-262-1 due to corrugation is 19% compared to 13% in G1. Although the ratio of the area of the corrugated web to the total steel area is larger in G1 compared to 100-262-1, the reduction of the flexural capacity due to corrugation is 19% in 100-262-1 compared to 13% in G1 since the height of 100-262-1 is 2.37 m compared to 0.98 m in G1 as discussed in 5.2.1.3.

The ultimate moment M_u, the plastic bending capacity M_{pl}, and the bending capacity M_s for 100-262-1 are listed in Table 5.16 and the detailed calculations are presented in Appendix C.

Table 5.16 Plastic bending capacity for models of (Bridge 100-262-1)

Bridge	Bridge 262-100-2				
	X_{pl}/h	M_{pl}	M_s	M_u	M_u/M_{pl}
262-FL-SS	0,152	73220	76260	91273,38	1,246564
262-FL-CS	0,148	64100		75106,47	1,171708
262-CR-SS	0,142	55810	62090	72263,22	1,294808
262-CR-CA	0,14	50720		60463,93	1,192112

The ultimate load was normalized with the corresponding plastic bending capacity and plotted against the cross-section slenderness (x.pl/h) as illustrated in Figure 5.44.

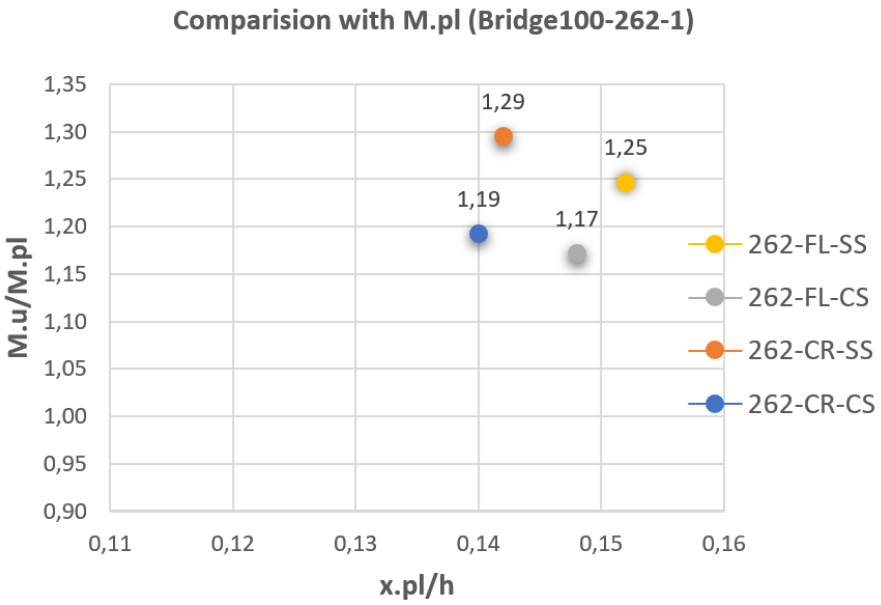

Figure 5.44 Ultimate bending moment normalized with plastic bending capacity against the ratio of depth of the neutral axis to the total depth

Compared to G1 and G2, similar results of the ratios M_u/M_{pl} were obtained from 100-262-1. The ratios are also larger than one. Furthermore, models with stainless steel have higher ratios than models with carbon steel since strain hardening in stainless steel is significantly remarkable. However, the difference of the ratio M_u/M_{pl} between stainless steel and carbon steel in 100-262-1 is about 8% for flat web models and 10% for corrugated web models compared to 8% for flat web models and 10% for corrugated web models in G2 and to 3% for flat web models and 1% for corrugated web models in G1. From that comparison, it's obvious that when the slenderness of the cross section is less than 0.15 wich is the case in G1 and G2, the strain hardening of stainless steel can affect the cross section flexural capacity to be increased with about 10% compared to carbon steel. However, when the slenderness of the cross section was about 0.18 which is the case in G1, the effect of strain hardening in stainless steel was not exploited effectively and was limited to 3% higher flexural capacity compared with carbon steel as discussed in 4.2.

An analogous result to G1 and G2, the ratio for the models with corrugated web is larger than the ratio for the models with flat web. However, the difference of the ratio M_u/M_{pl} between flat models and corrugated models in 100-262-1 is about 4% compared to 10% in G1 and 40% in G2. The ratio of the area of the corrugated web to the total cross-sectional area of the steel is 25% in 100-262-1 compared to a ratio of 38% in G1 and 49% in G2. As a result, the effect of the corrugation on the slenderness of the cross section is the most G2 and it is more notable in G1 compared to 100-262-1. It That agrees with the discussion in 5.2.1.3.

6 Discussion

By comparing the results from all the 12 models which were developed based on three real bridge girders, the bar chart shown in Figure 6.1 shows that models with FL-SS have 15-22% higher flexural capacity than models with FL-CS. Although, strain hardening is one reason for that, it can't be concluded that the increase is only caused by strain hardening since the yield strength of the used carbon steel is $f_y = 355$ for the web and $f_y = 420$ for the flanges compared to $f_y = 480$ for the web and $f_y = 450$ for the flanges in the used stainless steel. However, the strain hardening effect can be determined by comparing the ultimate bending capacity to the plastic bending capacity calculated according to Eurocode.

The comparison also shows that models with CR-CS have 13-21% lower flexural capacity than models with FL-CS. It has been noted that the larger the ratio of the area of the web to the area of the cross-section of the steel, the higher is the reduction of the ultimate load due to the corrugation. The web in a corrugated plate girder doesn't contribute to the flexural capacity due to the accordion effect as discussed in section 4.1. Based on that, the effective area of the steel will be reduced when using a corrugated web plate girder. Additionally, the height of the beam will affect the effect of corrugation on the flexural capacity since the corrugated area will be multiplied with its level arm when calculating the flexural capacity.

The effect of the area of the corrugated web on the flexural capacity can be easily noted by comparing G1 and G2. Since both has the same height of the beam, the difference of the reduction of the cross-section capacity cause by corrugation is only related to the area of the corrugated web. The ratio of the area of the corrugated web to the total steel area is 49% in G2 compared to a ratio of 38% in G1. The reduction of the flexural capacity is 21% in G2 compared with 13% in G1.

Although the ratio of the area of the corrugated web to the total steel area is 38% in G1 compared to 25% in 100-262-1, the reduction of the flexural capacity due to corrugation is 19% in 100-262-1 compared to 13% in G1 since the height of 100-262-1 is $2.37\ m$ compared to $0.98\ m$ in G1. This increased height has increased the reduction of the flexural capacity due to corrugation in 100-262-1 as discussed in 5.2.1.3.

This agrees with the discussion in section 4.1 concluding that using corrugated web plate girders results in a bending resistance that is about 10 to 20% less than the bending resistance of the same plate girder with a flat web due to the accordion effect. This reduction depends on the area of the corrugated web, the height of the plate girder and the geometry of the corrugated profile as discussed in section 4.1.

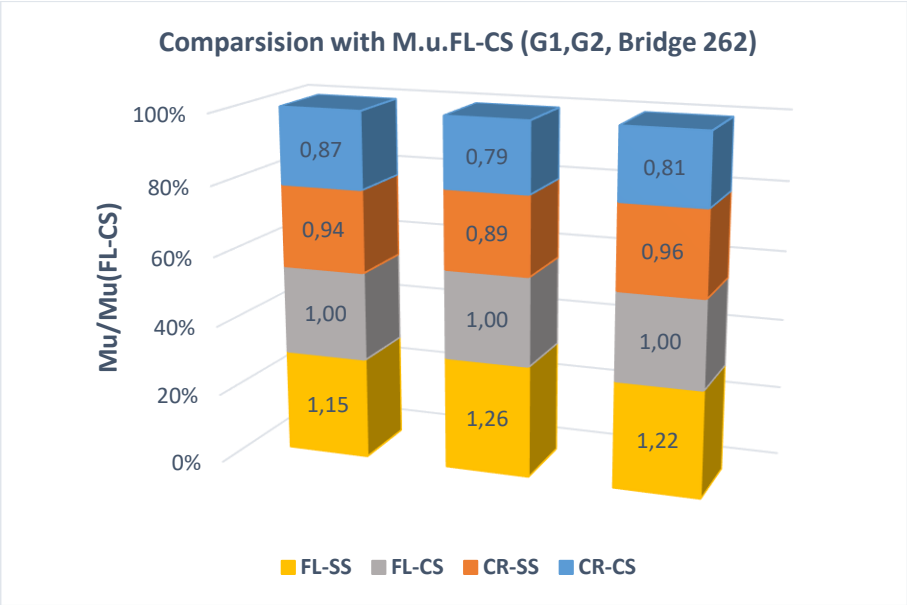

Figure 6.1 Comparison of ultimate bending resistance with M.u.FL-CS for all models

To exclude the effect of the difference of the yield strength of the stainless steel and the conventional steel on the obtained results, the ultimate bending capacity will be compared with the plastic bending capacity calculated according to Eurocode.

Figure 6.2 shows that M_u is always larger than M_{pl}. due to strain hardening and the conservatism in (EN 1994-2, 2005) that limits the bending resistance to the plastic bending resistance. One more reason is the safety factors that reduce the strength of concrete when calculating M.pl contribute to a larger difference between M_u and M_{pl}. The larger is the compressed area of concrete, the larger is the ratio M_u/M_{pl}. Another reason is that Eurocode neglects the contribution of the reinforcement to the flexural capacity.

To exclude all the mentioned factors from the comparison and to only keep the effect of strain hardening, the difference of the ratio M_u/M_{pl} in stainless steel and carbon steel can be calculated. Since both ratios are affected with other factors than strain hardening, the difference of the ratios will reflect the pure strain hardening effect.

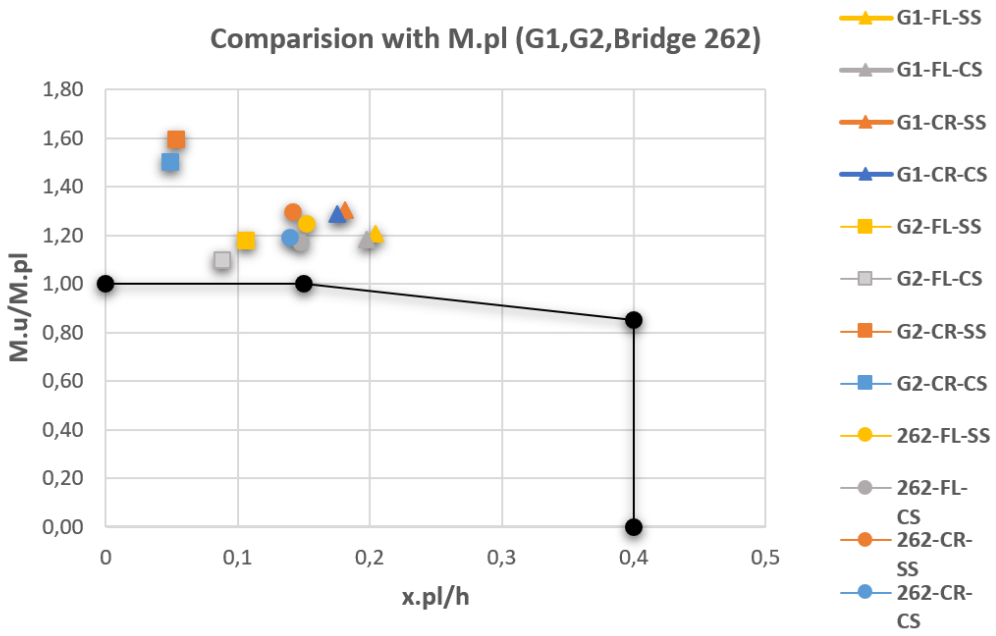

Figure 6.2 Mu/M.pl for all models

The difference of the ratio M_u/M_{pl} between stainless steel and carbon steel models in 100-262-1 is about 8% for flat web models and 10% for corrugated web models compared to 8% for flat web models and 10% for corrugated web models in G2 and to 3% for flat web models and 1% for corrugated web models in G1. These differences correspond to the effect of strain hardening in each model. From that comparison, it's obvious that when the slenderness of the cross section is less than 0.15 wich is the case in 100-262-1 and G2, the strain hardening of stainless steel can affect the cross section flexural capacity to be increased with about 10% compared to carbon steel. However, when the slenderness of the cross section was about 0.18 which is the case in G1, the effect of strain hardening in stainless steel was not exploited effectively and was limited to 3% higher flexural capacity compared with carbon steel. This comparison shows how the slenderness of the cross section is important to exploit the effect of strain hardening as discussed in 4.2. It also shows that strain hardening can contribute up to 10% higher flexural capacity.

Compared to the results of the bending tests (Zhou, et.al, 2021) reported in the literature review section 4.2, the resistance of the cross section using stainless steel is about 15% to 25% larger than the plastic bending resistance due to strain hardening. Although this increase is not only from strain hardening since the code neglects the contribution of the reinforcement to the flexural capacity and reduces the strength of the concrete, but however strain hardening is expected to be more significant in the specimens of the test since they have relatively small dimension to be in Class (1) and not near to the common dimension in bridge girders. G1 has the upper flange to be in Class (1), the lower flange and the web in Class (3). Moreover, G2 has an upper and lower flange of Class (1) and a web of class 3. 100-262-1 has a Class (4) web and Class (3) flanges. A stocky cross section is needed to have a sufficient ductility for strain hardening to develop in the lower flange of a ductile cross section before the collapse moment is reached (Shammas & Cashell, 2019). However, 100-262-1 reached an increase in the flexural capacity of

10% with a lower flange of Class (3) and a sufficient cross section slenderness x_{pl}/h. Reaching a higher increase in the flexural capacity need a more ductile cross section.

Moreover, the difference of the ratio M_u/M_{pl} between flat models and corrugated models in G2 is about 40% compared to 10% in G1. The ratio of the area of the corrugated web to the total steel area is 49% in G2 compared to a ratio of 38% in G1. Since the web in a corrugated plate girder doesn't contribute to the flexural capacity and the effective area of the steel will be reduced, the neutral axis will move upward causing a smaller x_{pl}/h and a slenderer cross-section. As a result, the beam will behave in a more ductile manner showing a more significant effect of strain hardening as discussed in 4.2, and the ratio M_u/M_{pl} will be larger also. However, the difference of the ratio M_u/M_{pl} between flat models and corrugated models in 100-262-1 is about 4% since the ratio of the area of the corrugated web to the total steel area is only 25% in 100-262-1. It can be concluded that the corrugation increases the ductility of the cross section and the effect of strain hardening and that increase is proportional to the ratio of the area of the corrugated web to the total steel area.

Finally, using the concept of corrugated stainless steel plate girder will be affected by both the accordion effect and the effect of strain hardening of the stainless steel. The accordion effect reduced the flexural capacity 21% in G2, and the corrugation increased the slenderness of the cross section x_{pl}/h and provided a sufficient ductility that the stainless steel reaches a 10% increased flexural strength. The comparison in Figure 6.1 shows that the model G2-CR-SS has 11% lower flexural capacity compared to G2-FL-CS combining both the effect of strain hardening and the accordion effect. Although the reduction of the flexural capacity in G1 was less than that in G2 to be 13%, and the corrugation was not able to provide a sufficient ductility that the increase of the flexural capacity caused by strain hardening was only 1%. The comparison in Figure 6.1 shows that the model G1-CR-SS has 6% lower flexural capacity compared to G1-FL-CS. It can be concluded that the concept of stainless-steel corrugated web plate girders combines the effect of strain hardening in stainless steel that depends on the ductility of the cross section having stocky elements and the global slenderness of the cross section x_{pl}/h, the reduction of the flexural capacity caused by corrugation that depends on the area of the corrugated web and the height of the cross section, and the effect of the corrugation on the slenderness of the cross section that depends on the area of the corrugated web.

7 Conclusion

From the literature review and the numerical study, it can be concluded that using stainless steel in composite bridges contributes to a higher flexural capacity due to its remarkable strain hardening. Strain hardening can develop in ductile cross-sections that has stocky elements and a sufficient cross-sectional slenderness x_{pl}/h . However, using a corrugated web in composite bridges contributes to a lower flexural capacity due to the so-called accordion effect that reduces the axial stiffness of the corrugated web. The reduction of the flexural capacity increases when the ratio of the area of the corrugated web to the total area of steel increases. The reduction increases also with the increased height of the cross section. On the other hand, the corrugated web increases the ductility of the cross section by increasing the slenderness of the cross section and this increase depends on the ratio of the area of the corrugated web also. This contributes to a more significant strain hardening effects when using the concept of stainless steel and corrugated web. The concept combines the effect of strain hardening, the reduction of the flexural capacity due to the corrugation, and the increase of the slenderness of the cross section due to corrugation. Finally, the design models for calculating M.pl according to Eurocode need to be updated for stainless steel since it neglects the effect of strain hardening.

8 References

Henrysson, A., & Yman , E. (2020). *Design of Composite Steel-Concrete Bridges using Stainless Steel Girders with Corrugated Web.* Master's thesis , Chalmers University of Technology, Department of Architecture and Civil Engineering, Gothenburg.

Inaam, Q., & Upadhyay , A. (2022, January 1). Accordion Effect in Bridge Girders with Corrugated Webs. *Journal of Constructional Steel Research*, 13.

Krona, K.-M. (2019). Krav Brobyggande.

Vayas, I., & Iliopoulos, A. (2014). *Design of Steel-Concrete Composite Bridges to Eurocodes.* New York: Taylor & Francis Group.

A.Jaafer, A., & L.Kareem, S. (2020). Behaviour of Curved Steel-Concrete Composite Beams under Monotonic Load.

Afshan, S., & Gardner, L. (2013). *The Continuous Strength Method for Structural Stainless Steel Design.*

Agampodi , M., Safat, A.-D., & Ashraf, M. (2018). *Flexural Shear Behaviour of Reinforced Crumbed Rubber Concrete Beam.* Canberra: The university of South Wales.

Design manual for structural stainless steel (4 ed.). (2018). United Kingdom: SCI.

Elammary, A., Saddek, A., & Alwetaishi, M. (2017). Effect of Corrugated Web on Flexural Capacity of Steel Beams.

ELgaaly, M., & Seshadri, A. (1997). Girders with Corrugated Webs Under Partial Compressive Edge Loading.

Ellobody, E. (2014). *Finite Element Analysis and Design of Steel and Steel-Concrete Composite Bridges.*

EN 1992-1-1. (2005). In *Eurocode 2: Design of concrete structures - Part 1-1: General rules and rules for buildings.* CEN.

EN 1993-1-1. (2005). In *Eurocode 3: Design of steel structures - Part 1-1: General rules and rules for building* (p. 91). CEN.

EN 1993-1-4. (2020). In *Eurocode 3- Design of steel structures-Part 1-4:General rules-Supplementary for stainless steels.* CEN.

EN 1993-1-5. (2005). In *Eurocode 3: Design of steel structures-Part 1-5: Plated Structural Elements.* CEN.

EN 1993-1-8. (2005). In *Eurocode 3: Design of steel structures- Part 1-8 : Design of jionts* (p. 133). CEN.

EN 1994-1-1. (2005). In *Eurocode 4: Design of composite steel and concrete structures-Part 1.1: General rules and rules for buildings.* Brussels: CEN.

EN 1994-2. (2005). In *Eurocode 4: Design of composite steel and concrete structures: Part 2: General rules and rules for bridges.* CEN.

EN10025. (2014). In *EN10025: The European Standard for grades of structural steel.*

Hafezolghorani, M., Hejazi, F., Vaghei, R., & Bin Jaafar, M. S. (2017, Febraury). *Simplified Damage Plasticity Model for Concrete.*

Hällmark, R. (2018). *Composite Bridges: Innovative Ways of Achieving Composite Action.* Luleå: Luleå university of technology.

Jankowiak, T., & Lodygowski, T. (2005). *Identification of Parameters OF Concrete Damage Plasticity Constitutive Model.* Poznan University of Technology, Institute of Structural Engineering (ISE), Poznan.

Jun , H., Yuqing, L., Airong , C., & Teruhiko, Y. (2012, September). Mechanical Behavior and Analysis of Composite Bridges with Corrugated Steel Webs: State-of-the-Art. *International Journal of Steel Structures*, *12*, 19.

Mans, P., Yakel, A., & Azizinamini, A. (2001). Full-Scale Testing Of Composite Plate Girders .

Plus, M., Zandi, K., Johansson, M., & Shu, J. (2021). Recommendations for Assessment of Reinforced Concrete Slabs. In *Enhanced structural analysis with the finite element method* (p. 171). Guthenberg.

Shammas, R., & Cashell, K. (2019). *Analysis of Stainless Steel-Concrete Composite Beams.*

Zhou, Y., Uy, B., Wang, J., Li, D., Huang, Z., & Liu, X. (2021). Behaviour and Design of Stainless Steel-Concrete Composite Beams. *Journal of constructional steel research*.

Appendix A

Table A.1 Material properties for concrete strength C30/37 in compression

$C30/37$			
ε_{true}	$\varepsilon_{inelastic}$	σ_{true} (MPa)	d_c
0,000495	3,38E-05	15,2076117	0
0,00055	4,48E-05	16,6664564	0
0,001099	0,000234	28,5600448	0
0,001649	0,000567	35,6945315	0
0,002198	0,001044	38,0836	0
0,002796	0,001727	35,2937068	0,071218
0,003095	0,002132	31,7925278	0,163355
0,003394	0,002579	26,8901064	0,292366
0,003793	0,003242	18,1775935	0,521642
0,004043	0,003696	11,4465812	0,698774

Table A.2 Material properties for concrete strength C35/45 in compression

$C35/45$			
ε_{true}	$\varepsilon_{inelastic}$	σ_{true} (MPa)	d_c
0,000532	2,57E-05	17,20901093	0
0,00055	2,85E-05	17,72561829	0
0,001099	0,00018	31,26327976	0
0,001649	0,000473	39,97635895	0
0,002198	0,00093	43,0946	0
0,002796	0,001649	39,00423419	0,092925
0,003095	0,002108	33,5790766	0,219091
0,003295	0,002454	28,5623519	0,335759
0,003494	0,002837	22,33958643	0,480475
0,003738	0,003357	12,95356874	0,698754

Table A.3 Stress and strain values for concrete strength C50/60 in compression

$C50/60$			
ε_{true}	$\varepsilon_{inelastic}$	σ_{true} (MPa)	d_c
0,000484	-1,2E-05	18,3543626	0
0,0005	-1,2E-05	18,9335715	0
0,001	1,6E-05	36,388991	0
0,001499	0,000123	50,8943313	0
0,001998	0,000427	58,116	0
0,002247	0,000772	54,5978418	0,058658
0,002397	0,001129	46,9362977	0,190753

0,002497	0,001488	37,3276543	0,35642
0,002597	0,002024	21,1779406	0,634863
0,002614	0,002142	17,4390785	0,699326

Table A.4 Material properties for concrete strength C30/37 in tension

C 30/37 (Tension)		
G_F	0,12	N/mm
f_{ctm}	2,9	MPa
Band width (h)	50	mm
ε	σ $(\boldsymbol{MPa})$	d_t
0	2,9	0
0,000827586	1,45	0,5
0,001655172	0	0,99

Table A.5 Material properties for concrete strength C35/45 in tension

C 35/45 (Tension)		
G_F	0,14	N/mm
f_{ctm}	3,2	MPa
Band width (h)	50	mm
ε	σ $(\boldsymbol{MPa})$	d_t
0	3,2	0
0,000875	1,6	0,5
0,00175	0	0,99

Table A.6 Stress and strain values for concrete strength C50/60 in tension

$C50/60$(Tension)		
$\boldsymbol{G_F}$	0,16	N/mm
$\boldsymbol{f_{ctm}}$	4,1	MPa
Band width $(\boldsymbol{h})$	50	mm
$\boldsymbol{\varepsilon}$	$\boldsymbol{\sigma}$ $(\boldsymbol{MPa})$	$\boldsymbol{d_t}$
0	4,1	0
0,000780488	2,05	0,5
0,001560976	0	0,99

Table A.7 Stress and strain values for steel strength HPS-556

High performance steel HPS-556					
	$\boldsymbol{\sigma}$ $(\boldsymbol{MPa})$	$\boldsymbol{\varepsilon}$	$\boldsymbol{\sigma_{true}}$ $(\boldsymbol{MPa})$	$\boldsymbol{\varepsilon_{true}}$	$\boldsymbol{\varepsilon_{inelastic}}$
$\boldsymbol{f_y}$ $(\boldsymbol{MPa})$	0	0	0	0	0
	556	0,002648	557,4721	0,002644	0
$\boldsymbol{f_u}$ $(\boldsymbol{MPa})$	700	0,071219	749,8533	0,068797	0,066149678
$\boldsymbol{E}$	210000	MPa			

Table A.8 Stress and strain values for steel strength HPS-583

High performance steel HPS-583					
	$\boldsymbol{\sigma}$ $(\mathbf{MPa})$	$\boldsymbol{\varepsilon}$	$\boldsymbol{\sigma_{true}}$ $(\mathbf{MPa})$	$\boldsymbol{\varepsilon_{true}}$	$\boldsymbol{\varepsilon_{inelastic}}$
$\boldsymbol{f_y}$ $(\boldsymbol{MPa})$	0	0	0	0	0
	583	0,002776	584,6185	0,002772	0
$\boldsymbol{f_u}$ $(\boldsymbol{MPa})$	656	0,037538	680,625	0,036851	0,0340745
$\boldsymbol{E}$	210000	MPa			

Table A.9 Stress and strain values for steel strength S420

Carbon steel S420					
	$\boldsymbol{\sigma}$ $(\boldsymbol{MPa})$	$\boldsymbol{\varepsilon}$	$\boldsymbol{\sigma_{true}}$ $(\boldsymbol{MPa})$	$\boldsymbol{\varepsilon_{true}}$	$\boldsymbol{\varepsilon_{inelastic}}$
$\boldsymbol{f_y}$ $(\boldsymbol{MPa})$	0	0			
	420	0,002	420,84	0,001998	0
$\boldsymbol{f_u}$ $(\boldsymbol{MPa})$	520	0,049619	545,8019	0,048427	0,045779667
$\boldsymbol{E}$	210000	MPa			

Table A.10 Stress and strain values for steel strength S355

Carbon steel S355					
	$\boldsymbol{\sigma}$ $(\boldsymbol{MPa})$	$\boldsymbol{\varepsilon}$	$\boldsymbol{\sigma_{true}}$ $(\boldsymbol{MPa})$	$\boldsymbol{\varepsilon_{true}}$	$\boldsymbol{\varepsilon_{inelastic}}$
$\boldsymbol{f_y}$ $(\boldsymbol{MPa})$	0	0			
	355	0,00169	355,6001	0,001689	0
$\boldsymbol{f_u}$ $(\boldsymbol{MPa})$	470	0,056452	496,5326	0,054916	0,052140294
$\boldsymbol{E}$	210000	MPa			

Table A.11 Stress and strain values for steel strength B 500

Carbon steel Reinforcement (413,7 MPa)					
	$\boldsymbol{\sigma}$ (MPa)	$\boldsymbol{\varepsilon}$	$\boldsymbol{\sigma_{true}}$ $(\boldsymbol{MPa})$	$\boldsymbol{\varepsilon_{true}}$	$\boldsymbol{\varepsilon_{inelastic}}$
	0	0			
$\boldsymbol{f_y}$ $(\boldsymbol{MPa})$	413,7	0,002069	414,5557	0,002066	0
$\boldsymbol{f_u}$ $(\boldsymbol{MPa})$	620,5	0,105469	685,9432	0,100269	0,097493037
$\boldsymbol{E}$	200000	MPa			

Table A.12 Material Properties for stainless-steel D1.1462 ($t \leq 8\ mm$)

Stainless Steel D 1.1462 ($\boldsymbol{t \leq 8\ mm}$)						
Stainless steel Parameters		$\boldsymbol{\sigma}$ (MPa)	$\boldsymbol{\varepsilon}$	$\boldsymbol{\sigma_{true}}$ $(\boldsymbol{MPa})$	$\boldsymbol{\varepsilon_{true}}$	$\boldsymbol{\varepsilon_{inelastic}}$
$\boldsymbol{n}$	5	0	0	0	0	0
$\boldsymbol{m}$	3.65	50	0.000250015	50.01250075	0.000249984	0
$\boldsymbol{\varepsilon_{0.002}}$	0.002	100	0.000500478	100.0500478	0.000500353	0
$\boldsymbol{E}$ $(\boldsymbol{MPa})$	200000	150	0.000753632	150.1130448	0.000753348	0
$\boldsymbol{f_y}$ $(\boldsymbol{MPa})$	530	199	0.001009925	199.2009751	0.001009415	0
$\boldsymbol{f_u}(\boldsymbol{MPa})$	700	200	0.001015304	200.2030608	0.001014789	0
$\boldsymbol{E_y}$	41897.2332	250	0.001296704	250.3241759	0.001295864	0
$\boldsymbol{e_u}$	0.242857143	300	0.001616214	300.4848641	0.001614909	0
		350	0.002001183	350.7004142	0.001999184	0
		382	0.002299016	382.8782241	0.002296377	0
		420	0.002725025	421.1445103	0.002721318	0
		450	0.003132497	451.4096236	0.003127601	0
		500	0.003994516	501.9972582	0.003986559	0
		525	0.004532424	527.3795224	0.004522183	0
		530	0.00465	532.4645	0.004639222	0
		535	0.004769964	537.5519307	0.004758624	0.002070864
		550	0.005225753	552.8741643	0.005212146	0.002447776
		575	0.007622676	579.3830389	0.007593771	0.004696855
		600	0.015844772	609.5068631	0.015720554	0.012673019
		625	0.035951226	647.4695162	0.035320063	0.032082716
		650	0.075626188	699.1570219	0.072902992	0.069407207
		675	0.14400649	772.2043808	0.134536566	0.130675544
		685	0.181699197	809.4639501	0.1669534	0.162906081
		700	0.25156469	876.095283	0.224394521	0.220014044

Table A.13 Material Properties for stainless-steel D1.1462 ($t \leq 13.5\ mm$)

Stainless Steel D 1.1462 ($t \leq 13.5\ mm$)						
Stainless Steel Parameters		σ (MPa)	ε	σ_{true} (MPa)	ε_{true}	$\varepsilon_{inelastic}$
n	5	0	0	0	0	0
m	3.470588235	50	0.000250025	50.01250123	0.000249993	0
$\varepsilon_{0.002}$	0.002	100	0.000500785	100.0500785	0.00050066	0
E(MPa)	200000	150	0.00075596	150.1133941	0.000755675	0
f_y(MPa)	480	200	0.001025117	200.2050235	0.001024592	0
f_u(MPa)	680	250	0.001326652	250.331663	0.001325773	0
E_y	38709.67742	300	0.001690735	300.5072205	0.001689307	0
e_u	0.294117647	350	0.002162253	350.7567886	0.002159919	0
		382	0.00254847	382.9735156	0.002545228	0
		420	0.003125818	421.3128435	0.003120943	0
		450	0.003698393	451.6642768	0.003691571	0
		480	0.0044	482.112	0.004390348	0
		500	0.005016192	502.5080959	0.005003653	0.002491112
		520	0.006536609	523.3990366	0.006515338	0.003898343
		525	0.007222902	528.7920238	0.007196942	0.004552982
		530	0.008085086	534.2850955	0.008052577	0.005381151
		535	0.009152609	539.8966457	0.009110978	0.006411494
		550	0.013902631	557.6464472	0.013806876	0.011018644
		575	0.029059522	591.7092252	0.0286453	0.025686754
		600	0.057454593	634.4727556	0.055864693	0.052692329
		625	0.10448698	690.3043626	0.099380956	0.095929434
		650	0.176117593	764.4764352	0.162218838	0.158396456
		675	0.278814574	863.1998376	0.245933535	0.241617536
		680	0.303684314	886.5053333	0.265194343	0.260761817

Table A.14 Material Properties for stainless-steel D1.1462 ($t \leq 75\ mm$)

Stainless Steel D 1.1462 ($t \leq 75\ mm$)						
Stainless Steel Parameters		σ (MPa)	ε	σ_{true} (MPa)	ε_{true}	$\varepsilon_{inelastic}$
n	5	0	0	0	0	0
m	3.423076923	50	0.000250034	50.01250169	0.000250003	-5.98916E-08
$\varepsilon_{0.002}$	0.002	100	0.000501084	100.0501084	0.000500958	7.07803E-07
E(MPa)	200000	150	0.00075823	150.1137346	0.000757943	7.37447E-06
f_y(MPa)	450	200	0.001034683	200.2069366	0.001034148	3.31135E-05
f_u(MPa)	650	250	0.001355844	250.3389611	0.001354926	0.000103231
E_y	36734.69388	300	0.001763374	300.5290123	0.001761822	0.000259177
e_u	0.307692308	350	0.002319256	350.8117396	0.002316571	0.000562512
		382	0.002791626	383.066401	0.002787736	0.000872404
		420	0.003516491	421.4769263	0.003510323	0.001402938
		450	0.00425	451.9125	0.004240994	0.001981432
		480	0.005532053	482.6553854	0.005516807	0.00310353
		500	0.008285466	504.1427328	0.00825133	0.005730616
		520	0.014616649	527.6006574	0.014510855	0.011872852
		525	0.017006685	533.9285094	0.01686369	0.014194047
		530	0.019791806	540.4896571	0.019598495	0.016896046
		535	0.023010005	547.3103529	0.022749267	0.020012716
		550	0.035658078	569.6119428	0.035037049	0.032188989
		575	0.069226901	614.8054681	0.066935865	0.063861838
		600	0.123265537	673.9593221	0.116240101	0.112870304
		625	0.203821421	752.3883878	0.185501014	0.181739072
		650	0.317386752	856.3013889	0.275650041	0.271368534

Table A 15 Classification of cross section G1

Bridge	h.w	tw	Fy.W	c/t	Limit	Class	Aw/A
G1-FL-HS	758,8	8,5	583	89,27059	78,72657	4	0,375173
G1-FL-SS	758,8	8,5	480	89,27059	61,45556	4	
G1-FL-CS	758,8	8,5	355	89,27059	67,53017	3	
G1-CR-SS	758,8	8,5	480	89,27059	61,45556	4	
G1-CR-CS	758,8	8,5	355	89,27059	67,53017	3	
	bfu	tfu	Fy.F	c/t	Limit	Class	
G1-FL-HS	184,2	19,6	556	4,482143	5,851121	2	
G1-FL-SS	184,2	19,6	450	4,482143	6,347103	1	
G1-FL-CS	184,2	19,6	420	4,482143	6,732119	1	
G1-CR-SS	184,2	19,6	450	4,482143	6,347103	1	
G1-CR-CS	184,2	19,6	420	4,482143	6,732119	1	

	bfl	tfl	F.y:F	C/t	Limit	Class
G1-FL-HS	362	19,7	556	8,972081	6,501245	3
G1-FL-SS	362	19,7	450	8,972081	7,052336	3
G1-FL-CS	362	19,7	420	8,972081	7,480132	3
G1-CR-SS	362	19,7	450	8,972081	7,052336	3
G1-CR-CS	362	19,7	420	8,972081	7,480132	3

Table A 16 Classification of cross section G2

Bridge	h.w	tw	Fy.W	c/t	Limit	Class	Aw/A
G2-FL-HS	760,4	8,9	583	85,4382	78,72657	4	0,485984
G2-FL-SS	760,4	8,9	480	85,4382	61,45556	4	
G2-FL-CS	760,4	8,9	355	85,4382	67,53017	3	
G2-CR-SS	760,4	8,5	480	89,45882	61,45556	4	
G2-CR-CS	760,4	8,5	355	89,45882	67,53017	3	
	bfu	tfu	Fy.F	c/t	Limit	Class	
G2-FL-HS	182,6	19,6	556	4,431122	5,851121	2	
G2-FL-SS	182,6	19,6	450	4,431122	6,347103	1	
G2-FL-CS	182,6	19,6	420	4,431122	6,732119	1	
G2-CR-SS	182,6	19,6	450	4,441327	6,347103	1	
G2-CR-CS	182,6	19,6	420	4,441327	6,732119	1	
	bfl	tfl	F.y:F	C/t	Limit	Class	
G2-FL-HS	182,6	19,6	556	4,431122	5,851121	1	
G2-FL-SS	182,6	19,6	450	4,431122	6,347103	1	
G2-FL-CS	182,6	19,6	420	4,431122	6,732119	1	
G2-CR-SS	182,6	19,6	450	4,441327	6,347103	1	
G2-CR-CS	182,6	19,6	420	4,441327	6,732119	1	

Table A 17 Classification of cross section 100-262-1

Bridge	h.w	tw	Fy.W	c/t	Limit	Class	Aw/A
262-FL-SS	1953	17	450	114,8824	64	4	0,2500056
262-FL-CS	1953	17	355	114,8824	101	4	
262-CR-SS	1955	6	530	325,8333	58	4	
262-CR-CS	1955	6	355	325,8333	101	4	
	bfu	tfu	Fy.F	c/t	Limit	Class	
262-FL-SS	800	42	450	9,321429	10	3	
262-FL-CS	800	42	420	9,321429	10	3	
262-CR-SS	850	45	450	9,377778	10	3	
262-CR-CS	850	45	420	9,377778	10	3	
	bfl	tfl	F.y:F	C/t	Limit	Class	
262-FL-SS	1200	55	450	10,75455	10	4	
262-FL-CS	1200	55	420	10,75455	10	4	
262-CR-SS	1225	50	450	12,19	10	4	
262-CR-CS	1225	50	420	12,19	10	4	

Appendix B

Table B.1 Values for load and displacement for model G1-HPS

High performance steel model (G1-HPS)		
Ultimate load $P_{ul}\ (kN)$	**Displacements** $U\ (mm)$	**Moment** $M_{ul}\ (kN*m)$
0	0	0
0,999997	0,0375588	3,04799086
1,99999	0,0751176	6,09596952
3,49996	0,131456	10,6678781
5,7499	0,215964	17,5256952
9,12475	0,342726	27,812238
14,1869	0,532871	43,2416712
21,7798	0,818092	66,3848304
33,1685	1,24593	101,097588
50,2501	1,8877	153,162305
75,8692	2,8504	231,249322
114,29	4,29453	348,35592
171,905	6,4609	523,96644
258,289	9,71087	787,264872
387,768	14,5874	1181,91686
581,683	21,9061	1772,96978
870,024	32,9229	2651,83315
1149,86	44,0414	3504,77328
1218,05	46,8291	3712,6164
1285,5	49,622	3918,204
1385,21	53,8219	4222,12008
1529,13	60,1625	4660,78824
1558,97	61,7902	4751,74056
1583,74	63,4529	4827,23952
1605,9	65,1359	4894,7832
1626,15	66,8277	4956,5052
1644,17	68,5416	5011,43016
1668,13	71,1242	5084,46024
1688,97	73,7311	5147,98056
1707,6	76,3399	5204,7648
1724,24	78,9427	5255,48352
1738,97	81,5638	5300,38056
1742,41	82,2214	5310,86568
1743,3	82,3843	5313,5784
1743,8	82,4755	5315,1024
1744,08	82,5269	5315,95584

Table B.2 Values for load and displacement for model G1-FL-CS

Flat Web-Carbon Steel (G1-FL-CS)		
Ultimate load P_{ul} (kN)	**Displacements U (mm)**	**Moment M_{ul} $(kN * m)$**
0	0	0
0,999997	0,0360975	3,047990856
1,99999	0,072195	6,09596952
3,49996	0,126341	10,66787808
5,7499	0,207561	17,5256952
9,12476	0,329392	27,81226848
14,1869	0,512139	43,2416712
21,7799	0,786262	66,3851352
33,1687	1,19745	101,0981976
50,2505	1,81425	153,163524
75,87	2,73949	231,25176
114,292	4,12742	348,362016
171,909	6,20948	523,978632
258,299	9,33294	787,295352
387,79	14,0196	1181,98392
581,732	21,0533	1773,119136
870,303	31,6381	2652,683544
1147,84	42,3355	3498,61632
1269,59	53,8229	3869,71032
1285,05	56,7724	3916,8324
1297,84	59,7435	3955,81632
1309,02	62,7226	3989,89296
1318,75	65,707	4019,55
1327,44	68,7058	4046,03712
1335	71,7273	4069,08
1342,35	74,7331	4091,4828
1349,19	77,7356	4112,33112
1355,49	80,7479	4131,53352
1361,38	83,7705	4149,48624
1361,47	83,8181	4149,76056
1361,56	83,8655	4150,03488

Table B.3 Values for load and displacement for model G1-FL-SS

Flat Web-Stainless Steel (G1-FL-SS)		
Ultimate load $P_{ul}\ (kN)$	**Displacements** $U\ (mm)$	**Moment** $M_{ul}\ (kN*m)$
0	0	0
0,999997	0,037559	3,047990856
1,99999	0,075118	6,09596952
3,49996	0,131456	10,66787808
5,7499	0,215964	17,5256952
9,12475	0,342726	27,812238
14,1869	0,532871	43,2416712
21,7798	0,818092	66,3848304
33,1685	1,24593	101,097588
50,2501	1,8877	153,1623048
75,8692	2,8504	231,2493216
114,29	4,29453	348,35592
171,905	6,4609	523,96644
258,289	9,71087	787,264872
387,768	14,5874	1181,916864
581,683	21,9061	1772,969784
870,024	32,9229	2651,833152
1149,86	44,0414	3504,77328
1364,41	55,5196	4158,72168
1397,03	58,4916	4258,14744
1424,93	61,4979	4343,18664
1449,64	64,5252	4418,50272
1471,59	67,5716	4485,40632
1491,22	70,6442	4545,23856
1509,19	73,7232	4600,01112
1525,77	76,7954	4650,54696
1541,19	79,8662	4697,54712
1555,41	82,9468	4740,88968
1558,76	83,7208	4751,10048
1559,57	83,9154	4753,56936
1560,83	84,2037	4757,40984
1560,84	84,2041	4757,44032
1560,84	84,2045	4757,44032
1560,85	84,2048	4757,4708
1560,86	84,2053	4757,50128
1560,88	84,2061	4757,56224
1560,9	84,2072	4757,6232
1560,94	84,2088	4757,74512
1560,88	84,2102	4757,56224

1560,9	84,2111	4757,6232
1560,9	84,2111	4757,6232

Table B.4 Values for load and displacement for model G1-CR-CS

Corrugated Web-Carbon Steel (G1-CR-CS)		
Ultimate load $P_{ul}\ (kN)$	**Displacements** $U\ (mm)$	**Moment** $M_{ul}\ (kN * m)$
0	0	0
0,999997	0,0412363	3,047990856
1,99999	0,0824727	6,09596952
3,49996	0,144327	10,66787808
5,7499	0,23711	17,5256952
9,12474	0,376284	27,81220752
14,1869	0,585048	43,2416712
21,7798	0,898197	66,3848304
33,1684	1,36793	101,0972832
50,2499	2,07255	153,1616952
75,8687	3,12953	231,2477976
114,289	4,71509	348,352872
171,903	7,09367	523,960344
258,284	10,6621	787,249632
387,762	16,0162	1181,898576
581,706	24,0519	1773,039888
870,727	36,1362	2653,975896
941,542	39,1763	2869,820016
973,831	42,4266	2968,236888
990,266	45,7435	3018,330768
1004,5	49,0727	3061,716
1016,02	52,4014	3096,82896
1026,71	55,7325	3129,41208
1036,72	59,0662	3159,92256
1050,08	64,0671	3200,64384
1061,76	69,0634	3236,24448
1072,68	74,0646	3269,52864
1087,69	81,5843	3315,27912
1101,05	89,1096	3356,0004
1113,33	96,6278	3393,42984
1124,85	104,168	3428,5428
1135,79	111,695	3461,88792
1145,94	119,229	3492,82512
1155,3	126,789	3521,3544
1163,99	134,407	3547,84152
1170,06	140,16	3566,34288
1176,05	145,895	3584,6004

1181,5	151,683	3601,212
1182,63	153,156	3604,65624
1183,69	154,634	3607,88712
1184,81	156,105	3611,30088
1185,91	157,576	3614,65368
1185,92	157,6	3614,68416
1185,93	157,623	3614,71464

Table B.5 Values for load and displacement for model G1-CR-SS

Corrugated Web-Stainless Steel (G1-CR-SS)		
Ultimate load $\boldsymbol{P_{ul}\ (kN)}$	**Displacements** $\boldsymbol{U\ (mm)}$	**Moment** $\boldsymbol{M_{ul}\ (kN*m)}$
0	0	0
0,999997	0,0429686	3,047990856
1,99999	0,0859373	6,09596952
3,49996	0,150391	10,66787808
5,74989	0,247071	17,52566472
9,12473	0,392092	27,81217704
14,1868	0,609626	43,2413664
21,7797	0,935931	66,3845256
33,1683	1,4254	101,0969784
50,2495	2,15962	153,160476
75,8678	3,26101	231,2450544
114,287	4,9132	348,346776
171,898	7,39175	523,945104
258,274	11,1101	787,219152
387,739	16,6894	1181,828472
581,653	25,0632	1772,878344
870,459	37,6603	2653,159032
1077,53	50,7782	3284,31144
1149,8	64,4921	3504,5904
1199,83	78,3404	3657,08184
1236,16	92,3094	3767,81568
1266,24	106,258	3859,49952
1272,75	109,769	3879,342
1272,84	109,824	3879,61632
1272,94	109,879	3879,92112
1273,04	109,934	3880,22592
1273,14	109,989	3880,53072
1273,29	110,071	3880,98792
1273,52	110,195	3881,68896
1273,53	110,201	3881,71944
1273,56	110,203	3881,81088
1273,57	110,203	3881,84136

1273,58	110,204	3881,87184

Table B.6 Values for load and displacement for model G2-HPS

High performance steel model (G2-HPS)		
P.ul (KN)	**U (mm)**	**M.ul (KN*m)**
0	0	0
0,999995	0,0496082	3,04798476
1,99998	0,0992166	6,09593904
3,49994	0,173629	10,66781712
5,74984	0,285249	17,52551232
9,12459	0,45268	27,81175032
14,1865	0,703829	43,240452
21,7789	1,08056	66,3820872
33,1664	1,64567	101,0911872
50,2453	2,49336	153,1476744
75,8582	3,76497	231,2157936
114,265	5,67255	348,27972
171,849	8,53428	523,795752
258,162	12,8277	786,877776
387,494	19,2696	1181,081712
581,18	28,9367	1771,43664
870,876	43,4643	2654,430048
1129,35	58,2629	3442,2588
1264,88	73,8455	3855,35424
1338,46	89,7726	4079,62608
1384,7	105,963	4220,5656
1393,71	110,043	4248,02808
1401,85	114,138	4272,8388
1409,39	118,243	4295,82072
1416,3	122,36	4316,8824
1423,06	126,473	4337,48688
1429,44	130,596	4356,93312
1435,41	134,733	4375,12968
1436,75	135,773	4379,214
1437,92	136,822	4382,78016
1438,27	137,423	4383,84696
1438,28	137,576	4383,87744
1438,32	137,578	4383,99936
1438,28	137,581	4383,87744
1438,29	137,581	4383,90792
1438,29	137,582	4383,90792
1438,29	137,582	4383,90792

Table B.7 Values for load and displacement for model G2-FL-CS

Flat Web-Carbon Steel (G2-FL-CS)

P.ul (KN)	U (mm)	M.ul (KN*m)
0,999995	0,047611	3,04798476
1,99998	0,0952221	6,09593904
3,49994	0,166639	10,66781712
5,74984	0,273765	17,52551232
9,12461	0,434455	27,81181128
14,1865	0,675492	43,240452
21,779	1,03705	66,382392
33,1667	1,57941	101,0921016
50,2459	2,39297	153,1495032
75,8595	3,61338	231,219756
114,268	5,44414	348,288864
171,855	8,1906	523,81404
258,177	12,311	786,923496
387,526	18,4933	1181,179248
581,253	27,7705	1771,659144
831,624	41,9721	2534,789952
923,105	57,1117	2813,62404
936,669	60,936	2854,967112
948,525	64,7724	2891,1042
959,019	68,6226	2923,089912
968,484	72,4838	2951,939232
976,859	76,3629	2977,466232
984,492	80,2559	3000,731616
991,512	84,1594	3022,128576
997,902	88,0748	3041,605296
1003,9	91,9989	3059,8872
1009,54	95,9313	3077,07792
1015,64	99,8404	3095,67072
1021,65	103,746	3113,9892
1030,29	109,609	3140,32392
1038,26	115,496	3164,61648
1040,13	116,973	3170,31624
1041,96	118,454	3175,89408
1043,74	119,937	3181,31952
1044,18	120,309	3182,66064
1044,61	120,68	3183,97128
1045,04	121,051	3185,28192
1045,46	121,424	3186,56208
1045,84	121,798	3187,72032
1046	122,182	3188,208
1046,04	122,277	3188,32992
1045,97	122,376	3188,11656
1046,01	122,473	3188,23848
1045,99	122,57	3188,17752
1045,83	122,67	3187,68984

1045,87	122,766	3187,81176
1045,8	122,865	3187,5984
1045,78	122,962	3187,53744
1045,85	123,058	3187,7508
1045,91	123,154	3187,93368
1045,94	123,251	3188,02512
1045,92	123,348	3187,96416
1045,88	123,446	3187,84224
1045,93	123,543	3187,99464
1046,03	123,637	3188,29944

Table B.8 Values for load and displacement for model G2-FL-SS

Flat Web-Carbon Steel (G2-FL-SS)		
P.ul (KN)	**U (mm)**	**M.ul (KN*m)**
0,999995	0,0496082	3,04798476
1,99998	0,0992166	6,09593904
3,49994	0,173629	10,66781712
5,74984	0,285249	17,52551232
9,12459	0,45268	27,81175032
14,1865	0,703829	43,240452
21,7789	1,08056	66,3820872
33,1664	1,64567	101,0911872
50,2453	2,49336	153,1476744
75,8582	3,76497	231,2157936
114,265	5,67255	348,27972
171,849	8,53428	523,795752
258,162	12,8277	786,877776
387,494	19,2696	1181,081712
581,18	28,9367	1771,43664
865,949	43,5025	2639,412552
1038,37	58,7857	3164,95176
1132,31	74,4435	3451,28088
1195,99	90,2591	3645,37752
1208,84	94,2384	3684,54432
1220,68	98,2336	3720,63264
1231,57	102,245	3753,82536
1241,56	106,27	3784,27488
1255,06	112,331	3825,42288
1267,12	118,423	3862,18176
1278,39	124,524	3896,53272
1289,13	130,62	3929,26824
1299,09	136,731	3959,62632
1312,72	145,935	4001,17056
1315,92	148,241	4010,92416
1319,01	150,551	4020,34248

1323,13	154,045	4032,90024
1323,19	154,1	4033,08312
1323,25	154,103	4033,266
1323,26	154,104	4033,29648
1323,22	154,105	4033,17456

Table B.9 Values for load and displacement for model G2-CR-CS

Corrugated Web-Carbon Steel (G2-CR-CS)		
P.ul (KN)	**U (mm)**	**M.ul (KN*m)**
0	0	0
0,999994	0,0659965	3,047981712
1,99998	0,131993	6,09593904
3,49993	0,230989	10,66778664
5,7498	0,379484	17,5253904
9,1245	0,602228	27,811476
14,1863	0,93635	43,2398424
21,7784	1,43754	66,3805632
33,1653	2,18936	101,0878344
50,2426	3,31716	153,1394448
75,8521	5,00898	231,1972008
114,252	7,54703	348,240096
171,817	11,3548	523,698216
258,091	17,068	786,661368
387,334	25,6414	1180,594032
534,806	38,9671	1630,088688
547,494	42,4995	1668,761712
558,349	46,0379	1701,847752
567,986	49,5797	1731,221328
576,866	53,1229	1758,287568
585,228	56,6631	1783,774944
592,954	60,1962	1807,323792
600,194	63,729	1829,391312
601,95	64,6128	1834,7436
603,685	65,4963	1840,03188
605,39	66,3794	1845,22872
607,064	67,262	1850,331072
609,53	68,5853	1857,84744
611,962	69,9082	1865,260176
614,365	71,2312	1872,58452
616,726	72,5538	1879,780848
619,043	73,8756	1886,843064
621,316	75,1972	1893,771168
623,554	76,5189	1900,592592
626,862	78,5018	1910,675376

631,717	81,4767	1925,473416
636,432	84,4506	1939,844736
640,992	87,4244	1953,743616
645,419	90,3977	1967,237112
649,688	93,3687	1980,249024
653,79	96,3448	1992,75192
657,927	99,3123	2005,361496
662,037	102,277	2017,888776
666,088	105,243	2030,236224
672,001	109,687	2048,259048
677,693	114,125	2065,608264
683,256	118,562	2082,564288
688,726	122,999	2099,236848
694,082	127,435	2115,561936
701,843	134,086	2139,217464
709,333	140,742	2162,046984
716,495	147,399	2183,87676
723,411	154,047	2204,956728
730,132	160,693	2225,442336
736,523	167,348	2244,922104
742,526	174,009	2263,219248
748,153	180,68	2280,370344
753,479	187,357	2296,603992
758,54	194,035	2312,02992
763,166	200,716	2326,129968
767,775	207,397	2340,1782
772,212	214,092	2353,702176
776,495	220,791	2366,75676
780,595	227,5	2379,25356
784,606	234,207	2391,479088
788,51	240,916	2403,37848
792,282	247,635	2414,875536
795,885	254,368	2425,85748
799,257	261,116	2436,135336
804,07	271,236	2450,80536
808,668	281,368	2464,820064
813,084	291,501	2478,280032
817,244	301,631	2490,959712
821,066	311,773	2502,609168
824,695	321,926	2513,67036
824,752	322,085	2513,844096
824,81	322,244	2514,02088
824,867	322,403	2514,194616
824,925	322,562	2514,3714
824,982	322,72	2514,545136
825,04	322,879	2514,72192

825,097	323,038	2514,895656
825,155	323,197	2515,07244
825,212	323,355	2515,246176
825,27	323,514	2515,42296
825,327	323,673	2515,596696
825,385	323,832	2515,77348
825,442	323,991	2515,947216
825,499	324,149	2516,120952
825,556	324,308	2516,294688
825,613	324,467	2516,468424
825,671	324,626	2516,645208
825,728	324,785	2516,818944
825,785	324,943	2516,99268
825,842	325,102	2517,166416
825,899	325,261	2517,340152
825,956	325,42	2517,513888

Table B.10 Values for load and displacement for model G2-CR-SS

Corrugated Web-Stainless Steel (G2-CR-SS)		
P.ul (KN)	**U (mm)**	**M.ul (KN*m)**
0	0	0
0,999994	0,0688836	3,047981712
1,99997	0,137767	6,09590856
3,49992	0,241094	10,66775616
5,74979	0,396084	17,52535992
9,12448	0,628573	27,81141504
14,1862	0,977312	43,2395376
21,7783	1,50043	66,3802584
33,165	2,28515	101,08692
50,242	3,46228	153,137616
75,8506	5,22814	231,1926288
114,248	7,87726	348,227904
171,81	11,8517	523,67688
258,074	17,8151	786,609552
387,284	26,7647	1180,441632
564,231	40,384	1719,776088
584,176	44,0146	1780,568448
600,82	47,6558	1831,29936
615,44	51,3007	1875,86112
628,798	54,9483	1916,576304
640,83	58,5936	1953,24984
651,793	62,2464	1986,665064
661,859	65,898	2017,346232
671,153	69,551	2045,674344
673,401	70,4648	2052,526248
675,605	71,379	2059,24404
678,849	72,7504	2069,131752

683,58	74,8081	2083,55184
688,14	76,8661	2097,45072
692,544	78,9233	2110,874112
696,809	80,9802	2123,873832
700,958	83,0378	2136,519984
704,997	85,097	2148,830856
708,957	87,1569	2160,900936
712,827	89,2174	2172,696696
716,588	91,2789	2184,160224
720,227	93,3409	2195,251896
723,762	95,4025	2206,026576
727,203	97,464	2216,514744
730,578	99,5259	2226,801744
733,885	101,589	2236,88148
738,737	104,684	2251,670376
745,825	109,324	2273,2746
756,166	116,268	2304,793968
765,974	123,208	2334,688752
775,327	130,151	2363,196696
784,355	137,1	2390,71404
793,039	144,055	2417,182872
801,36	151,007	2442,54528
809,364	157,96	2466,941472
817,076	164,916	2490,447648
824,492	171,883	2513,051616
831,686	178,844	2534,978928
838,606	185,801	2556,071088
845,204	192,765	2576,181792
851,363	199,74	2594,954424
857,22	206,725	2612,80656
862,823	213,717	2629,884504
868,168	220,715	2646,176064
873,258	227,725	2661,690384
878,12	234,746	2676,50976
882,763	241,781	2690,661624
887,222	248,823	2704,252656
891,53	255,869	2717,38344
895,621	262,923	2729,852808
899,585	269,98	2741,93508
903,449	277,038	2753,712552
907,19	284,098	2765,11512
908,109	285,864	2767,916232
909,021	287,629	2770,696008
910,377	290,277	2774,829096
912,375	294,251	2780,919
915,31	300,214	2789,86488
918,174	306,18	2798,594352
921,008	312,143	2807,232384
923,789	318,102	2815,708872
926,525	324,056	2824,0482

929,154	330,007	2832,061392
931,664	335,958	2839,711872
934,148	341,906	2847,283104
934,761	343,394	2849,151528
934,793	343,472	2849,249064
934,826	343,551	2849,349648
934,859	343,629	2849,450232
934,892	343,708	2849,550816
934,924	343,787	2849,648352
934,957	343,865	2849,748936
934,99	343,944	2849,84952
935,023	344,022	2849,950104
935,055	344,101	2850,04764
935,088	344,179	2850,148224
935,121	344,258	2850,248808
935,153	344,336	2850,346344
935,186	344,415	2850,446928
935,218	344,494	2850,544464
935,251	344,572	2850,645048
935,283	344,651	2850,742584
935,316	344,729	2850,843168
935,348	344,808	2850,940704
935,381	344,886	2851,041288
935,413	344,965	2851,138824
935,445	345,044	2851,23636
935,478	345,122	2851,336944
935,51	345,201	2851,43448
935,543	345,279	2851,535064
935,575	345,358	2851,6326
935,608	345,436	2851,733184
935,64	345,515	2851,83072
935,673	345,594	2851,931304
935,706	345,672	2852,031888
935,738	345,751	2852,129424
935,771	345,829	2852,230008
935,803	345,908	2852,327544
935,836	345,986	2852,428128

Table B.11 Values for load and displacement for model 100-262-1-FL-CS

Flat Web-Carbon Steel (100-262-1-FL-CS)		
P.ul (KN)	**U (mm)**	**M.ul (KN*m)**
1,02553	0,0520301	10,5116825
2,03723	0,103358	20,8816075
3,04892	0,154687	31,25143
4,06062	0,206015	41,621355
5,57816	0,283008	57,17614
7,85447	0,398498	80,5083175
11,2689	0,571732	115,506225
16,3905	0,831584	168,002625
24,0729	1,22136	246,747225
35,5964	1,80604	364,8631
52,8812	2,68305	542,0323
78,8076	3,99859	807,7779
117,696	5,97193	1206,384
176,024	8,93203	1804,246
263,507	13,3723	2700,94675
394,713	20,0332	4045,80825
591,478	30,0255	6062,6495
886,527	45,0159	9086,90175
1328,88	67,506	13621,02
1991,91	101,251	20417,0775
2985,33	151,892	30599,6325
4471,43	227,908	45832,1575
5913,14	304,865	60609,685
6163,7	324,928	63177,925
6260,1	345,88	64166,025
6335,94	366,9	64943,385
6398,09	387,973	65580,4225
6450,94	409,07	66122,135
6494,57	430,221	66569,3425
6534,23	451,387	66975,8575
6568,82	472,573	67330,405
6615,46	504,39	67808,465
6676,38	552,137	68432,895
6727,36	599,959	68955,44
6775,54	647,743	69449,285
6817,52	695,602	69879,58
6856,61	743,538	70280,2525
6893,72	791,457	70660,63
6928,21	839,417	71014,1525
6960,89	887,355	71349,1225
7008,23	959,187	71834,3575
7054,12	1031,01	72304,73
7098,15	1102,79	72756,0375

7140,54	1174,59	73190,535
7180,47	1246,45	73599,8175
7217,88	1318,42	73983,27
7250,9	1390,85	74321,725
7281,51	1463,46	74635,4775
7310,43	1536,1	74931,9075
7317,36	1554,29	75002,94
7319,07	1558,84	75020,4675
7320,79	1563,39	75038,0975
7322,49	1567,94	75055,5225
7324,18	1572,49	75072,845
7324,6	1573,63	75077,15
7325,03	1574,77	75081,5575
7325,45	1575,91	75085,8625
7325,87	1577,05	75090,1675
7326,28	1578,19	75094,37
7326,7	1579,34	75098,675
7326,8	1579,62	75099,7
7326,91	1579,91	75100,8275
7327,01	1580,19	75101,8525
7327,11	1580,48	75102,8775
7327,17	1580,48	75103,4925
7327,23	1580,48	75104,1075
7327,32	1580,49	75105,03
7327,46	1580,5	75106,465

Table B.12 Values for load and displacement for model 100-262-1-FL-SS

Flat Web-Carbon Steel (100-262-1-FL-SS)		
P.ul (KN)	**U (mm)**	**M.ul (KN*m)**
0	0	0
1,04062	0,05489	10,666355
1,29508	0,0683119	13,27457
1,54953	0,0817337	15,8826825
1,93122	0,101866	19,795005
2,50374	0,132066	25,663335
3,36252	0,177364	34,46583
4,2213	0,222663	43,268325
5,08009	0,267962	52,0709225
6,36826	0,33591	65,274665
8,30051	0,437832	85,0802275
11,1989	0,590716	114,788725
15,5464	0,820042	159,3506
22,0676	1,16403	226,1929
31,8494	1,68002	326,45635
46,5217	2,45401	476,847425

68,5297	3,615	702,429425
101,54	5,35652	1040,785
151,053	7,96886	1548,29325
225,317	11,8875	2309,49925
336,696	17,7658	3451,134
503,733	26,5839	5163,26325
754,214	39,8127	7730,6935
1129,77	59,6594	11580,1425
1692,72	89,4375	17350,38
2536,3	134,122	25997,075
3799,6	201,19	38945,9
5657,97	302,586	57994,1925
7215,7	406,379	73960,925
7699,67	516,411	78921,6175
7789,49	543,991	79842,2725
7869,91	571,617	80666,5775
7946,98	599,21	81456,545
8016,84	626,877	82172,61
8081,28	654,613	82833,12
8140,59	682,389	83441,0475
8195,63	710,19	84005,2075
8249,09	737,957	84553,1725
8326,93	779,567	85351,0325
8398,8	821,217	86087,7
8463,73	863,037	86753,2325
8539,52	926,367	87530,08
8604,31	989,834	88194,1775
8664,08	1053,3	88806,82
8720,6	1116,83	89386,15
8772,96	1180,61	89922,84
8818,63	1244,74	90390,9575
8857,58	1309,23	90790,195
8874,38	1341,64	90962,395
8889,41	1374,17	91116,4525
8902,39	1406,78	91249,4975
8903,75	1411,41	91263,4375
8904,74	1416,05	91273,585
8904,72	1416,05	91273,38
8904,72	1416,06	91273,38
8904,72	1416,06	91273,38

Table B.13 Values for load and displacement for model 100-262-1-CR-CS

Corrugated Web-Carbon Steel (100-262-1-CR-CS)		
P.ul (KN)	**U (mm)**	**M.ul (KN*m)**
0	0	0

0,999999	0,0656998	10,24998975
2	0,1314	20,5
2,99999	0,197099	30,7498975
4,49999	0,295649	46,1248975
6,74997	0,443474	69,1871925
10,1249	0,665212	103,780225
15,1873	0,99782	155,669825
22,7809	1,49673	233,504225
34,171	2,24511	350,25275
51,256	3,36768	525,374
76,8825	5,05156	788,045625
115,321	7,57744	1182,04025
172,974	11,3664	1772,9835
259,445	17,05	2659,31125
389,132	25,5761	3988,603
583,617	38,3665	5982,07425
875,243	57,555	8971,24075
1312,46	86,3443	13452,715
1967,76	129,543	20169,54
2949,56	194,372	30232,99
4416,97	291,69	45273,9425
4779,65	316,131	48991,4125
4975,12	342,23	50994,98
5004,42	369,553	51295,305
5030,41	396,761	51561,7025
5054,84	423,888	51812,11
5078,25	450,961	52052,0625
5100,86	477,982	52283,815
5122,81	504,963	52508,8025
5144,28	531,914	52728,87
5165,24	558,826	52943,71
5185,74	585,713	53153,835
5205,82	612,577	53359,655
5225,51	639,428	53561,4775
5244,68	666,258	53757,97
5263,45	693,078	53950,3625
5268,07	699,784	53997,7175
5269,22	701,46	54009,505
5270,37	703,137	54021,2925
5271,52	704,813	54033,08
5272,67	706,49	54044,8675
5273,81	708,166	54056,5525
5274,95	709,843	54068,2375
5276,09	711,519	54079,9225
5277,23	713,196	54091,6075
5278,36	714,872	54103,19

5279,49	716,549	54114,7725
5280,62	718,225	54126,355
5281,75	719,902	54137,9375
5283,44	722,417	54155,26
5285,96	726,19	54181,09
5289,72	731,85	54219,63
5295,3	740,341	54276,825
5303,54	753,082	54361,285
5315,75	772,195	54486,4375
5327,8	791,307	54609,95
5339,73	810,409	54732,2325
5351,54	829,505	54853,285
5363,25	848,592	54973,3125
5380,66	877,216	55151,765
5397,82	905,836	55327,655
5414,71	934,453	55500,7775
5439,62	977,383	55756,105
5475,68	1041,84	56125,72
5509,77	1106,39	56475,1425
5542,91	1170,92	56814,8275
5575,27	1235,41	57146,5175
5607,02	1299,86	57471,955
5638,14	1364,27	57790,935
5668,64	1428,64	58103,56
5698,43	1493	58408,9075
5705,76	1509,09	58484,04
5713,05	1525,19	58558,7625
5723,9	1549,33	58669,975
5734,65	1573,48	58780,1625
5745,28	1597,63	58889,12
5761,01	1633,86	59050,3525
5784,16	1688,23	59287,64
5817,69	1769,89	59631,3225
5849,35	1851,84	59955,8375
5856,9	1872,37	60033,225
5864,32	1892,91	60109,28
5875,2	1923,72	60220,8
5890,92	1969,96	60381,93
5894,68	1981,53	60420,47
5898,35	1993,1	60458,0875
5898,54	1993,71	60460,035
5898,73	1994,32	60461,9825
5898,92	1994,93	60463,93

Table B.14 Values for load and displacement for model 100-262-1-CR-SS

Corrugated Web-Stainless Steel (100-262-1-CR-SS)		
P.ul (KN)	**U (mm)**	**M.ul (KN*m)**
0	0	0
0,999999	0,0690805	10,24998975
2	0,138161	20,5
2,99999	0,207242	30,7498975
3,99999	0,276322	40,9998975
5,49998	0,379943	56,374795
7,74996	0,535375	79,43709
11,1249	0,768523	114,030225
16,1873	1,11825	165,919825
23,7808	1,64283	243,7532
35,171	2,42972	360,50275
52,2558	3,61006	535,62195
77,8823	5,38059	798,293575
116,32	8,03645	1192,28
173,973	12,0204	1783,22325
260,443	17,9965	2669,54075
390,127	26,9614	3998,80175
584,607	40,4102	5992,22175
876,223	60,5865	8981,28575
1313,41	90,8582	13462,4525
1968,66	136,282	20178,765
2950,34	204,452	30240,985
4417,11	306,793	45275,3775
5751,35	411,162	58951,3375
5988,82	524,021	61385,405
6186,65	635,925	63413,1625
6351,72	747,617	65105,13
6489,86	859,562	66521,065
6584,86	972,472	67494,815
6669,56	1085,46	68362,99
6749,19	1198,3	69179,1975
6819,88	1311,44	69903,77
6879,15	1425,02	70511,2875
6931,96	1538,84	71052,59
6979,17	1653,04	71536,4925
6989,62	1681,76	71643,605
6999,46	1710,55	71744,465
7013,4	1753,8	71887,35
7026,12	1797,15	72017,73
7037,81	1840,58	72137,5525
7048,43	1884,08	72246,4075
7048,59	1884,77	72248,0475
7048,74	1885,45	72249,585

7048,89	1886,13	72251,1225
7049,04	1886,81	72252,66
7049,19	1887,49	72254,1975
7049,34	1888,18	72255,735
7049,49	1888,86	72257,2725
7049,64	1889,54	72258,81
7049,78	1890,22	72260,245
7049,92	1890,9	72261,68
7050,07	1891,58	72263,2175

Appendix C

Bending resistance M_{pl} of G1-FL-HS

Geometry:

$t_c := 181mm$

$b_c := 1524mm$

$b_{fl} := 362mm$

$t_{fl} := 19.7mm$

$b_{fu} := 184.2mm$

$t_{fu} := 19.6mm$

$h_w := 758.8mm$

$t_w := 8.5mm$

Material Properties:

$f_c := \frac{30.5}{1.5} \cdot MPa = 2.033 \times 10^7 Pa$

$E := 200000MPa$

$F_{y.F} := 556MPa$

$F_{y.W} := 583MPa$

Center of steel section:

$h_a := t_{fl} + t_{fu} + h_w$

$A_s := b_{fl} \cdot t_{fl} + h_w \cdot t_w + b_{fu} \cdot t_{fu} = 0.017m^2$

$$Y_a := \frac{b_{fu} \cdot t_{fu} \cdot \left(h_a - \frac{t_{fu}}{2} \right) + b_{fl} \cdot t_{fl} \cdot \frac{t_{fl}}{2} + h_w \cdot t_w \cdot \left(t_{fl} + \frac{h_w}{2} \right)}{A_s} = 0.319m$$

Position of the neutral axis:

$A_F := b_{fl} \cdot t_{fl} + b_{fu} \cdot t_{fu} = 0.011m^2$

$A_w := h_w \cdot t_w = 6.45 \times 10^{-3} m^2$

$N_a := F_{y.F} \cdot A_F + F_{y.W} \cdot A_w = 9.733 \times 10^6 N$

$N_c := 0.85 \cdot b_c \cdot t_c \cdot f_c = 4.768 \times 10^6 N$

$N_f := t_{fu} \cdot b_{fu} \cdot F_{y.F} = 2.007 \times 10^6 N$

$$N_{af} := \frac{N_a - N_c}{2} = 2.483 \times 10^6 N$$

$$N_{aw} := \frac{N_a - N_c - F_{y.F} \cdot b_{fl} \cdot t_{fl} - F_{y.F} \cdot b_{fu} \cdot t_{fu}}{2} = -5.036 \times 10^5 N$$

The neutral axis lies at the upper flange of the plate girder

Selenderness of the cross section:

$h := t_c + t_{fl} + t_{fu} + h_w = 0.979\,m$

$x_{pl.f} := t_c + \frac{N_{af}}{b_{fu} \cdot F_{y.F}} = 0.205\,m$ $\qquad \frac{x_{pl.f}}{h} = 0.21$

Bending Resistance:

$M_{pl.f} := N_c \cdot \left(h - Y_a - \frac{t_c}{2} \right) + N_{af} \cdot \left[h_a - \left(x_{pl.f} - t_c \right) \right] = 4.635 \times 10^3 \cdot kN \cdot m$

Bending resistance M_{pl} of G1-FL-CS

Geometry:

$t_c := 181\,mm$

$b_c := 1524\,mm$

$b_{fl} := 362\,mm$

$t_{fl} := 19.7\,mm$

$b_{fu} := 184.2\,mm$

$t_{fu} := 19.6\,mm$

$h_w := 758.8\,mm$

$t_w := 8.5\,mm$

Material Properties:

$f_c := \frac{30.5}{1.5} \cdot MPa = 2.033 \times 10^7\,Pa$

$E := 210000\,MPa$

$F_{y.F} := 420\,MPa$

$F_{y.W} := 355\,MPa$

Center of steel section:

$h_a := t_{fl} + t_{fu} + h_w$

$A_s := b_{fl} \cdot t_{fl} + h_w \cdot t_w + b_{fu} \cdot t_{fu} = 0.017\,m^2$

$Y_a := \frac{b_{fu} \cdot t_{fu} \cdot \left(h_a - \frac{t_{fu}}{2} \right) + b_{fl} \cdot t_{fl} \cdot \frac{t_{fl}}{2} + h_w \cdot t_w \cdot \left(t_{fl} + \frac{h_w}{2} \right)}{A_s} = 0.319\,m$

Position of the neutral axis:

$A_F := b_{fl}\cdot t_{fl} + b_{fu}\cdot t_{fu} = 0.011\,m^2$

$A_w := h_w\cdot t_w = 6.45\times 10^{-3}\,m^2$

$N_a := F_{y.F}\cdot A_F + F_{y.W}\cdot A_w = 6.801\times 10^6\,N$

$N_c := 0.85\cdot b_c\cdot t_c\cdot f_c = 4.768\times 10^6\,N$

$N_f := t_{fu}\cdot b_{fu}\cdot F_{y.F} = 1.516\times 10^6\,N$

$N_{af} := \frac{N_a - N_c}{2} = 1.017\times 10^6\,N$

$N_{aw} := \frac{N_a - N_c - F_{y.F}\cdot b_{fl}\cdot t_{fl} - F_{y.F}\cdot b_{fu}\cdot t_{fu}}{2} = -1.239\times 10^6\,N$

The neutral axis lies at the upper flange of the plate girder

Selenderness of the cross section:

$h := t_c + t_{fl} + t_{fu} + h_w = 0.979\,m$

$x_{pl.f} := t_c + \frac{N_{af}}{b_{fu}\cdot F_{y.F}} = 0.194\,m$

$\frac{x_{pl.f}}{h} = 0.198$

Bending Resistance:

$M_{pl.f} := N_c\cdot\left(h - Y_a - \frac{t_c}{2}\right) + N_{af}\cdot\left[h_a - \left(x_{pl.f} - t_c\right)\right] = 3.512\times 10^3\cdot kN\cdot m$

Bending resistance M_{pl} of G1-FL-SS

Geometry:

$t_c := 181mm$

$b_c := 1524mm$

$b_{fl} := 362mm$

$t_{fl} := 19.7mm$

$b_{fu} := 184.2mm$

$t_{fu} := 19.6mm$

$h_w := 758.8mm$

$t_w := 8.5mm$

Material Properties:

$f_c := \frac{30.5}{1.5} \cdot MPa = 2.033 \times 10^7 Pa$

$E := 200000MPa$

$F_{y.F} := 450MPa$

$F_{y.W} := 480MPa$

Center of steel section:

$h_a := t_{fl} + t_{fu} + h_w$

$A_s := b_{fl} \cdot t_{fl} + h_w \cdot t_w + b_{fu} \cdot t_{fu} = 0.017m^2$

$$Y_a := \frac{b_{fu} \cdot t_{fu} \cdot \left(h_a - \frac{t_{fu}}{2} \right) + b_{fl} \cdot t_{fl} \cdot \frac{t_{fl}}{2} + h_w \cdot t_w \cdot \left(t_{fl} + \frac{h_w}{2} \right)}{A_s} = 0.319m$$

Position of the neutral axis:

$A_F := b_{fl} \cdot t_{fl} + b_{fu} \cdot t_{fu} = 0.011m^2$

$A_w := h_w \cdot t_w = 6.45 \times 10^{-3} m^2$

$N_a := F_{y.F} \cdot A_F + F_{y.W} \cdot A_w = 7.93 \times 10^6 N$

$N_c := 0.85 \cdot b_c \cdot t_c \cdot f_c = 4.768 \times 10^6 N$

$N_f := t_{fu} \cdot b_{fu} \cdot F_{y.F} = 1.625 \times 10^6 N$

$$N_{af} := \frac{N_a - N_c}{2} = 1.581 \times 10^6 N$$

$$N_{aw} := \frac{N_a - N_c - F_{y.F} \cdot b_{fl} \cdot t_{fl} - F_{y.F} \cdot b_{fu} \cdot t_{fu}}{2} = -8.358 \times 10^5 N$$

The neutral axis lies at the upper flange of the plate girder

Slenderness of the cross section:

$$h := t_c + t_{fl} + t_{fu} + h_w = 0.979\,m$$

$$x_{pl.f} := t_c + \frac{N_{af}}{b_{fu} \cdot F_{y.F}} = 0.2\,m \qquad \frac{x_{pl.f}}{h} = 0.204$$

Bending Resistance:

$$M_{pl.f} := N_c \cdot \left(h - Y_a - \frac{t_c}{2} \right) + N_{af} \cdot \left[h_a - \left(x_{pl.f} - t_c \right) \right] = 3.946 \times 10^3 \cdot kN \cdot m$$

Bending resistance M.s of G1-FL-SS

Material Parameters:

$\sigma_{0.2} := F_{y.F} = 4.5 \times 10^{8}\,Pa$

$\varepsilon_{0.2} := \frac{\sigma_{0.2}}{E} + 0.002 = 4.25 \times 10^{-3}$

$ee := \frac{\sigma_{0.2}}{E} = 2.25 \times 10^{-3}$

$n := 8.01$

$E_2 := \frac{E}{1 + 0.002 \cdot \frac{n}{ee}} = 2.463 \times 10^{10}\,Pa$

$r_2 := E_2 \cdot \frac{\varepsilon_{0.2}}{\sigma_{0.2}} = 0.233$

$\sigma_u := \sigma_{0.2} \cdot \frac{[1 - 0.0375 \cdot (n - 5)]}{0.2 + 185 \cdot ee} = 6.478 \times 10^{8}\,Pa$

$\varepsilon_u := 0.28$

$m_1 := 1 + 3.5 \cdot \frac{\sigma_{0.2}}{\sigma_u} = 3.431$

$r_1 := E_2 \cdot \frac{(\varepsilon_u - \varepsilon_{0.2})}{\sigma_u - \sigma_{0.2}} = 34.337$

$E_u := \frac{E_2}{1 + (r_1 - 1) \cdot m_1} = 2.135 \times 10^{8}\,Pa$

$r_u := E_u \cdot \frac{(\varepsilon_u - \varepsilon_{0.2})}{\sigma_u - \sigma_{0.2}} = 0.298$

$p_1 := r_1 \cdot \left(\frac{1 - r_u}{r_1 - 1} \right) = 0.723$

Stress in steel σ_m:

Given

$y_1 := 304.54\text{mm}$ $\varepsilon_{cu} := 0.003$

$\kappa_a := \frac{\varepsilon_u}{h - y_1} = 0.415\frac{1}{m}$ $\kappa_c := \frac{\varepsilon_{cu}}{y_1} = 0.011\frac{1}{m}$

$\kappa := \min(\kappa_a, \kappa_c) = 0.011\frac{1}{m}$ $y_2 := t_c + 0.6 \cdot h - y_1 = 0.464\text{m}$

$\varepsilon_2 := \kappa \cdot y_2$

$$\sigma_m := \sigma_{0.2} \cdot \left[\frac{1 + r_2 \cdot \left(\frac{\varepsilon_2}{\varepsilon_{0.2}} - 1 \right)}{1 + (r_1 - 1) \cdot \left(\frac{\frac{\varepsilon_2}{\varepsilon_{0.2}} - 1}{\frac{\varepsilon_u}{\varepsilon_{0.2}} - 1} \right)^{p_1}} \right] = 466.598 \cdot \text{MPa}$$

$y_1 := \sigma_m \cdot \frac{A_s}{0.85 \cdot f_c \cdot b_c} = 304.54 \cdot \text{mm}$

Position of the neutral axis:

$$N_{a.s} := \sigma_m \cdot A_s = 8.022 \times 10^3 \frac{1}{m} \cdot kN \cdot m$$

$$N_{c.s} := 0.85 \cdot b_c \cdot t_c \cdot f_c = 4.768 \times 10^6 N$$

$$N_{f.s} := t_{fu} \cdot b_{fu} \cdot \sigma_m = 1.685 \times 10^6 N$$

$$N_{af.s} := \frac{N_{a.s} - N_{c.s}}{2} = 1.627 \times 10^6 N$$

$$N_{aw.s} := \frac{N_{a.s} - N_{c.s} - \sigma_m \cdot b_{fl} \cdot t_{fl} - \sigma_m \cdot b_{fu} \cdot t_{fu}}{2} = -8.79 \times 10^5 N$$

The neutral axis lies at the upper flange of the plate girder

Selenderness of the cross section:

$$x_{pl.f.s} := t_c + \frac{N_{af.s}}{b_{fu} \cdot \sigma_m} = 0.2 m \qquad \frac{x_{pl.f.s}}{h} = 0.204$$

Bending Resistance:

$$M_s := N_{c.s} \cdot \left(h - Y_a - \frac{t_c}{2} \right) + N_{af.s} \cdot \left[h_a - \left(x_{pl.f.s} - t_c \right) \right] = 3.982 \times 10^3 \cdot kN \cdot m$$

Bending resistance M_{pl} of G1-CR-CS

Geometry:

$t_c := 181mm$

$b_c := 1524mm$

$b_{fl} := 362mm$

$t_{fl} := 19.7mm$

$b_{fu} := 184.2mm$

$t_{fu} := 19.6mm$

$h_w := 758.8mm$

$t_w := 0mm$

Material Properties:

$f_c := \frac{30.5}{1.5} \cdot MPa = 2.033 \times 10^7 Pa$

$E := 210000MPa$

$F_{y.F} := 420MPa$

$F_{y.W} := 355MPa$

Center of steel section:

$h_a := t_{fl} + t_{fu} + h_w$

$A_s := b_{fl} \cdot t_{fl} + h_w \cdot t_w + b_{fu} \cdot t_{fu} = 0.011m^2$

$$Y_a := \frac{b_{fu} \cdot t_{fu} \cdot \left(h_a - \frac{t_{fu}}{2} \right) + b_{fl} \cdot t_{fl} \cdot \frac{t_{fl}}{2} + h_w \cdot t_w \cdot \left(t_{fl} + \frac{h_w}{2} \right)}{A_s} = 0.271m$$

Position of the neutral axis:

$A_F := b_{fl} \cdot t_{fl} + b_{fu} \cdot t_{fu} = 0.011m^2$

$A_w := h_w \cdot t_w = 0$

$N_a := F_{y.F} \cdot A_F + F_{y.W} \cdot A_w = 4.512 \times 10^6 N$

$N_c := 0.85 \cdot b_c \cdot t_c \cdot f_c = 4.768 \times 10^6 N$

$N_f := t_{fu} \cdot b_{fu} \cdot F_{y.F} = 1.516 \times 10^6 N$

$$N_{af} := \frac{N_a - N_c}{2} = -1.28 \times 10^5 N$$

$$N_{aw} := \frac{N_a - N_c - F_{y.F} \cdot b_{fl} \cdot t_{fl} - F_{y.F} \cdot b_{fu} \cdot t_{fu}}{2} = -2.384 \times 10^6 N$$

The neutral axis lies at the Concrete

Selenderness of the cross section:

$h := t_c + t_{fl} + t_{fu} + h_w = 0.979\,m$

$x_{pl.c} := \frac{N_a}{0.85 \cdot f_c \cdot b_c} = 0.171\,m \qquad \frac{x_{pl.c}}{h} = 0.175$

Bending Resistance:

$M_{pl.c} := N_a \cdot \left(h - Y_a - \frac{x_{pl.c}}{2} \right) = 2.806 \times 10^3\,m \cdot kN$

Bending resistance M.pl of G1-CR-SS

Geometry:

$t_c := 181\,mm$

$b_c := 1524\,mm$

$b_{fl} := 362\,mm$

$t_{fl} := 19.7\,mm$

$b_{fu} := 184.2\,mm$

$t_{fu} := 19.6\,mm$

$h_w := 758.8\,mm$

$t_w := 0\,mm$

Material Properties:

$f_c := \frac{30.5}{1.5} \cdot MPa = 2.033 \times 10^7\,Pa$

$E := 200000\,MPa$

$F_{y.F} := 450\,MPa$

$F_{y.W} := 480\,MPa$

Center of steel section:

$h_a := t_{fl} + t_{fu} + h_w$

$A_s := b_{fl} \cdot t_{fl} + h_w \cdot t_w + b_{fu} \cdot t_{fu} = 0.011\,m^2$

$Y_a := \frac{b_{fu} \cdot t_{fu} \cdot \left(h_a - \frac{t_{fu}}{2}\right) + b_{fl} \cdot t_{fl} \cdot \frac{t_{fl}}{2} + h_w \cdot t_w \cdot \left(t_{fl} + \frac{h_w}{2}\right)}{A_s} = 0.271\,m$

Position of the neutral axis:

$A_F := b_{fl} \cdot t_{fl} + b_{fu} \cdot t_{fu} = 0.011\,m^2$

$A_w := h_w \cdot t_w = 0$

$N_a := F_{y.F} \cdot A_F + F_{y.W} \cdot A_w = 4.834 \times 10^6\,N$

$N_c := 0.85 \cdot b_c \cdot t_c \cdot f_c = 4.768 \times 10^6\,N$

$N_f := t_{fu} \cdot b_{fu} \cdot F_{y.F} = 1.625 \times 10^6\,N$

$N_{af} := \frac{N_a - N_c}{2} = 3.314 \times 10^4\,N$

$N_{aw} := \frac{N_a - N_c - F_{y.F} \cdot b_{fl} \cdot t_{fl} - F_{y.F} \cdot b_{fu} \cdot t_{fu}}{2} = -2.384 \times 10^6\,N$

The neutral axis lies at the upper flange of the plate girder

Selenderness of the cross section:

$h := t_c + t_{fl} + t_{fu} + h_w = 0.979\,m$

$x_{pl.f} := t_c + \frac{N_{af}}{b_{fu} \cdot F_{y.F}} = 0.181\,m$

$\frac{x_{pl.f}}{h} = 0.185$

Bending Resistance:

$M_{pl.f} := N_c \cdot \left(h - Y_a - \frac{t_c}{2}\right) + N_{af} \cdot \left[h_a - \left(x_{pl.f} - t_c\right)\right] = 2.969 \times 10^3 \cdot kN \cdot m$

Bending resistance M.s of G1-CR-SS

Material Parameters:

$\sigma_{0.2} := F_{y.F} = 4.5 \times 10^{8}\,Pa$

$\varepsilon_{0.2} := \frac{\sigma_{0.2}}{E} + 0.002 = 4.25 \times 10^{-3}$

$ee := \frac{\sigma_{0.2}}{E} = 2.25 \times 10^{-3}$

$n := 8.01$

$E_2 := \frac{E}{1 + 0.002 \cdot \frac{n}{ee}} = 2.463 \times 10^{10}\,Pa$

$r_2 := E_2 \cdot \frac{\varepsilon_{0.2}}{\sigma_{0.2}} = 0.233$

$\sigma_u := \sigma_{0.2} \cdot \frac{[1 - 0.0375 \cdot (n - 5)]}{0.2 + 185 \cdot ee} = 6.478 \times 10^{8}\,Pa$

$\varepsilon_u := 0.28$

$m_1 := 1 + 3.5 \cdot \frac{\sigma_{0.2}}{\sigma_u} = 3.431$

$r_1 := E_2 \cdot \frac{(\varepsilon_u - \varepsilon_{0.2})}{\sigma_u - \sigma_{0.2}} = 34.337$

$E_u := \frac{E_2}{1 + (r_1 - 1) \cdot m_1} = 2.135 \times 10^{8}\,Pa$

$r_u := E_u \cdot \frac{(\varepsilon_u - \varepsilon_{0.2})}{\sigma_u - \sigma_{0.2}} = 0.298$

$p_1 := r_1 \cdot \left(\frac{1 - r_u}{r_1 - 1} \right) = 0.723$

Stress in steel σ_m:

Given

$y_1 := 202.248\text{mm}$ $\varepsilon_{cu} := 0.003$

$\kappa_a := \frac{\varepsilon_u}{h - y_1} = 0.36\frac{1}{m}$ $\kappa_c := \frac{\varepsilon_{cu}}{y_1} = 0.017\frac{1}{m}$

$\kappa := \min(\kappa_a, \kappa_c) = 0.017\frac{1}{m}$ $y_2 := t_c + 0.6 \cdot h - y_1 = 0.566\text{m}$

$\varepsilon_2 := \kappa \cdot y_2$

$$\sigma_m := \sigma_{0.2} \cdot \left[\frac{1 + r_2 \cdot \left(\frac{\varepsilon_2}{\varepsilon_{0.2}} - 1 \right)}{1 + (r_1 - 1) \cdot \left(\frac{\frac{\varepsilon_2}{\varepsilon_{0.2}} - 1}{\frac{\varepsilon_u}{\varepsilon_{0.2}} - 1} \right)^{p_1}} \right] = 495.933 \cdot \text{MPa}$$

$$y_1 := \sigma_m \cdot \frac{A_s}{0.85 \cdot f_c \cdot b_c} = 202.248 \cdot \text{mm}$$

Position of the neutral axis:

$$N_{a.s} := \sigma_m \cdot A_s = 5.327 \times 10^3 \frac{1}{m} \cdot kN \cdot m$$

$$N_{c.s} := 0.85 \cdot b_c \cdot t_c \cdot f_c = 4.768 \times 10^6 N$$

$$N_{f.s} := t_{fu} \cdot b_{fu} \cdot \sigma_m = 1.79 \times 10^6 N$$

$$N_{af.s} := \frac{N_{a.s} - N_{c.s}}{2} = 2.798 \times 10^5 N$$

$$N_{aw.s} := \frac{N_{a.s} - N_{c.s} - \sigma_m \cdot b_{fl} \cdot t_{fl} - \sigma_m \cdot b_{fu} \cdot t_{fu}}{2} = -2.384 \times 10^6 N$$

The neutral axis lies at the upper flange of the plate girder

Selenderness of the cross section:

$$x_{pl.f.s} := t_c + \frac{N_{af.s}}{b_{fu} \cdot \sigma_m} = 0.184 m \qquad \frac{x_{pl.f.s}}{h} = 0.188$$

Bending Resistance:

$$M_s := N_{c.s} \cdot \left(h - Y_a - \frac{t_c}{2} \right) + N_{af.s} \cdot \left[h_a - \left(x_{pl.f.s} - t_c \right) \right] = 3.165 \times 10^3 \cdot kN \cdot m$$

Bending resistance M_{pl} of G2-FL-HS

Geometry:

$t_c := 181mm$

$b_c := 2184.4mm$

$b_{fl} := 182.6mm$

$t_{fl} := 19.6mm$

$b_{fu} := 182.6mm$

$t_{fu} := 19.6mm$

$h_w := 760.4mm$

$t_w := 8.9mm$

Material Properties:

$f_c := \frac{50.5}{1.5} \cdot MPa = 3.367 \times 10^7 Pa$

$E := 200000MPa$

$F_{y.F} := 556MPa$

$F_{y.W} := 583MPa$

Center of steel section:

$h_a := t_{fl} + t_{fu} + h_w$

$A_s := b_{fl} \cdot t_{fl} + h_w \cdot t_w + b_{fu} \cdot t_{fu} = 0.014m^2$

$$Y_a := \frac{b_{fu} \cdot t_{fu} \cdot \left(h_a - \frac{t_{fu}}{2} \right) + b_{fl} \cdot t_{fl} \cdot \frac{t_{fl}}{2} + h_w \cdot t_w \cdot \left(t_{fl} + \frac{h_w}{2} \right)}{A_s} = 0.4m$$

Position of the neutral axis:

$A_F := b_{fl} \cdot t_{fl} + b_{fu} \cdot t_{fu} = 7.158 \times 10^{-3} m^2$

$A_w := h_w \cdot t_w = 6.768 \times 10^{-3} m^2$

$N_a := F_{y.F} \cdot A_F + F_{y.W} \cdot A_w = 7.925 \times 10^6 N$

$N_c := 0.85 \cdot b_c \cdot t_c \cdot f_c = 1.131 \times 10^7 N$

$N_f := t_{fu} \cdot b_{fu} \cdot F_{y.F} = 1.99 \times 10^6 N$

$$N_{af} := \frac{N_a - N_c}{2} = -1.695 \times 10^6 N$$

$$N_{aw} := \frac{N_a - N_c - F_{y.F} \cdot b_{fl} \cdot t_{fl} - F_{y.F} \cdot b_{fu} \cdot t_{fu}}{2} = -3.684 \times 10^6 N$$

The neutral axis lies at the concrete

Selenderness of the cross section:

$h := t_c + t_{fl} + t_{fu} + h_w = 0.981\,m$

$x_{pl.c} := \frac{N_a}{0.85 \cdot f_c \cdot b_c} = 0.127\,m \qquad \frac{x_{pl.c}}{h} = 0.129$

Bending Resistance:

$M_{pl.c} := N_a \cdot \left(h - Y_a - \frac{x_{pl.c}}{2} \right) = 4.101 \times 10^3 \cdot kN \cdot m$

Bending resistance M_{pl} of G2-FL-CS

Geometry:

$t_c := 181\,mm$
$b_c := 2184.4\,mm$
$b_{fl} := 182.6\,mm$
$t_{fl} := 19.6\,mm$
$b_{fu} := 182.6\,mm$
$t_{fu} := 19.6\,mm$
$h_w := 760.4\,mm$
$t_w := 8.9\,mm$

Material Properties:

$f_c := \frac{50.5}{1.5} \cdot MPa = 3.367 \times 10^7\,Pa$

$E := 210000\,MPa$

$F_{y.F} := 420\,MPa$

$F_{y.W} := 355\,MPa$

Center of steel section:

$h_a := t_{fl} + t_{fu} + h_w$

$A_s := b_{fl} \cdot t_{fl} + h_w \cdot t_w + b_{fu} \cdot t_{fu} = 0.014\,m^2$

$Y_a := \frac{b_{fu} \cdot t_{fu} \cdot \left(h_a - \frac{t_{fu}}{2} \right) + b_{fl} \cdot t_{fl} \cdot \frac{t_{fl}}{2} + h_w \cdot t_w \cdot \left(t_{fl} + \frac{h_w}{2} \right)}{A_s} = 0.4\,m$

Position of the neutral axis:

$A_F := b_{fl} \cdot t_{fl} + b_{fu} \cdot t_{fu} = 7.158 \times 10^{-3} m^2$

$A_w := h_w \cdot t_w = 6.768 \times 10^{-3} m^2$

$N_a := F_{y.F} \cdot A_F + F_{y.W} \cdot A_w = 5.409 \times 10^6 N$

$N_c := 0.85 \cdot b_c \cdot t_c \cdot f_c = 1.131 \times 10^7 N$

$N_f := t_{fu} \cdot b_{fu} \cdot F_{y.F} = 1.503 \times 10^6 N$

$$N_{af} := \frac{N_a - N_c}{2} = -2.953 \times 10^6 N$$

$$N_{aw} := \frac{N_a - N_c - F_{y.F} \cdot b_{fl} \cdot t_{fl} - F_{y.F} \cdot b_{fu} \cdot t_{fu}}{2} = -4.456 \times 10^6 N$$

The neutral axis lies at the concrete

Selenderness of the cross section:

$h := t_c + t_{fl} + t_{fu} + h_w = 0.981 m$

$$x_{pl.c} := \frac{N_a}{0.85 \cdot f_c \cdot b_c} = 0.087 m \qquad \frac{x_{pl.c}}{h} = 0.088$$

Bending Resistance:

$$M_{pl.c} := N_a \cdot \left(h - Y_a - \frac{x_{pl.c}}{2} \right) = 2.907 \times 10^3 \cdot kN \cdot m$$

Bending resistance M.pl of G2-FL-SS

Geometry:

$t_c := 181mm$

$b_c := 2184.4mm$

$b_{fl} := 182.6mm$

$t_{fl} := 19.6mm$

$b_{fu} := 182.6mm$

$t_{fu} := 19.6mm$

$h_w := 760.4mm$

$t_w := 8.9mm$

Material Properties:

$f_c := \frac{50.5}{1.5} \cdot MPa = 3.367 \times 10^7 Pa$

$E := 200000MPa$

$F_{y.F} := 450MPa$

$F_{y.W} := 480MPa$

Center of steel section:

$h_a := t_{fl} + t_{fu} + h_w$

$A_s := b_{fl} \cdot t_{fl} + h_w \cdot t_w + b_{fu} \cdot t_{fu} = 0.014m^2$

$$Y_a := \frac{b_{fu} \cdot t_{fu} \cdot \left(h_a - \frac{t_{fu}}{2} \right) + b_{fl} \cdot t_{fl} \cdot \frac{t_{fl}}{2} + h_w \cdot t_w \cdot \left(t_{fl} + \frac{h_w}{2} \right)}{A_s} = 0.4m$$

Position of the neutral axis:

$A_F := b_{fl} \cdot t_{fl} + b_{fu} \cdot t_{fu} = 7.158 \times 10^{-3} m^2$

$A_w := h_w \cdot t_w = 6.768 \times 10^{-3} m^2$

$N_a := F_{y.F} \cdot A_F + F_{y.W} \cdot A_w = 6.469 \times 10^6 N$

$N_c := 0.85 \cdot b_c \cdot t_c \cdot f_c = 1.131 \times 10^7 N$

$N_f := t_{fu} \cdot b_{fu} \cdot F_{y.F} = 1.611 \times 10^6 N$

$$N_{af} := \frac{N_a - N_c}{2} = -2.422 \times 10^6 N$$

$$N_{aw} := \frac{N_a - N_c - F_{y.F} \cdot b_{fl} \cdot t_{fl} - F_{y.F} \cdot b_{fu} \cdot t_{fu}}{2} = -4.033 \times 10^6 N$$

The neutral axis lies in the concrete

Selenderness of the cross section:

$h := t_c + t_{fl} + t_{fu} + h_w = 0.981\text{m}$

$x_{pl.c} := \frac{N_a}{0.85 \cdot f_c \cdot b_c} = 0.103\text{m}$ $\qquad \frac{x_{pl.c}}{h} = 0.106$

Bending Resistance:

$M_{pl.c} := N_a \cdot \left(h - Y_a - \frac{x_{pl.c}}{2} \right) = 3.423 \times 10^3 \cdot \text{kN} \cdot \text{m}$

Bending resistance M.s of G2-FL-SS

Material Parameters:

$\sigma_{0.2} := F_{y.F} = 4.5 \times 10^8\,\text{Pa}$ $\qquad \varepsilon_{0.2} := \frac{\sigma_{0.2}}{E} + 0.002 = 4.25 \times 10^{-3}$

$ee := \frac{\sigma_{0.2}}{E} = 2.25 \times 10^{-3}$ $\qquad n := 8.01$

$E_2 := \frac{E}{1 + 0.002 \cdot \frac{n}{ee}} = 2.463 \times 10^{10}\,\text{Pa}$ $\qquad r_2 := E_2 \cdot \frac{\varepsilon_{0.2}}{\sigma_{0.2}} = 0.233$

$\sigma_u := \sigma_{0.2} \cdot \frac{[1 - 0.0375 \cdot (n - 5)]}{0.2 + 185 \cdot ee} = 6.478 \times 10^8\,\text{Pa}$ $\qquad \varepsilon_u := 0.28$

$$m_1 := 1 + 3.5 \cdot \frac{\sigma_{0.2}}{\sigma_u} = 3.431$$

$$r_1 := E_2 \cdot \frac{\left(\varepsilon_u - \varepsilon_{0.2}\right)}{\sigma_u - \sigma_{0.2}} = 34.337$$

$$E_u := \frac{E_2}{1 + \left(r_1 - 1\right) \cdot m_1} = 2.135 \times 10^8\,\text{Pa}$$

$$r_u := E_u \cdot \frac{\left(\varepsilon_u - \varepsilon_{0.2}\right)}{\sigma_u - \sigma_{0.2}} = 0.298$$

$$p_1 := r_1 \cdot \left(\frac{1 - r_u}{r_1 - 1}\right) = 0.723$$

Stress in steel σ_m:

Given

$y_1 := 116.673\text{mm}$

$\varepsilon_{cu} := 0.003$

$$\kappa_a := \frac{\varepsilon_u}{h - y_1} = 0.324\frac{1}{\text{m}}$$

$$\kappa_c := \frac{\varepsilon_{cu}}{y_1} = 0.03\frac{1}{\text{m}}$$

$$\kappa := \min\left(\kappa_a, \kappa_c\right) = 0.03\frac{1}{\text{m}}$$

$y_2 := t_c + 0.6 \cdot h - y_1 = 0.653\text{m}$

$\varepsilon_2 := \kappa \cdot y_2$

$$\sigma_m := \sigma_{0.2} \cdot \left[1 + \frac{r_2 \cdot \left(\frac{\varepsilon_2}{\varepsilon_{0.2}} - 1\right)}{1 + \left(r_1 - 1\right) \cdot \left(\frac{\frac{\varepsilon_2}{\varepsilon_{0.2}} - 1}{\frac{\varepsilon_u}{\varepsilon_{0.2}} - 1}\right)^{p_1}}\right] = 523.738 \cdot \text{MPa}$$

$$y_1 := \sigma_m \cdot \frac{A_s}{0.85 \cdot f_c \cdot b_c} = 116.674 \cdot mm$$

Position of the neutral axis:

$$N_{a.s} := \sigma_m \cdot A_s = 7.293 \times 10^3 \frac{1}{m} \cdot kN \cdot m$$

$$N_{c.s} := 0.85 \cdot b_c \cdot t_c \cdot f_c = 1.131 \times 10^7 N$$

$$N_{f.s} := t_{fu} \cdot b_{fu} \cdot \sigma_m = 1.874 \times 10^6 N$$

$$N_{af.s} := \frac{N_{a.s} - N_{c.s}}{2} = -2.011 \times 10^6 N$$

$$N_{aw.s} := \frac{N_{a.s} - N_{c.s} - \sigma_m \cdot b_{fl} \cdot t_{fl} - \sigma_m \cdot b_{fu} \cdot t_{fu}}{2} = -3.885 \times 10^6 N$$

The neutral axis lies in the concrete

Selenderness of the cross section:

$$x_{pl.c.s} := \frac{N_{a.s}}{0.85 \cdot f_c \cdot b_c} = 0.117 m \qquad \frac{x_{pl.c.s}}{h} = 0.119$$

Bending Resistance:

$$M_s := N_{a.s} \cdot \left(h - Y_a - \frac{x_{pl.c.s}}{2} \right) = 3.81 \times 10^3 \cdot kN \cdot m$$

Bending resistance M_{pl} of G2-CR-CS

Geometry:

$t_c := 181mm$

$b_c := 2184.4mm$

$b_{fl} := 182.6mm$

$t_{fl} := 19.6mm$

$b_{fu} := 182.6mm$

$t_{fu} := 19.6mm$

$h_w := 760.4mm$

$t_w := 0mm$

Material Properties:

$f_c := \frac{50.5}{1.5} \cdot MPa = 3.367 \times 10^{7} Pa$

$E := 210000MPa$

$F_{y.F} := 420MPa$

$F_{y.W} := 355MPa$

Center of steel section:

$h_a := t_{fl} + t_{fu} + h_w$

$A_s := b_{fl} \cdot t_{fl} + h_w \cdot t_w + b_{fu} \cdot t_{fu} = 7.158 \times 10^{-3} m^2$

$$Y_a := \frac{b_{fu} \cdot t_{fu} \cdot \left(h_a - \frac{t_{fu}}{2} \right) + b_{fl} \cdot t_{fl} \cdot \frac{t_{fl}}{2} + h_w \cdot t_w \cdot \left(t_{fl} + \frac{h_w}{2} \right)}{A_s} = 0.4m$$

Position of the neutral axis:

$A_F := b_{fl} \cdot t_{fl} + b_{fu} \cdot t_{fu} = 7.158 \times 10^{-3} m^2$

$A_w := h_w \cdot t_w = 0$

$N_a := F_{y.F} \cdot A_F + F_{y.W} \cdot A_w = 3.006 \times 10^{6} N$

$N_c := 0.85 \cdot b_c \cdot t_c \cdot f_c = 1.131 \times 10^{7} N$

$N_f := t_{fu} \cdot b_{fu} \cdot F_{y.F} = 1.503 \times 10^{6} N$

$$N_{af} := \frac{N_a - N_c}{2} = -4.154 \times 10^{6} N$$

$$N_{aw} := \frac{N_a - N_c - F_{y.F} \cdot b_{fl} \cdot t_{fl} - F_{y.F} \cdot b_{fu} \cdot t_{fu}}{2} = -5.657 \times 10^{6} N$$

The neutral axis lies in the Concrete

Selenderness of the cross section:

$h := t_c + t_{fl} + t_{fu} + h_w = 0.981\,m$

$x_{pl.c} := \frac{N_a}{0.85 \cdot f_c \cdot b_c} = 0.048\,m$ $\qquad \frac{x_{pl.c}}{h} = 0.049$

Bending Resistance:

$M_{pl.c} := N_a \cdot \left(h - Y_a - \frac{x_{pl.c}}{2} \right) = 1.674 \times 10^3\,m \cdot kN$

Bending resistance M.pl of G2-CR-SS

Geometry:

$t_c := 181\,mm$
$b_c := 2184.4\,mm$
$b_{fl} := 182.6\,mm$
$t_{fl} := 19.6\,mm$
$b_{fu} := 182.6\,mm$
$t_{fu} := 19.6\,mm$
$h_w := 760.4\,mm$
$t_w := 0\,mm$

Material Properties:

$f_c := \frac{50.5}{1.5} \cdot MPa = 3.367 \times 10^7\,Pa$

$E := 200000\,MPa$

$F_{y.F} := 450\,MPa$

$F_{y.W} := 480\,MPa$

Center of steel section:

$h_a := t_{fl} + t_{fu} + h_w$

$A_s := b_{fl} \cdot t_{fl} + h_w \cdot t_w + b_{fu} \cdot t_{fu} = 7.158 \times 10^{-3}\,m^2$

$Y_a := \frac{b_{fu} \cdot t_{fu} \cdot \left(h_a - \frac{t_{fu}}{2} \right) + b_{fl} \cdot t_{fl} \cdot \frac{t_{fl}}{2} + h_w \cdot t_w \cdot \left(t_{fl} + \frac{h_w}{2} \right)}{A_s} = 0.4\,m$

Position of the neutral axis:

$A_F := b_{fl} \cdot t_{fl} + b_{fu} \cdot t_{fu} = 7.158 \times 10^{-3} m^2$

$A_w := h_w \cdot t_w = 0$

$N_a := F_{y.F} \cdot A_F + F_{y.W} \cdot A_w = 3.221 \times 10^6 N$

$N_c := 0.85 \cdot b_c \cdot t_c \cdot f_c = 1.131 \times 10^7 N$

$N_f := t_{fu} \cdot b_{fu} \cdot F_{y.F} = 1.611 \times 10^6 N$

$$N_{af} := \frac{N_a - N_c}{2} = -4.047 \times 10^6 N$$

$$N_{aw} := \frac{N_a - N_c - F_{y.F} \cdot b_{fl} \cdot t_{fl} - F_{y.F} \cdot b_{fu} \cdot t_{fu}}{2} = -5.657 \times 10^6 N$$

The neutral axis lies in the concrete

Selenderness of the cross section:

$h := t_c + t_{fl} + t_{fu} + h_w = 0.981 m$

$$x_{pl.c} := \frac{N_a}{0.85 \cdot f_c \cdot b_c} = 0.052 m \qquad \frac{x_{pl.c}}{h} = 0.053$$

Bending Resistance:

$$M_{pl.c} := N_a \cdot \left(h - Y_a - \frac{x_{pl.c}}{2} \right) = 1.788 \times 10^3 \cdot kN \cdot m$$

Bending resistance M.s of G2-CR-SS

Material Parameters:

$\sigma_{0.2} := F_{y.F} = 4.5 \times 10^{8}\,Pa$

$\varepsilon_{0.2} := \frac{\sigma_{0.2}}{E} + 0.002 = 4.25 \times 10^{-3}$

$ee := \frac{\sigma_{0.2}}{E} = 2.25 \times 10^{-3}$

$n := 8.01$

$E_2 := \frac{E}{1 + 0.002 \cdot \frac{n}{ee}} = 2.463 \times 10^{10}\,Pa$

$r_2 := E_2 \cdot \frac{\varepsilon_{0.2}}{\sigma_{0.2}} = 0.233$

$\sigma_u := \sigma_{0.2} \cdot \frac{[1 - 0.0375 \cdot (n - 5)]}{0.2 + 185 \cdot ee} = 6.478 \times 10^{8}\,Pa$

$\varepsilon_u := 0.28$

$m_1 := 1 + 3.5 \cdot \frac{\sigma_{0.2}}{\sigma_u} = 3.431$

$r_1 := E_2 \cdot \frac{(\varepsilon_u - \varepsilon_{0.2})}{\sigma_u - \sigma_{0.2}} = 34.337$

$E_u := \frac{E_2}{1 + (r_1 - 1) \cdot m_1} = 2.135 \times 10^{8}\,Pa$

$r_u := E_u \cdot \frac{(\varepsilon_u - \varepsilon_{0.2})}{\sigma_u - \sigma_{0.2}} = 0.298$

$p_1 := r_1 \cdot \left(\frac{1 - r_u}{r_1 - 1} \right) = 0.723$

Stress in steel σ_m:

Given

$y_1 := 63.146\text{mm}$ $\varepsilon_{cu} := 0.003$

$\kappa_a := \frac{\varepsilon_u}{h - y_1} = 0.305\frac{1}{m}$ $\kappa_c := \frac{\varepsilon_{cu}}{y_1} = 0.055\frac{1}{m}$

$\kappa := \min(\kappa_a, \kappa_c) = 0.055\frac{1}{m}$ $y_2 := t_c + 0.6\cdot h - y_1 = 0.706\text{m}$

$\varepsilon_2 := \kappa \cdot y_2$

$$\sigma_m := \sigma_{0.2}\cdot\left[\frac{1 + r_2\cdot\left(\frac{\varepsilon_2}{\varepsilon_{0.2}} - 1\right)}{1 + (r_1 - 1)\cdot\frac{\frac{\varepsilon_2}{\varepsilon_{0.2}} - 1}{\frac{\varepsilon_u}{\varepsilon_{0.2}} - 1}}\right]^{p_1} = 551.454\cdot\text{MPa}$$

$y_1 := \sigma_m\cdot\frac{A_s}{0.85\cdot f_c\cdot b_c} = 63.146\cdot\text{mm}$

Position of the neutral axis:

$$N_{a.s} := \sigma_m \cdot A_s = 3.947 \times 10^3 \frac{1}{m} \cdot kN \cdot m$$

$$N_{c.s} := 0.85 \cdot b_c \cdot t_c \cdot f_c = 1.131 \times 10^7 N$$

$$N_{f.s} := t_{fu} \cdot b_{fu} \cdot \sigma_m = 1.974 \times 10^6 N$$

$$N_{af.s} := \frac{N_{a.s} - N_{c.s}}{2} = -3.684 \times 10^6 N$$

$$N_{aw.s} := \frac{N_{a.s} - N_{c.s} - \sigma_m \cdot b_{fl} \cdot t_{fl} - \sigma_m \cdot b_{fu} \cdot t_{fu}}{2} = -5.657 \times 10^6 N$$

The neutral axis lies in the concrete

Selenderness of the cross section:

$$x_{pl.c.s} := \frac{N_{a.s}}{0.85 \cdot f_c \cdot b_c} = 0.063 m \qquad \frac{x_{pl.c.s}}{h} = 0.064$$

Bending Resistance:

$$M_{pl.c.s} := N_{a.s} \cdot \left(h - Y_a - \frac{x_{pl.c.s}}{2} \right) = 2.168 \times 10^3 \cdot kN \cdot m$$

Bending resistance M.pl of 100-262-1-FL-CS

Geometry:

$t_c := 320mm$

$b_c := 4925mm$

$b_{fl} := 1200mm$

$t_{fl} := 55mm$

$b_{fu} := 800mm$

$t_{fu} := 42mm$

$h_w := 1953mm$

$t_w := 17mm$

Material Properties:

$f_c := \frac{35}{1.5} \cdot MPa = 2.333 \times 10^7 Pa$

$E := 210000MPa$

$F_{y.F} := 390MPa$

$F_{y.W} := 355MPa$

Center of steel section:

$h_a := t_{fl} + t_{fu} + h_w$

$A_s := b_{fl} \cdot t_{fl} + h_w \cdot t_w + b_{fu} \cdot t_{fu} = 0.133m^2$

$$Y_a := \frac{b_{fu} \cdot t_{fu} \cdot \left(h_a - \frac{t_{fu}}{2} \right) + b_{fl} \cdot t_{fl} \cdot \frac{t_{fl}}{2} + h_w \cdot t_w \cdot \left(t_{fl} + \frac{h_w}{2} \right)}{A_s} = 0.785m$$

Position of the neutral axis:

$A_F := b_{fl} \cdot t_{fl} + b_{fu} \cdot t_{fu} = 0.1m^2$

$A_w := h_w \cdot t_w = 0.033m^2$

$N_a := F_{y.F} \cdot A_F + F_{y.W} \cdot A_w = 5.063 \times 10^7 N$

$N_c := 0.85 \cdot b_c \cdot t_c \cdot f_c = 3.126 \times 10^7 N$

$N_f := t_{fu} \cdot b_{fu} \cdot F_{y.F} = 1.31 \times 10^7 N$

$$N_{af} := \frac{N_a - N_c}{2} = 9.687 \times 10^6 N$$

$$N_{aw} := \frac{N_a - N_c - F_{y.F} \cdot b_{fl} \cdot t_{fl} - F_{y.F} \cdot b_{fu} \cdot t_{fu}}{2} = -9.735 \times 10^6 N$$

The neutral axis lies in the upper flange of the plate girder

Selenderness of the cross section:

$h := t_c + t_{fl} + t_{fu} + h_w = 2.37\text{m}$

$x_{pl.f} := t_c + \frac{N_{af}}{b_{fu} \cdot F_{y.F}} = 0.351\text{m}$ $\qquad \frac{x_{pl.f}}{h} = 0.148$

Bending Resistance:

$M_{pl.f} := N_c \cdot \left(h - Y_a - \frac{t_c}{2} \right) + N_{af} \cdot \left[h - t_c - \left(x_{pl.f} - t_c \right) \right] = 6.41 \times 10^4 \cdot \text{kN} \cdot \text{m}$

Bending resistance M.pl of 100-262-1-FL-SS

Geometry:

$t_c := 320\text{mm}$
$b_c := 4925\text{mm}$
$b_{fl} := 1200\text{mm}$
$t_{fl} := 55\text{mm}$
$b_{fu} := 800\text{mm}$
$t_{fu} := 42\text{mm}$
$h_w := 1953\text{mm}$
$t_w := 17\text{mm}$

Material Properties:

$f_c := \frac{35}{1.5} \cdot \text{MPa} = 2.333 \times 10^7\ \text{Pa}$

$E := 201000\text{MPa}$

$F_{y.F} := 450\text{MPa}$

$F_{y.W} := 450\text{MPa}$

Center of steel section:

$h_a := t_{fl} + t_{fu} + h_w$

$A_s := b_{fl} \cdot t_{fl} + h_w \cdot t_w + b_{fu} \cdot t_{fu} = 0.133\text{m}^2$

$Y_a := \frac{b_{fu} \cdot t_{fu} \cdot \left(h_a - \frac{t_{fu}}{2} \right) + b_{fl} \cdot t_{fl} \cdot \frac{t_{fl}}{2} + h_w \cdot t_w \cdot \left(t_{fl} + \frac{h_w}{2} \right)}{A_s} = 0.785\text{m}$

Position of the neutral axis:

$A_F := b_{fl} \cdot t_{fl} + b_{fu} \cdot t_{fu} = 0.1\,m^2$

$A_w := h_w \cdot t_w = 0.033\,m^2$

$N_a := F_{y.F} \cdot A_F + F_{y.W} \cdot A_w = 5.976 \times 10^7\,N$

$N_c := 0.85 \cdot b_c \cdot t_c \cdot f_c = 3.126 \times 10^7\,N$

$N_f := t_{fu} \cdot b_{fu} \cdot F_{y.F} = 1.512 \times 10^7\,N$

$N_{af} := \frac{N_a - N_c}{2} = 1.425 \times 10^7\,N$

$N_{aw} := \frac{N_a - N_c - F_{y.F} \cdot b_{fl} \cdot t_{fl} - F_{y.F} \cdot b_{fu} \cdot t_{fu}}{2} = -8.158 \times 10^6\,N$

The neutral axis lies in the upper flange og the plate girder

Selenderness of the cross section:

$h := t_c + t_{fl} + t_{fu} + h_w = 2.37\,m$

$x_{pl.f} := t_c + \frac{N_{af}}{b_{fu} \cdot F_{y.F}} = 0.36\,m$

$\frac{x_{pl.f}}{h} = 0.152$

Bending Resistance:

$M_{pl.f} := N_c \cdot \left(h - Y_a - \frac{t_c}{2} \right) + N_{af} \cdot \left[h - t_c - \left(x_{pl.f} - t_c \right) \right] = 7.32 \times 10^4 \cdot kN \cdot m$

Bending resistance M.s of 100-262-1-FL-SS

Material Parameters:

$\sigma_{0.2} := F_{y.F} = 4.5 \times 10^{8}\,\text{Pa}$

$\varepsilon_{0.2} := \frac{\sigma_{0.2}}{E} + 0.002 = 4.239 \times 10^{-3}$

$ee := \frac{\sigma_{0.2}}{E} = 2.239 \times 10^{-3}$

$n := 8.01$

$E_2 := \frac{E}{1 + 0.002 \cdot \frac{n}{ee}} = 2.465 \times 10^{10}\,\text{Pa}$

$r_2 := E_2 \cdot \frac{\varepsilon_{0.2}}{\sigma_{0.2}} = 0.232$

$\sigma_u := \sigma_{0.2} \cdot \frac{[1 - 0.0375 \cdot (n - 5)]}{0.2 + 185 \cdot ee} = 6.5 \times 10^{8}\,\text{Pa}$

$\varepsilon_u := 0.28$

$m_1 := 1 + 3.5 \cdot \frac{\sigma_{0.2}}{\sigma_u} = 3.423$

$r_1 := E_2 \cdot \frac{\left(\varepsilon_u - \varepsilon_{0.2}\right)}{\sigma_u - \sigma_{0.2}} = 33.984$

$E_u := \frac{E_2}{1 + \left(r_1 - 1\right) \cdot m_1} = 2.164 \times 10^{8}\,\text{Pa}$

$r_u := E_u \cdot \frac{\left(\varepsilon_u - \varepsilon_{0.2}\right)}{\sigma_u - \sigma_{0.2}} = 0.298$

$p_1 := r_1 \cdot \left(\frac{1 - r_u}{r_1 - 1}\right) = 0.723$

Stress in steel σ_m:

Given

$y_1 := 643.348\text{mm}$ $\varepsilon_{cu} := 0.003$

$\kappa_a := \frac{\varepsilon_u}{h - y_1} = 0.162\frac{1}{m}$ $\kappa_c := \frac{\varepsilon_{cu}}{y_1} = 5.44\times 10^{-3}\frac{1}{m}$

$\kappa := \min(\kappa_a, \kappa_c) = 5.44\times 10^{-3}\frac{1}{m}$ $y_2 := t_c + 0.6\cdot h - y_1 = 1.099\text{m}$

$\varepsilon_2 := \kappa \cdot y_2$

$$\sigma_m := \sigma_{0.2}\cdot\left[\frac{1 + r_2\cdot\left(\frac{\varepsilon_2}{\varepsilon_{0.2}} - 1\right)}{1 + (r_1 - 1)\cdot\left(\frac{\frac{\varepsilon_2}{\varepsilon_{0.2}} - 1}{\frac{\varepsilon_u}{\varepsilon_{0.2}} - 1}\right)^{p_1}}\right] = 473.202\cdot\text{MPa}$$

$$y_1 := \sigma_m\cdot\frac{A_s}{0.85\cdot f_c\cdot b_c} = 643.348\cdot\text{mm}$$

Position of the neutral axis:

$$N_{a.s} := \sigma_m \cdot A_s = 6.284 \times 10^4 \frac{1}{m} \cdot kN \cdot m$$

$$N_{c.s} := 0.85 \cdot b_c \cdot t_c \cdot f_c = 3.126 \times 10^7 N$$

$$N_{f.s} := t_{fu} \cdot b_{fu} \cdot \sigma_m = 1.59 \times 10^7 N$$

$$N_{af.s} := \frac{N_{a.s} - N_{c.s}}{2} = 1.579 \times 10^7 N$$

$$N_{aw.s} := \frac{N_{a.s} - N_{c.s} - \sigma_m \cdot b_{fl} \cdot t_{fl} - \sigma_m \cdot b_{fu} \cdot t_{fu}}{2} = -7.773 \times 10^6 N$$

The neutral axis lies in the upper flange of the plate girder

Selenderness of the cross section:

$$x_{pl.f.s} := t_c + \frac{N_{af.s}}{b_{fu} \cdot \sigma_m} = 0.362 m \qquad \frac{x_{pl.f.s}}{h} = 0.153$$

Bending Resistance:

$$M_s := N_{c.s} \cdot \left(h - Y_a - \frac{t_c}{2} \right) + N_{af.s} \left[h_a - \left(x_{pl.f.s} - t_c \right) \right] = 7.626 \times 10^4 \cdot kN \cdot m$$

Bending resistance of 100-262-1-CR-CS

Geometry:

$t_c := 320mm$

$b_c := 4925mm$

$b_{fl} := 1225mm$

$t_{fl} := 50mm$

$b_{fu} := 850mm$

$t_{fu} := 45mm$

$h_w := 1955mm$

$t_w := 0mm$

Material Properties:

$f_c := \frac{35}{1.5}\cdot MPa = 2.333\times 10^7\,Pa$

$E := 210000MPa$

$F_{y.F} := 390MPa$

$F_{y.W} := 355MPa$

Center of steel section:

$h_a := t_{fl} + t_{fu} + h_w$

$A_s := b_{fl}\cdot t_{fl} + h_w\cdot t_w + b_{fu}\cdot t_{fu} = 0.1\,m^2$

$$Y_a := \frac{b_{fu}\cdot t_{fu}\cdot\left(h_a - \frac{t_{fu}}{2}\right) + b_{fl}\cdot t_{fl}\cdot\frac{t_{fl}}{2} + h_w\cdot t_w\cdot\left(t_{fl} + \frac{h_w}{2}\right)}{A_s} = 0.795m$$

Position of the neutral axis:

$A_F := b_{fl}\cdot t_{fl} + b_{fu}\cdot t_{fu} = 0.1\,m^2$

$A_w := h_w\cdot t_w = 0$

$N_a := F_{y.F}\cdot A_F + F_{y.W}\cdot A_w = 3.88\times 10^7\,N$

$N_c := 0.85\cdot b_c\cdot t_c\cdot f_c = 3.126\times 10^7\,N$

$N_f := t_{fu}\cdot b_{fu}\cdot F_{y.F} = 1.492\times 10^7\,N$

$$N_{af} := \frac{N_a - N_c}{2} = 3.774\times 10^6\,N$$

$$N_{aw} := \frac{N_a - N_c - F_{y.F}\cdot b_{fl}\cdot t_{fl} - F_{y.F}\cdot b_{fu}\cdot t_{fu}}{2} = -1.563\times 10^7\,N$$

The neutral axis lies in the upper flange of the plate girder

Selenderness of the cross section:

$h := t_c + t_{fl} + t_{fu} + h_w = 2.37\,m$

$x_{pl.f} := t_c + \frac{N_{af}}{b_{fu} \cdot F_{y.F}} = 0.331\,m$ $\qquad \frac{x_{pl.f}}{h} = 0.14$

Bending Resistance:

$M_{pl.f} := N_c \cdot \left(h - Y_a - \frac{t_c}{2} \right) + N_{af} \cdot \left[h_a - t_c - \left(x_{pl.f} - t_c \right) \right] = 5.072 \times 10^4 \cdot kN \cdot m$

Bending resistance M.pl of 100-262-1-CR-SS

Geometry:

$t_c := 320\,mm$

$b_c := 4925\,mm$

$b_{fl} := 1225\,mm$

$t_{fl} := 50\,mm$

$b_{fu} := 850\,mm$

$t_{fu} := 45\,mm$

$h_w := 1955\,mm$

$t_w := 0\,mm$

Material Properties:

$f_c := \frac{35}{1.5} \cdot MPa = 2.333 \times 10^7\,Pa$

$E := 201000\,MPa$

$F_{y.F} := 450\,MPa$

$F_{y.W} := 530\,MPa$

Center of steel section:

$h_a := t_{fl} + t_{fu} + h_w$

$A_s := b_{fl} \cdot t_{fl} + h_w \cdot t_w + b_{fu} \cdot t_{fu} = 0.1\,m^2$

$Y_a := \frac{b_{fu} \cdot t_{fu} \cdot \left(h_a - \frac{t_{fu}}{2} \right) + b_{fl} \cdot t_{fl} \cdot \frac{t_{fl}}{2} + h_w \cdot t_w \cdot \left(t_{fl} + \frac{h_w}{2} \right)}{A_s} = 0.795\,m$

Position of the neutral axis:

$A_F := b_{fl} \cdot t_{fl} + b_{fu} \cdot t_{fu} = 0.1\,m^2$

$A_w := h_w \cdot t_w = 0$

$N_a := F_{y.F} \cdot A_F + F_{y.W} \cdot A_w = 4.478 \times 10^7\,N$

$N_c := 0.85 \cdot b_c \cdot t_c \cdot f_c = 3.126 \times 10^7\,N$

$N_f := t_{fu} \cdot b_{fu} \cdot F_{y.F} = 1.721 \times 10^7\,N$

$N_{af} := \frac{N_a - N_c}{2} = 6.759 \times 10^6\,N$

$N_{aw} := \frac{N_a - N_c - F_{y.F} \cdot b_{fl} \cdot t_{fl} - F_{y.F} \cdot b_{fu} \cdot t_{fu}}{2} = -1.563 \times 10^7\,N$

The neutral axis lies in the upper flange of the plate girder

Selenderness of the cross section:

$h := t_c + t_{fl} + t_{fu} + h_w = 2.37m$

$x_{pl.f} := t_c + \frac{N_{af}}{b_{fu} \cdot F_{y.F}} = 0.338m$

$\frac{x_{pl.f}}{h} = 0.142$

Bending Resistance:

$M_{pl.f} := N_c \cdot \left(h - Y_a - \frac{t_c}{2} \right) + N_{af} \cdot \left[h_a - t_c - \left(x_{pl.f} - t_c \right) \right] = 5.581 \times 10^4 \cdot kN \cdot m$

Bending resistance M.s of 100-262-1-CR-SS

Material Parameters:

$\sigma_{0.2} := F_{y.F} = 4.5 \times 10^{8}\,Pa$

$\varepsilon_{0.2} := \frac{\sigma_{0.2}}{E} + 0.002 = 4.239 \times 10^{-3}$

$ee := \frac{\sigma_{0.2}}{E} = 2.239 \times 10^{-3}$

$n := 8.01$

$E_2 := \frac{E}{1 + 0.002 \cdot \frac{n}{ee}} = 2.465 \times 10^{10}\,Pa$

$r_2 := E_2 \cdot \frac{\varepsilon_{0.2}}{\sigma_{0.2}} = 0.232$

$\sigma_u := \sigma_{0.2} \cdot \frac{[1 - 0.0375 \cdot (n - 5)]}{0.2 + 185 \cdot ee} = 6.5 \times 10^{8}\,Pa$

$\varepsilon_u := 0.28$

$m_1 := 1 + 3.5 \cdot \frac{\sigma_{0.2}}{\sigma_u} = 3.423$

$r_1 := E_2 \cdot \frac{(\varepsilon_u - \varepsilon_{0.2})}{\sigma_u - \sigma_{0.2}} = 33.984$

$E_u := \frac{E_2}{1 + (r_1 - 1) \cdot m_1} = 2.164 \times 10^{8}\,Pa$

$r_u := E_u \cdot \frac{(\varepsilon_u - \varepsilon_{0.2})}{\sigma_u - \sigma_{0.2}} = 0.298$

$p_1 := r_1 \cdot \left(\frac{1 - r_u}{r_1 - 1} \right) = 0.723$

Stress in steel σ_m:

Given

$y_1 := 500.229\text{mm}$ $\varepsilon_{cu} := 0.003$

$\kappa_a := \frac{\varepsilon_u}{h - y_1} = 0.15\frac{1}{m}$ $\kappa_c := \frac{\varepsilon_{cu}}{y_1} = 6.997 \times 10^{-3}\frac{1}{m}$

$\kappa := \min(\kappa_a, \kappa_c) = 6.997 \times 10^{-3}\frac{1}{m}$ $y_2 := t_c + 0.6 \cdot h - y_1 = 1.242\text{m}$

$\varepsilon_2 := \kappa \cdot y_2$

$$\sigma_m := \sigma_{0.2} \cdot \left[\frac{1 + r_2 \cdot \left(\frac{\varepsilon_2}{\varepsilon_{0.2}} - 1 \right)}{1 + (r_1 - 1) \cdot \frac{\frac{\varepsilon_2}{\varepsilon_{0.2}} - 1}{\frac{\varepsilon_u}{\varepsilon_{0.2}} - 1}} \right]^{p_1} = 491.075 \cdot \text{MPa}$$

$$y_1 := \sigma_m \cdot \frac{A_s}{0.85 \cdot f_c \cdot b_c} = 500.229 \cdot \text{mm}$$

Position of the neutral axis:

$$N_{a.s} := \sigma_m \cdot A_s = 4.886 \times 10^4 \frac{1}{m} \cdot kN \cdot m$$

$$N_{c.s} := 0.85 \cdot b_c \cdot t_c \cdot f_c = 3.126 \times 10^7 N$$

$$N_{f.s} := t_{fu} \cdot b_{fu} \cdot \sigma_m = 1.878 \times 10^7 N$$

$$N_{af.s} := \frac{N_{a.s} - N_{c.s}}{2} = 8.802 \times 10^6 N$$

$$N_{aw.s} := \frac{N_{a.s} - N_{c.s} - \sigma_m \cdot b_{fl} \cdot t_{fl} - \sigma_m \cdot b_{fu} \cdot t_{fu}}{2} = -1.563 \times 10^7 N$$

The neutral axis lies in the upper flange of the plate girder

Selenderness of the cross section:

$$x_{pl.f.s} := t_c + \frac{N_{af.s}}{b_{fu} \cdot \sigma_m} = 0.341 m \qquad \frac{x_{pl.f.s}}{h} = 0.144$$

Bending Resistance:

$$M_{pl.f.s} := N_{c.s} \cdot \left(h - Y_a - \frac{t_c}{2} \right) + N_{af.s} \cdot \left[h_a - \left(x_{pl.f.s} - t_c \right) \right] = 6.209 \times 10^4 \cdot kN \cdot m$$

Appendix D

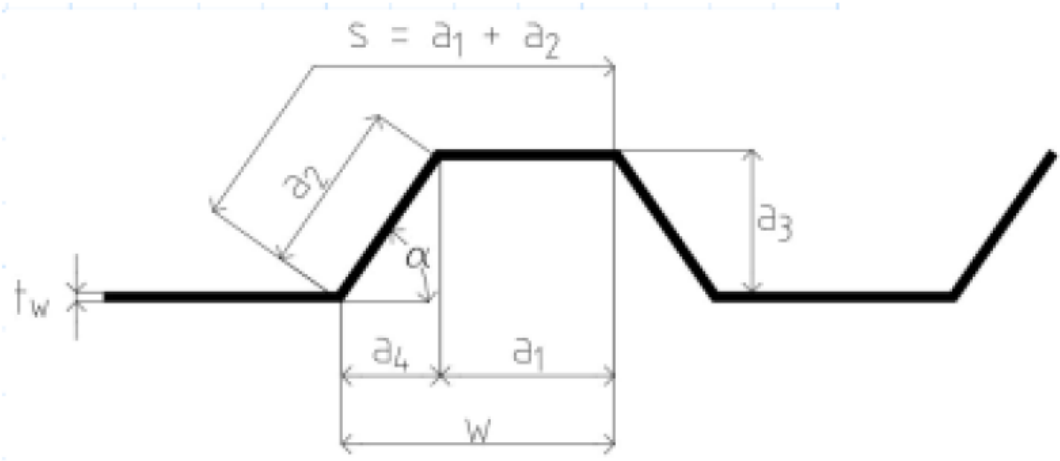

Figure D 1 Corrugated profile from (Henrysson & Yman , 2020)